מכון ויצמן למדע
WEIZMANN INSTITUTE OF SCIENCE

Thesis for the degree
Doctor of Philosophy

עבודת גמר (תזה) לתואר
דוקטור לפילוסופיה

Submitted to the Scientific Council of the
Weizmann Institute of Science
Rehovot, Israel

מוגשת למועצה המדעית של
מכון ויצמן למדע
רחובות, ישראל

By
Rafat Qubaja

מאת
ראפת קבאגה

שטפי של CO_2 ו H_2O ביער חצי ארידי
Fluxes of CO_2 and H_2O in a Semi-arid Forest Ecosystem

Advisor:
Prof. Dan Yakir

מנחה:
פרופי דן יקיר

October 2019

אוקטובר 2019

Fluxes of CO_2 and H_2O in a Semi-arid Forest Ecosystem

PhD thesis

to obtain the degree of PhD at
Weizmann Institute of Science
Rehovot, Israel
under the supervision of
Prof. Dan Yakir

This thesis will be defended in public
Thursday 31 October 2019

by

Rafat A.I. Qubaja

To my Parents;

To my lovely wife, Nuha;

and

To my children, Bara, Mohammad,

Abed Al-Rahman and Tala;

... with love and respect.

ACKNOWLEDGEMENTS

I am grateful to my supervisor, Prof. Dan Yakir, for his guidance through this project. Through providing me the freedom to develop and pursue my own ideas, his sound advice and developing and involving me in interesting discussions, he has helped make me become, I believe, a better scientist. I also appreciate him taking an interest in my family life.

I wish to thank for my advisory committee, Profs. Jose Grünzweig and Itay Halevy, for their interest in the work, constructive ideas and advice for improvements.

The members of Dan Yakir's group with whom I have shared time: Efrat Schwartz, Dr. Fedor Tatarinov, Dr. Fulin Yang, Dr. Gil Yosef, Dr. Amnon Cochavi, Yakir Preisler, Huanhuan Wang, Shani Rohatyn, Efrat Ramati, Jonathan Muller, Rafael Stern, Madi Amer, and Itay Oz; have not only educated me in their various areas of scientific expertise that broadened my knowledge and opened my thinking to new areas, but have been very good friends in life outside the lab and a pleasure to work with.

Particular mention must be made of Dr. Eyal Rotenberg, whose attention to detail has motivated a level of excellence in the running of the tower, and with whom I have had many thought-provoking discussions about Yatir and more.

Various folk around the department have been indispensable and I am happy to thank them for their help. Hagai Sagi, Avraham and Boaz Ninyo-Setter always provided excellent technical assistance and advice in a friendly manner. Ofra Ashkenazi, Dalia Madhala, Alona Surdin and Dror Barzilay were great at taking care of administrative issues and always happy to help.

My family, although at a distance, were always encouraging and supportive and took an interest in my work, and were never far from my heart.

Finally Nuha, my lovely wife whose patience has been phenomenal, I thank you deeply for everything.

Rafat Qubaja
October 2019, Rehovot, Israel.

DECLARATION

All group members associated with the Yatir Forest flux tower research site have been involved in the maintenance and operation of the flux tower, under the direction of Dr. Eyal Rotenberg. The database of flux and meteorological data is maintained by Miss. Efrat Schwartz. Interpretation and analysis of flux data is my own.

All other work presented in this thesis is my own.

Rafat Qubaja
October 2019, Rehovot, Israel.

CONTENTS

ABSTRACT

The objective was to quantify soil CO_2 and H_2O fluxes as a basis for partitioning net ecosystem-atmosphere exchange of carbon and water vapor, which, in-turn, is a critical limiting factor in understanding ecosystem and the land biosphere response to climate change. Within this framework, this work focused on semi-arid ecosystems that represent large spatial fraction of the land biosphere (~18%) for which information remains scarce. **In the 1st part** we combined carbon stock (CS) and eddy covariance (EC) flux measurements that were collected over a period of 15 years (2001-2016) in our semi-arid pine forest. The forest accumulated 145-160 g C m^{-2} y^{-1} over the study period, reaching the current ecosystem C stock of 7943±323 g C m^{-2} with a long C turnover time of 59±4 y. The soil organic C is ~71% of the current ecosystem C and where most C accumulates. The results imply that afforestation of even 10% of semi-arid land area under conditions similar to that of the study site, could sequester ~0.4 Pg C y^{-1}. **In the 2nd part**, we applied carbon flux partitioning methodology, together with stable isotopes (^{13}C) and a radiocarbon (^{14}C) data in the semi-arid pine forest to partition the ecosystem CO_2 flux and estimate gross primary productivity, (GPP) and ecosystem respiration (Re) and the soil respiration flux to its autotropic (Rsa), heterotrophic (Rh) and inorganic (Ri) components. On annual scale, gross GPP and Re were 655 and 488 g C m^{-2}, with net primary productivity, NPP, of 282 g C m^{-2} and carbon use efficiency (NPP/GPP) of 0.42. Rs made up 0.60 of total ecosystem respiration comprised of 24±4, 23±4, and 13±1%, from Rsa, Rh, and Ri, respectively. Results obtained at the site 15 years earlier indicated that annual Rs decreased by 27% (~2% per year), associated with 36% decrease in the Q_{10}. Low rates of soil carbon loss combined with high belowground carbon allocation (38% of canopy CO_2 uptake) help explain the high soil organic carbon accumulation, and reflects highe resilience of pine forest to climate change. **In the 3rd part**, we used a citrus orchard on the Weizmann campus as a model system to further develop and test our flux partitioning approach based on combined ecosystem canopy scale eddy covariance and soil flux measurements to partition the net CO_2 exchange (NEE), and total evapotranspiration (ET) into their main components. We show that in such system, the ratio of soil to ecosystem respiration (Rs/Re) and soil evaporation to ET (Es/ET) were 0.65, 0.41 during the wet period, and change to 0.71, and 0.18 during the dry period, respectively. Spatial variations showed the sensitivity of the fluxes to the proportions of shaded and sun exposed microsites. Estimated C stock together with that of gross primary productivity (GPP) indicated fast carbon turnover time of 5±1 y. **In the 4th part** of this work, we focused on our new extension of the flux partitioning approach to the partitioning of ecosystem water vapor fluxes. We used chamber-based direct measurements of soil evaporation (Es) in the semi-arid forest to partition ET to Es and tree transpiration (Et). The ecosystem is characterized by a high annual Es/ET ratio of 0.26, and an Et/ET of 0.63. Es diminishes in the long dry season, and as much as 74±5% of the residual flux was due to the re-evaporation of nighttime moisture adsorption, which may provide critical protection from soil drying. Over a 10 years observation period, concurrent increase in the transpiration ratio (TR=Et/ET; +29%) and in leaf area index (LAI; +44%) indicated a ratio of TR/LAI that remain near constant at ~0.31, and with persistently closed hydrological balance (ET/P of 0.94-1.07). The observed Et/ET values are similar to the estimated global mean values, but are attained at a much higher aridity index of 5.5, demonstrating the potential for expanding forestation into dry regions.

תקציר

הפרדת חילופי הגזים בין האקוסיסטמה לאטמוספרה, למקורם הצמחי או הקרקעי, היא מרכיב מכריע וגורם מגביל בהבנתנו את תגובת הביוספרה היבשתית לשינויי אקלים. מטרת העל של המחקר הייתה לכמת בצורה ישירה את השטפים הקרקעיים, כשיטה להפרדה זו. במסגרת המחקר, התמקדנו במערכות אקולוגיות באקלים היובשני למחצה (semi-arid) אשר מהוות אחוז נכבד (18%) משטח הביוספרה היבשתית ועם זאת המידע לגביהם חסר במידה ניכרת. **בחלק הראשון**, שילבנו נתונים ומדידות משתי שיטות: מאגר הפחמן (carbon stock; CS) וקורלציית הערבלים (eddy covariance; EC) אשר נמדדו ונאספו במהלך 15 שנה (2001 – 2016) ביתיר, יער אורנים באזור יובשני-למחצה. מצאנו כי לאורך תקופת המחקר, הצטברו במערכת כ- 160–145 *גר׳ פחמן מ׳$^{-2}$ שנה$^{-1}$*, שטף המביא את צבר הפחמן של היער ל 323±7,943 *גר׳ פחמן מ׳$^{-2}$* וזמן תחלופה ארוך של כ 4±59 שנים. בנוסף, מרבית הפחמן (כ~ 71%)מצטבר בפרקציה האורגנית בקרקע. התוצאות מרמזות שייעור, אפילו של כ10% מהשטח המאופיין כאקלים יובשני למחצה, בתנאים דומים לאלה שבהם נערך מחקר זה, עשוי להביא לקיבוע של כ ~0.4 פטה גרם פחמן בשנה. **בחלק השני**, יישמנו את מתודולוגיית הפרדת שטפי הפחמן, לצד נתוני האיזוטופ היציב (^{13}C) וזה הרדיואקטיבי (^{14}C) מיער יתיר, על מנת לחלק את סך השטף האקו-סיסטמי לנשימה (Re) לעומת יצרנות ראשונית ברוטו (GPP). וכן, הפרדנו את שטף הנשימה הקרקעי לרכיב האוטו-טרופי (Rsa) וההטרו-טרופי (Rh) לעומת הרכיב האי-אורגני (Ri). ברמה השנתית, GPP ו Re היו 655 ו 488 *גר׳ פחמן מ׳$^{-2}$, כאשר היצרנות הראשונית נטו* (NPP) מהווה 282 גר׳ פחמן מ׳$^{-2}$ ויעילות ניצול הפחמן (NPP/GPP) שווה ל0.42. החלק הנשימתי של הקרקע הוא 0.6 מסך הנשימה של האקוסיסטמה, כאשר Rsa, Rh ו Ri שווים ל4%±24, 4%±23 ו1%±13, בהתאמה. תוצאות שהונפקו מהאתר 15 שנים קודם לכן, מראות שכיום ישנה ירידה של ~27% (~2% לשנה) בנשימת הקרקע השנתית מלווה בירידה של כ36% ב Q_{10}. קצב נמוך של איבוד פחמן הקרקע, יחד עם רמה גבוהה של הסעת פחמן אל תת הקרקע (כ38% מהפחמן הנקלט על ידי הצמחייה), מסבירים את צבר הפחמן האורגני הקרקעי ומשקף את יכולת ההתמודדות של יער האורנים עם שינויי האקלים. **בחלק השלישי**, השתמשנו בפרדס ההדרים בקמפוס מכון ויצמן, כמערכת מודל לבחינה מורחבת של שיטתנו להפרדת השטפים; זו המבוססת על מדידת השטפים ברמת האקוסיסטמה באמצעות שיטת קורלציית הערבלים, יחד עם מדידה ישירה של השטפים הקרקעיים. הפעם, שאפנו להפריד את תחלופת הפחמן הדו חמצני נטו (NEE) ואת שטף ההתאיידות הכולל (ET) לרכיביהם העיקריים. אנו מראים כי במערכת מסוג זה, היחס בין הנשימה הקרקעית לאקוסיסטמית (Rs/Re) והאידוי הקרקעי לעומת ההתאיידות הכללית (Es/ET) היו 0.65 ו 0.41 במהלך העונה הרטובה, ויחסים אלו השתנו ל 0.71 ו0.18 במהלך העונה היבשה, בהתאמה. השונות המרחבית משקפת את רגישות השטפים לחשיפתם לשמש והצללה של המיקרו-אתרים. כאן, הערכת צבר הפחמן לצד הערכת הGPP מראים זמן תחלופה מהיר של 1±5 שנים. **בחלק הרביעי** של עבודה זו, התמקדנו בהרחבה שלנו את שיטת הפרדת שטפי הפחמן והנשימה, ליישומה החדשני על הפרדת שטפי אדי המים ברמת האקוסיסטמה. לצורך כך, נעזרנו במדידה ישירה של אידוי מהקרקע (Es), המבוססת על תאי קרקע סגורים, על מנת לכמת את רכיבי הET לEs ולדיות הצמחי (Et) ביער יתיר היובשני למחצה. מערכת זו מאופיינת ביחס שנתי גבוה של Es/ET העומד על 0.26 ויחס Et/ET של 0.63. אידוי הקרקע מצטמצם בעונה היבשה הארוכה וכמעט כ5%±74 מהשטף החסר הוא כתוצאה מאידוי חוזר של לחות לילה שסופחה, תהליך שכנראה מספק הגנה קריטית מייבוש כליל של הקרקע ותמותת העצים. במהלך עשר שנות מדידה, עליית בקצב הדיות הצמחי (TR=ET/ET; +29%), במקביל לעליה באינדקס שטח העלווה (LAI; +44%), מראים יחס TR/LAI כמעט קבוע השווה ל~0.31, לצד מחזור הידרולוגי מאוזן באופן עקבי (ET/P = 0.94 – 1.07). ערכי הפרופורציה המוצגים כאן של Et/ET, דומים לערכים הממוצעים הגלובליים, אך אלו כאן מגיעים מאזור בעל אינדקס יובשנות (Aridity Index) גבוה מאוד (5.5) ביחס לזה הגלובלי, ומדגימים את היכולות הצפונות של התפשטות היערות לאזורים היבשים.

1

INTRODUCTION

1

1.1. INTRODUCTION

1.1.1. CLIMATE CHANGE AND THE BIOSPHERE

The biosphere, upon which humanity is inextricably dependent, is an important component of the global carbon cycle and climate system (Le Quéré et al., 2018a & b). The terrestrial biosphere exchanges with the atmosphere about 120 Pg C annually, which is an order of magnitude greater than the amount released through fossil fuel burning (~9.5 Pg C y^{-1}; Schimel et al., 2000). Plants and soils in the terrestrial ecosystems currently absorb the equivalent of ~25% of anthropogenic greenhouse gas emissions (Griscom et al., 2017; Le Quéré et al., 2018a & b), which is partly offset by emissions from land use change (IPCC, 2014; Le Quéré et al., 2018a & b). The land ecosystems and natural climate solutions can provide opportunities for climate change mitigation by enhancing the land sinks combined with reduced emissions (Griscom et al., 2017). Clearly, a mechanistic knowledge of the physiological processes influencing plant, soil and ecosystem functioning is essential for estimating or forecasting the response of the land biosphere to short- and long-term climate variations (Hulme, 2005). To better understand the processes underlying changes in photosynthesis and respiration, measurements of these fluxes across biomes and ecosystems are needed. However, a major limitation in the existing global measurement networks is our ability to measure only the net biosphere-atmosphere fluxes, reflecting the residual of the opposing fluxes of photosynthesis and respiration. Indeed this limitation provided an important motivation for this PhD research.

1.1.2. ECOSYSTEM RESEARCH

The interactions of the global carbon and water cycles have emerged as a critical topic in Earth system science (Ito and Inatomi, 2012; Hartmann et al., 2013) and provided the impetus in the last few decades to establish a large number of research sites worldwide to investigate biosphere-atmosphere interactions. At the core of these measurements are the continuous measurement of CO_2, H_2O and energy fluxes between ecosystems and the atmosphere, using the micrometeorological techniques, in about 600 "flux sites" around the world (Baldocchi et al., 2001). This is often complemented with smaller scale physiological and ecological measurements, as well as with experimental manipulations. A central element of the flux-site studies is to determine the underlying controls over ecosystem functioning, including both the canopy and soil components (Buchmann and Schulze, 1999). Such measurements monitor the variations in the fluxes, but also perform critical eco-physiological studies of the interactions among them to assess the efficiency of process. This include studies related to ecosystem water use efficiency (the ratio of carbon uptake to water loss), carbon use efficiency (the ratio of gross carbon uptake to net ecosystem productivity), or light use efficiency (the ratio of the flux of carbon uptake to that of the solar energy input). Other processes, e.g. soil CO_2 flux (Rs), are studied by manipulations of key parameters, such as water availability (drought or irrigation experiments), or temperature (e.g. soil heating), see e.g., Maseyk et al., 2008a; Grünzweig et al., 2009; Raz-Yaseef et al., 2010.

In practice, relatively few EC flux towers are available with long-term datasets (Campioli et al., 2016; Pilegaard et al., 2011), and those are mostly concentrated in the temperate regions. Almost no such measurements were carried out in the semi-arid

regions, despite their large spatial coverage (~18% of the earth's land surface area, with 35% of global population; Lal, 2004), and their importance to the climate system (Ahlström et al., 2015; Poulter et al., 2014).

Furthermore, despite the low soil organic carbon (SOC) concentrations, total SOC pool in the drylands is 10% of the large world's total of 2352 Pg to 1-meter depth (Carvalhais et al., 2014; Lal et al., 2018). Management of SOC pool in dryland ecosystems can play a major role in reducing the rate of increase in atmospheric CO_2 concentrations because of the vast areas involved and because the dry soil environment enhances long-term carbon storage.

1.1.3. FORESTRY IN THE MEDITERRANEAN, ISRAEL, AND THE PALESTINIAN TERRITORIES

There is a long history of human interaction with forests in the Mediterranean. Wood is still an important economic resource that remains the basic source of energy in many countries and is a desired fuel source in many industrialised countries (Scarascia-Mugnozza et al., 2000). In addition to fuel wood, forests provide a range of traditional products (e.g. food, resins, aromatic plants) and a range of environmental (e.g. soil and slope stabilisation, mitigation of desertification) and social (e.g. recreation and landscape aesthetics) benefits. Reforestation and afforestation programs and forest conservation and sustainable management policies are therefore quite developed and remain important economic and activities in southern Europe and west Asian countries (FAO, 2001).

The dry climate of much of the region is an important factor affecting forest productivity, and one of the important roles of forests is in preventing desertification and protecting watersheds. However, the positive aspects of forestry need to be balanced by considerations for the potential effects on other species and on water resources downstream of forest regions in arid catchments (Maestre et al., 2003; Farley et al., 2005; Jackson et al., 2005).

Following many years of exploitation and degradation of the forest resources, reforestation and afforestation efforts were started in Israel in 1890, by independently operating settlers, and there is now widespread management and afforestation activity in Israel under the administration of the Keren Keyemet L'Israel (KKL; Bonneh, 2000). By 2000, there were 91,000 ha of planted forest in Israel, being nearly 70% of the total forested area (132,000 ha), and in the Palestinian territories, there were 2792 ha (~20% in Tarqumia's Forest-Hebron) of planted forest, being nearly 13% of the total (21,118 ha) forested area (FAO, 2001). The majority of the afforestation has been with Pinus halepensis (Aleppo pine) trees, which is one of ten Pinus species in the Mediterranean Basin (Klaus, 1989). The use of P. halepensis was predominant from the 1930s through the 1970s, but the use of the closely related P. brutia has since increased due to the susceptibility of P. halepensis to the pine bast scale Matsucoccus josephi (Bonneh, 2000). In the arid regions, due to high level of drought tolerance of P. halepensis, it is the species that has been used most extensively in reforestation and afforestation efforts and is therefore one of the most important ecological and economic tree species in the region (Maestre and Cortina, 2004). However, in recent years changes in forest management in Israel has increased the use of other tree species, such as Oak, Pistacia, Ceratonia (carob tree), Olives, and other local species (FAO, 2010).

1

1.1.4. RESEARCH AT THE DRY TIMBERLINE

The only "flux site" in Israel was established in the Yatir Forest in 2000 (Grünzweig et al., 2003), and is the site of the present research. The Yatir forest is part of the long-term forest planting efforts in Israel over the last 100 years; it is the largest and southern-most forest in Israel, and it is likely the driest forest in the global Fluxnet network (Bladocchi, 2001). It is composed predominantly of *Pinus halepensis*, planted mostly between 1964 and 1969.

One of the key results to emerge from the flux measurements at Yatir is the high annual net ecosystem productivity (i.e., annual rate of carbon sequestration), considering the local dry and stressful conditions. Despite the low annual precipitation level of ~290 mm, annual productivity in Yatir between 2000-2006 has been in the range of 200-300 g C m-2 (Maseyk et al., 2008a; Rotenberg and Yakir, 2010), which is similar to that observed in many pine and conifer forests in the temperate and boreal ecosystems (Luyssaert et al., 2007). Such results highlighted the potential of dryland regions for carbon sequestration and for the extension of afforestation beyond the conventional precipitation limits (Grünzweig et al., 2003). At the same time, it was also observed that evapotranspiration (ET), which on global average is ~57% of annual precipitation (Wei et al., 2017), can reach in the dryland ecosystem 95% of annual precipitation (Raz-Yaseef et al., 2010; Stoy et al., 2019), with great impact on local hydrology (Rohatyn et al., 2018). Other effects unique to dry land forest plantations were also identified, such as its effect on surface albedo and surface roughness, in turn, on local atmospheric circulations. Such effects further enhance the interactions of dryland forest ecosystems and the climate (Rotenberg and Yakir, 2010).

Afforestation, and agroforestry is one of the few key strategies available to us for mitigating the effects of climate change, drought and desertification (Bastin et al., 2017, 2019; Le Houérou, 1997). Understanding ecosystem functioning under water limited conditions is, in turn, key for the successful developing these approaches on large scales. Our study site, for which extensive information is available over almost 20 year (e.g., Bar Masada et al., 2006; Grünzweig et al., 2007; Maseyk et al., 2008a; Rotenberg and Yakir, 2010; Gelfand et al., 2012) provided an excellent test bed for the present study that addresses key questions in biosphere-atmosphere in general, and its special characteristics in semi-arid environments.

1.2. OBJECTIVES AND GOALS OF THIS THESIS

The objectives were to quantify the potential productivity and carbon storage of forestry activity in dry regions. We hypothesized first, that low soil CO_2 efflux (Rs) in dry land ecosystems is a key to the observation of high NEE (similar to temperate conditions) and the high carbon use efficiency (CUE; higher than in temperate conditions). And second, that the soil evaporation (Es) is a critical component of the water budget in these ecosystems.

Specifically, the aims of this study were to:

- Partition ecosystem fluxes in order to determine the rates, and quantify dependence on temperature (Ts) and soil moisture (SWC), of the soil-atmosphere CO_2 flux under field conditions in semi-arid Pinus halepensis plantation.

- Test the hypothesis that variations in Rs are driven by temporal (both daily and seasonal) and spatial (distances from trees) differences in the Rs components, autotropic, heterotrophic, and inorganic.

- To use our analysis of the spatiotemporal variations in Rs to improve the up-scaling of Rs from single soil chambers to the whole ecosystem.

- Using our new methodology to estimate soil evaporation, and test the hypothesis that the link of Rs and SWC is driven by variation in Es and, and the ET partitioning to soil evaporation and transpiration.

2

EVIDENCE FOR LARGE CARBON SINK AND LONG RESIDENCE TIME IN SEMI-ARID FORESTS BASED ON 15-YEARS FLUX AND INVENTORY RECORDS

The rate of change in atmospheric CO_2 is significantly affected by the terrestrial carbon sink, but the size and spatial distribution of this sink, and the extent to which it can be enhanced to mitigate climate change are highly uncertain. We combined carbon stock (CS) and eddy covariance (EC) flux measurements that were collected over a period of 15 years (2001–2016) in a 55-year-old 30 km² pine forest growing at the semi-arid timberline (with no irrigation or fertilization). The objective was to constrain estimates of the carbon (C) storage potential in forest plantations in such semi-arid lands, which cover ~18% of the global land area. The forest accumulated 145–160 g C m^{-2} y^{-1} over the study period based on the EC and CS approaches, with a mean value of 152.5 ± 30.1 g C m^{-2} y^{-1} indicating 20% uncertainty in carbon uptake estimates. Current total stocks are estimated at 7943 ± 323 g carbon m^{-2} and 372 g nitrogen m^{-2}. Carbon accumulated mostly in the soil (~71% and 29% for soil and standing biomass carbon, respectively) with long soil carbon turnover time (59 y). Regardless of unexpected disturbances beyond those already observed at the study site, the results support a considerable carbon sink potential in semi-arid soils and forest plantations, and imply that afforestation of even 10% of semi-arid land area under conditions similar to that of the study site, could sequester ~0.4 Pg C y^{-1} over several decades.

Key words: *Carbon sequestration; Semi-arid; Carbon sink; Ecosystem productivity; Soil carbon; Carbon turnover time*

This chapter is published as: Qubaja, R., Grünzweig, J., Rotenberg, E., & Yakir, D. (2019). Evidence for large carbon sink and long residence time in semi-arid forests based on 15-year flux and inventory records. Global Change Biology. doi:10.1111/gcb.14927

2.1. INTRODUCTION

The magnitude of the terrestrial carbon sink over the decade 2007–2016 averaged 3.0 ± 0.8 Pg C y^{-1} (Le Quéré et al., 2018b). Constraining these C sink estimates, its spatial distribution, and the potential to enhance it is critical to support future climate change mitigation actions. Sequestration of atmospheric CO_2 as soil organic matter has recently been promoted (Minasny et al., 2017), but its potential has also been challenged (Amundson and Biardeau, 2018; Schlesinger and Amundson, 2019). Semi-arid lands cover ~18% of the land surface and play a significant role in the trend, magnitude and inter-annual variability of the terrestrial carbon storage (Ahlstöm et al., 2015; Ma et al., 2016; Poulter et al., 2014). The semi-arid ecosystems usually support shrublands, dry savannas or grasslands, with a wide range in productivity and water use (Biederman et al., 2017; Scott et al., 2015; Yan et al., 2019), and are seldom considered as offering significant C sequestration potential (Lal, 2004). Clearly, carbon storage in soils will not provide the solution to global warming, but should be explored together with any other potential means at our disposal (e.g., Pacala and Socolow, 2004).

Detailed measurements of ecosystem C uptake over the last two decades used eddy covariance methodology (EC; Baldocchi et al., 2001) that provided half-hourly based estimates of net ecosystem exchange (NEE) of CO_2 and other scalars (e.g., water vapor and heat). However, uncertainties in this approach persist due to advective flux losses and low turbulence periods (typically at night), sensitivity to variable topography, and the persistent inability to close the surface energy budget (Aubinet et al., 2008, 2012; Finnigan and Belcher, 2004; Thomas et al., 2013). Notably, the EC method provides information on only the net fluxes, while the component fluxes of uptake and emission, which are critical to understanding ecosystem processes, must be estimated indirectly by postprocessing (Lasslop et al., 2010; Reichstein et al., 2005).

Ecosystem-scale accounts of carbon stocks (CS) are commonly estimated in permanent study plots involving tree size parameters and soil organic carbon (SOC), which are converted to CS with allometric equations and soil sample analyses (e.g., Parresol, 1999; West et al., 1997). Nitrogen (N) is considered one of the most significant nutrients limiting primary production and decomposition processes in dry ecosystems (Gebauer and Ehleringer, 2000; Turpin-Jelfs et al., 2019), with important implications for biogeochemical cycles at the global scale (Delgado-Baquerizo et al., 2013; Turpin-Jelfs et al., 2019). Nitrogen stocks (NS) are therefore often assessed together with CS and using the same approach. This stock-based approach has drawbacks; in particular, it is performed on a few replicated individuals or small plots that need to be scaled up. The physical sampling approach can potentially miss important components of the C and N budgets, such as mycorrhizae production, ground flora productivity, or biomass losses, such as to herbivory. The physical sampling approach can also cause disturbances that influence subsequent measurements and cannot be linked to specific events due to non-continuous measurements.

In practice, relatively few EC flux towers are available with long-term datasets, and fewer still carry out simultaneous long-term CS inventories (Campioli et al., 2016; Curtis et al., 2002; Granier et al., 2008; Pilegaard et al., 2011). Obtaining information in the semi-arid regions is important because of the large spatial cover of approximately 0.3 Gha in the Mediterranean regions (Rambal, 2001) and 2.3 Gha globally (~18% of the earth's land surface area; Lal, 2004), and because of their significant effects on the global C cycle (Ahlström et al., 2015; Poulter et al., 2014)

and their C sequestration potential (Lal, 2004; Le Houérou, 1997; Yosef et al., 2018).

Our study was carried out in the semi-arid Yatir pine forest (31°20'49" N; 35°03'07" E), for which extensive information is available from long-term flux measurements, C and N stock inventories, and aerial photography (Bar Massada et al., 2006; Gelfand et al., 2012; Grünzweig et al., 2007; Maseyk et al., 2008; Rotenberg and Yakir, 2010). With 15 years of quantitative data on carbon accumulation at this site, the main objective was to test the idea that dry, semi-arid forest plantations can provide a significant carbon sink as part of our efforts to slow down the increase in atmospheric CO_2. Within this framework, we also sought to estimate the ecosystem's carbon uptake and to assess associated uncertainty by comparing stock-based and flux-based approaches.

2.2. FLUXES, INVENTORY, AND TURNOVER TIME BASICS

Both the EC and CS approaches are applied to estimate net ecosystem productivity, NEP, which can be related to gross primary productivity (GPP) and ecosystem respiration (Re), as follows:

$$GPP = NEP + Re \quad (2.1)$$

where Re is often obtained from nighttime measurements. However, in long-term studies, some caveats must be addressed when assessing the ecosystem C balance since C fluxes other than GPP and Re can be substantial. For example, the effects of ecosystem disturbances (e.g., harvest, forest clearance, fire, grazing) are usually included only when assessing regional-scale net biome productivity (Schulze and Heimann, 1998). The concept introduced by Chapin et al. (2006) includes the combined contributions of disturbances such as harvest, thinning, fire, insect damage, and grazing, and the contribution of non-CO_2 carbon losses, including CO, CH_4, and VOC emissions. For consistency with most recent studies, we use the term NEP (Campioli et al., 2016; Gielen et al., 2013; Luyssaert et al., 2007), recognizing that in our semi-arid system, contributions other than GPP and Re are either negligible (e.g., Seco et al., 2017) or reasonably constrained (for example, by available thinning and mortality records, grazing estimates, limited insect damage, and the absence of fire).

Once the ecosystem C pool and the associated C fluxes are constrained, another critical factor controlling ecosystem C sequestration potential to be considered is the mean C turnover time (τ, years; Carvalhais et al., 2014; Körner, 2017; Luo and Weng, 2011; Wu et al., 2018). It is increasingly recognized that ecosystems are not at steady state with respect to carbon fluxes (e.g. Le Quéré et al., 2018a), and for non-steady-state systems, 'turnover time' (or 'residence time') should be obtained as the ratio of the ecosystem C stock (vegetation and soil; kg m^{-2}) to the rate of the total removal flux (F_{out}, kg m^{-2} y^{-1}; e.g., Rhode, 1992):

$$\tau = C_{stock}/F_{out} \quad (2.2)$$

At the ecosystem scale, F_{out} estimates can be based on Re (Carvalhais et al., 2014; Reichstein et al., 2005; Wu et al., 2018; Yan et al., 2017), which can be further partitioned to its autotrophic and heterotrophic components (Re = Ra+Rh; e.g., Grünzweig et al., 2009; Maseyk et al., 2008; Qubaja et al., 2019b). If C removals can be accounted for (e.g., thinning and mortality records) or

considered negligible (e.g., VOC flux is small), C turnover at the ecosystem (τ_{eco}), tree (τ_{tree}), and soil (τ_{soil}) scales in non-steady-state systems could be estimated by inserting Re, Ra, and Rh, respectively, as F_{out} in Eq. 2.2, recognizing that differences between GPP and Re or between NPP (GPP-Ra) and Rh can be large in non-steady-state systems. For example, previous estimates of the C balance in our study site indicated values of ~830 vs. ~619 g C m^{-2} y^{-1} for GPP vs. Re and 350 vs. 142 g C m^{-2} y^{-1} for NPP vs. Rh values (Grünzweig et al., 2009; Maseyk et al., 2008). Such reduced outflux compared to influx (by 25–60%) reflects the influence of a C sink (Luyssaert et al., 2007, 2010) and underscores the need to account for it in estimating τ.

Finally, we note that the C sequestration potential of an ecosystem ultimately depends on the 'C saturation' level, which may be controlled in crop fields by the soil clay content (e.g., Kemanian and Stöckle, 2010). In turn, the time remaining to reach soil C saturation (T_{sat}, y) can then be estimated from the soil C sequestration potential (C_{seq}; g C m^{-2}) and the sequestration rate during a period of time ($\Delta C_{soil}/t$; g C m^{-2} y^{-1}), neglecting the potential effects of climate change, as follows (West and Six, 2007):

$$T_{sat} = C_{seq}/(\Delta C_{soil}/t) \quad (2.3)$$

For standing biomass, which is a smaller C stock than the soil C stock in semi-arid forests, estimating C saturation and the time remaining to reach the soil C saturation is difficult because of the lack of information on the limit of the amount of biomass accumulation.

2.3. MATERIALS AND METHODS

2.3.1. SITE DESCRIPTION

Yatir Forest is a *Pinus halepensis* Mill. forest established at the edge of the Negev Desert between 1965 and 1969. It covers an area of 3000 ha of undulating terrain (31°20'49" N; 35°03'07" E, at a mean elevation of 650 m a.s.l.) with a mild slope from ~700 to ~600 m a.s.l. across the 6 km length of the forest. In 2004, the tree density was ~300 trees ha^{-1}; tree height (H), ~8.7 ± 0.2 m; diameter at breast height (DBH), ~15.9 ± 0.4 cm; leaf area index (LAI), ~1.5 (with small variations during the study period, associated with variations in precipitation); and plant area index (PAI), ~2.0 (Sprintsin et al., 2007). The trees are neither irrigated nor fertilized, with management limited to thinning to a final density of 300 trees ha^{-1}, and fire prevention. The soil type is a Rendzic Leptosol (Haploxeroll); it is approximately 0.2–1.0 m deep (0.79 ± 0.46 m on average) and has a clay-loam texture (31% sand, 41% silt and 28% clay; bulk density of 1.65 ± 0.14 g cm^{-3}). The soil is underlain by chalk and limestone (FAO classification), and is associated with high fractions of surface rock outcrops (36.8%) and stoniness (48% down to 1.2 m of soil depth; Preisler et al., 2019). The mean annual potential evapotranspiration and precipitation are 1600 mm and 285 mm, respectively, the evapotranspiration (ET) to precipitation (P) ratio is 0.94 (Qubaja et al., 2019a; Raz-Yaseef et al., 2010), with negligible runoff and with inaccessible groundwater table at >300 m depth. Only winter precipitation (December to April) occurs in this region. The mean annual global radiation is 7.5 GJ m^{-2} y^{-1}, and the mean diurnal (24-h) air temperature and relative humidity are 10 °C and 65% in January and 25 °C and 50%

in July, respectively. Further detail on the Yatir research sites can be found in other recent publications and references there in (e.g., Preisler et al., 2019; Maseyk et al., 2019; Tatarinov et al., 2016).

2.3.2. STOCK-BASED APPROACH

The original forest inventory assessment was performed in 2001 (Grünzweig et al., 2007) and was repeated 15 years later (2016) on the same five 30×30 m plots in the central part of the forest (Fig. A2.1). A detailed recent forest inventory included estimates of the following four main components: standing biomass, litter, soil, and removal (mortality, thinning and sanitation).

Standing biomass: Aboveground biomass, including trees and belowground stem-root transition sections, was estimated by applying site-specific allometric equations to measurements of diameter at breast height (DBH; 1.3 m; 107 trees in total) using a metric steel diameter tape and tree height using a clinometer; dry matter contents of individual tree parts were also examined (Grünzweig et al., 2007; see Table A2.4). For the C balance of the predominantly annual herbaceous understory, 3 subplots of 25 m^2 were randomly selected at 3 of the studied plots (Fig. A2.1; plots 1, 4 and 6) during 2002. The understory vegetation within the subplots was harvested at the end of the growing season. Total fresh biomass was weighed, and subsamples were used to determine dry weight and C and N content. However, this vegetation was subjected to a moderate to heavy grazing regime that removed an estimated ~50% of the aboveground understory by the end of the dry period; the understory contribution to the forest carbon was previously assumed to be negligible (Grünzweig et al., 2007). The carbon removal that accumulated over the 15-year study period was nevertheless accounted for in the present C budget analysis, while herbaceous root biomass and grazed biomass replaced by defecation of domestic animals were included in the belowground C stocks as before (Grünzweig et al., 2007).

Thinning and mortality: Carbon removal ($C_{tree\_t,m}$) associated with thinning and mortality in 2011–2012 (following the severe drought events of 2008 and 2009) was estimated based on the following steps: First, the average annual increment in aboveground tree biomass C was estimated for plot 1 where removal during 15-year was minimal (I) with applying our allometric equations. Second, the missing tree C due to tree removal between 2001 and 2012 was estimated from the mean annual tree C increment in the first step (I), the difference in tree numbers in each plot between the 2016 and 2001 surveys (N; no removal was reported between 2013 and 2016), and the mean tree biomass in 2001 (B). The total removed C in each plot was expressed on an area basis rather than on a plot basis as follows:

$$C_{tree\_t,m}=(I*N+B)/A \quad (2.4)$$

where A is the plot size of 900 m2.

Sanitation: The coarse woody debris removed in sanitation campaigns consisted of dead and dying trees. Sanitation estimates were based on local forestry management records (Abed Abulkean, KKL, personal communication), which showed that 360 tons of trees was removed in 2016 from a 75 ha forest area in a typical sanitation campaign. The C and N concentrations of the coarse woody debris were assumed to be similar to

those of the individual living tree parts (Grünzweig et al., 2007).

Litter and soil: The shallow litter layer was sampled in 2016 within a grid of 40×40 cm at 7 subplots from each of the five plots. The litter C and N stocks were presented as part of the soil. The mean annual litter C production (P_l; g C m^{-2} y^{-1}) was derived from 25 litter traps of 0.5 m^2 that were in place in three plots during 2001–2006 (59 ± 2 g C m^{-2} y^{-1}; Maseyk et al., 2008); this mean P_l was assumed to represent the current study period.

Soil was sampled in a 5-cm diameter core in each of the seven litter subplots during 2016 (AMS Multi-Stage Soil Core Sampler, AMS Inc., Idaho, USA). Coring of the mineral soil was carried out at different depths according to the procedure described in Schulze et al. (2000): 0–5, 5–10, 10–20 and 20–50 cm depths in the field. Roots (other than the main stem-to-root transition included in the tree biomass as noted above) were included in C stocks of mineral soils since it was impossible to manually separate myriads of fine root segments from dry soil particles.

In the lab, the soil samples were air-dried, sieved (2 mm) and mixed. The subsamples were dried at 105 °C to determine the moisture content used in the dry mass estimates. The soil texture and pH were determined as in Grünzweig et al. (2007). For the C analyses, each sample was treated separately (5 plots x 7 cores x 4 layers), but for the N analyses, all cores in a plot were combined into one composite sample per plot and depth (5 plots x 4 layers). The 2-mm sieved soil was ground to pass a 250-µm sieve, and concentrations of total C and N were determined in an elemental analyzer (EA 1108, Carlo-Erba, Milan, Italy). The SOC was measured by the EA 1108 following the removal of carbonates by treating ground soil samples with 1N HCl and shaking samples at 180 revolutions min^{-1} for 24 h according to the procedure of Midwood and Boutton (1998). The coarse organic matter (>2 mm) and the fine fraction were combined in estimating the SOC concentration and stocks. C and N stocks were corrected for differences in bulk density by the method of equivalent soil mass (Grünzweig et al., 2004). All area-based values of C and N inventories were corrected for surface rock cover. Clay content was estimated at 36.5% to 41.7% and silt at 17% to 43% across the soil profile (increasing with depth).

Stock-based NEP: The mean annual net ecosystem productivity based on CS (NEP_{CS}) and the annual changes in NS (ΔNS) over the observation period t (15 years) were calculated as follows:

$$NEP_{CS} = (\Delta C_{soil} + \Delta C_{tree} + C_u + C_{tree\_t,m} + C_s)/t \quad (2.5)$$

$$\Delta NS/t = (\Delta N_{soil} + \Delta N_{tree} + N_u + N_{tree\_t,m} + N_s)/t \quad (2.6)$$

where Δ is the difference in soil or tree CS or NS over the observation period. The equations also accounted for C or N removed by grazing (u), mortality and thinning (tree_t, m), and sanitation (s).

2.3.3. FLUX-BASED APPROACH

A micrometeorological tower in the geographical center of the Yatir Forest was constructed in 2000 according to the Euroflux methodology (Aubinet et al., 2000; Grünzweig et al., 2003). The system is instrumented by a 3D sonic anemometer (Gill R-50; Gill Instruments, Lymington, UK), a closed path LI-COR 7000 CO_2/H_2O infrared gas analyzer (IRGA, LI-7000; Li-Cor, Lincoln, NE, USA) to measure evapotranspiration flux (ET) and NEE by EC methodology, and EddyPro 5 software

(Li-Cor, Lincoln, NE, USA). The flux tower's footprint was estimated according to Gockede et al. (2008), indicating that the largest contribution to the flux during the day was from an area 34 m away from the tower and that 95% of the recorded flux originated from an area within 1300 m of the tower, which is well within the forest boundaries. The wind direction was from the northwest to southwest sector during 64% of the day (see more detail in Rotenberg and Yakir, 2010; Tatarinov et al., 2016). EC flux measurements were used to estimate the annual scale NEP_{EC} by integrating half-hour NEE values. The 15-year record was obtained after U* night-time correction, gap filling, and quality control as described in Tatarinov et al. (2016). We used our own site-specific algorithm for flux partitioning into ecosystem respiration (Re) and GPP, which was based on measured nighttime flux values averaged for the first three half-hours of each night as described in Tatarinov et al. (2016) and based on Afik (2009) and Maseyk et al. (2008). Rates of heterotrophic respiration were estimated based on the relationships observed at the site for Rh relative to total respiration fluxes, Re, for the study period 2001–2016 according to Grünzweig et al. (2009) and Maseyk et al. (2008) as: Rh = 0.19*Re (g C m^{-2} y^{-1}); this was recently validated with $\delta^{13}C$ and $\Delta^{14}C$ methods (unpublished data, see Fig. A2.2). Note that estimating uncertainty in flux measurements is difficult (e.g. Loescher et al, 2006), but it is likely better than the generally acceptable ±20%. The most common test of the EC measurements is based on the 'energy closure' assessment (ratio of all other measured energy fluxes to net radiation) and the Yatir site showed an average energy closure of 1.07 ± 0.04 (Rotenberg and Yakir, 2010). The water budget at this dry site, which has no runoff or recharge to depth, showed that ET flux measurements are 0.94 of annual precipitation (Qubaja et al., 2019a; Raz-Yaseef et al., 2010). Simultaneous measurements of NEE of CO_2 and COS indicated an uncertainty of ±15% (Asaf et al., 2013).

2.3.4. CARBON TURNOVER

The mean apparent ecosystem carbon turnover time (τ) was estimated according to Eq. 2.2 (Introduction). Recognizing that our ecosystem is not at a steady-state, we also estimated the apparent τ_{eco} and τ_{soil} based on Re and Rh, respectively, which we obtained as described above.

To fully separate estimates of the C turnover time for the soil and the standing biomass, we subtracted the live-root C from the total soil C stock and added it to the standing biomass. The live-root C was estimated to be 10 ± 2% (mean ± SE, n=5) of the total SOC based on earlier measurements at the site (Grünzweig et al., 2007). The resulting soil, tree and ecosystem CS (C_{soil}, C_{tree} and $C_{eco} = C_{soil}+C_{tree}$) were used to calculate the respective τ values (years).

The soil turnover times were calculated from the 2016 stocks and the following fluxes: Rh for soil (τ_{soil_Rh}), and Ra for standing biomass (τ_{tree_Ra}), and Re for the ecosystem (τ_{eco_Re}). Non-respiratory carbon loss to VOC, which could have influenced our estimates, was recently shown to be a very minor flux (Seco et al., 2017).

2.3.5. STATISTICAL ANALYSES

The paired *t*-test was used to detect significant differences between 2001 and 2016 (identical plots) in C and N concentrations, soil stocks at all depths, tree stock components, and ecosystem stocks. Calculations of the soil C and N stocks was

normalized using soil bulk density and gravel content from the present study, and rock cover (Grünzweig et al., 2007). Statistical analysis of linear regression for the k estimation and Student's *t*-test for analyses of the differences between the two periods were performed using MATLAB software, Version R2017b (MathWorks, Inc., MA, USA).

2.4. RESULTS

2.4.1. CARBON AND NITROGEN STOCKS

Table 2.1 | Breakdown of the carbon (CS) and nitrogen stocks (NS) in Yatir forest as estimated from soil cores and from plant samples using site-specific allometric equations of *P. halepensis* trees (see Methods). Mean (±SE) for n=5 plots (same plots used in both the 2001 and 2016 analyses). The difference (Δ) in the CS and NS between the 2016 and the 2001 study is indicated.

	Carbon stock (g m^{-2})		**Nitrogen stock (g m^{-2})**	
	2016	**ΔCS**	**2016**	**ΔNS**
1. Standing biomass				
Stem	923(148)	108(96)	1.3(0.2)	0.1(0.1)
Branches	742(138)	160(90)	4.2(0.6)	0.8(0.5)
Foliage	164(25)	9(16)	3.1(0.4)	0.1(0.3)
Stem-root transition section	214(32)	0(19)	0.3(0.0)	0.0(0.0)
Total standing biomass	**2043(341)**	**276(220)**	**9.0(1.2)**	**1.1(1.0)**
2. Soil				
Litter layer	88(23)	-37(38)	1.4(0.3)	-1.1(0.7)
0–5 cm	521(85)	-304(127)	58.3(4.0)	-12.4(6.0)
5-10 cm	582(128)	43(121)	46.5(6.9)	-4.2(5.2)
10–20 cm	1150(202)	157(125)	87.5(8.5)	1.4(0.8)
20–50 cm	2562(347)	973(352)	165.5(18.2)	32.7(14.9)
Total soil	**4903(297)**	**831(432)**	**359.2(10.5)**	**16.4(6.6)**
Total ecosystem, current (2016)	**6946(326)**	**1107 (286)**	**368.2(11.4)**	**17.5(6.9)**
3. Removed understory vegetation	**240(48)**	**240(48)**	**0.6(0.0)**	**0.6(0.1)**
4. Removed by thinning	**620(123)**	**620(123)**	**3.0(0.7)**	**3.0(0.7)**
5. Removed by sanitation	**137**	**137**	**0.7**	**0.7**
Total ecosystem(current+removed)	**7943(323)**	**2014(375)**	**372(11)**	**22(7)**

Both carbon and nitrogen accumulated in the Yatir Forest over the observation period (Fig. 2.1) both in the standing biomass and in the soil (Table 2.1). The relative increase in C stock was similar for the above- and belowground pools (~20% increase in both pools), but for N the increase was smaller and was relatively greater in the standing biomass than in the soil (+14% and +5% respectively). Carbon, was mainly stored in the soil (70% vs. 30% and 71% vs. 29% for the soil and standing biomass pools in 2001 and 2016, respectively; Table 2.1, see also Table A2.2). Furthermore, a large part of soil C and N (53% and 46% respectively) was stored in the deeper layers (below 20 cm, Table 2.1). Soil C showed the largest change across the study period (+831 g C m^{-2}; p = 0.07), which translates into a mean annual C accumulation rate of ~57 g C m^{-2}

y^{-1} in the SOC pool (0–50 cm layer, with little or no soil below this depth at the study site). The tree C storage increased by only +276 g C m^{-2} (19 g C m^{-2} y^{-1}). Variations in N storage were relatively small and had positive net trends.

The depth distribution of changes in the C and N stocks indicated a loss of stored SOC in the top layer (0–5 cm) over the study period, while the bottom layer (20–50 cm) gained SOC; no change was observed in the litter layer (Table 2.1). Changes in the N stocks over the study period consisted of an 18% decrease in the top layer, which was compensated by an increase of 25% in the bottom layer. No significant changes were observed in the middle or the litter layers. In the aboveground standing biomass, most of the C was stored in the stems (~45%) and branches (~36%), with small changes over time. Nitrogen was almost exclusively stored in the soil (~98%). The C/N ratio aboveground was >200 compared with ~61 for the litter layer (7% higher than in the 2001 study) and 13.7 belowground (17% higher). The total standing ecosystem C/N ratio increased from 16.6 in 2001 to 18.9 in 2016.

Estimating long-term changes in C and N using the stock approach (Table 2.1) was complicated by a major drought in 2008–2009. The drought was followed by removal of biomass by mortality, thinning, and subsequent sanitation, mainly in 2012. In addition, grazing activities in the periods between stock analyses were estimated to have removed biomass. Combined, the total C removal component from the study plots amounted to 997 g C m^{-2} on average (Table 2.1 and Table A2.2). The biomass removal also included N, but due to the high C/N ratio in the aboveground biomass, the estimated N removal was small (approximately 4 g N m^{-2}).

2.4.2. CARBON STOCK-BASED NET ECOSYSTEM PRODUCTION

The stocks reported above were also used to reconstruct the forest C evolution over the course of the study period, as illustrated in Fig. 2.1. This reconstructing was the basis for our estimated NEP_{CS} values (long-term and annual). The current (2016) mean C stock is 6946 g C m^{-2} compared with 5839 g C m^{-2} estimated for 2001; this difference indicates an addition of 1108 g C m^{-2} on average to the forest ecosystem. Accounting for the C removal (997 g C m^{-2}), the forest captured a total of 2104 g C m^{-2} in the 2001-2016 observation period, which translates into annual NEP_{CS} of 145±26 g C m^{-2} y^{-1}. For N, the current stock is 368 g N m^{-2} vs. 350 g N m^{-2} in 2001, indicating a small increase of 18 g N m^{-2}. Accounting for N removal of 4 g N m^{-2}, during the observation period, the forest captured 22 g N m^{-2}, which translates into a minor ΔNS/t of 1.5±0.5 g N m^{-2} y^{-1}.

2.4.3. EDDY COVARIANCE-BASED APPROACH OF NET ECOSYSTEM PRODUCTION (NEP) AND COMPARISON WITH CARBON STOCK-BASED NEP

The EC-based cumulative net ecosystem CO_2 uptake (NEP_{EC}) during the 15-year observation period was 2317 ± 307 g C m^{-2}, and on average 160 ± 32 g C m^{-2} y^{-1} (Figs. 2.2 and 2.3). Large interannual variations (associated mostly with variations in rainfall; Fig. 2.2) resulted in NEP_{EC} ranging between 33 g C m^{-2} y^{-1} in 2011 and 354 g C m^{-2} y^{-1} in 2005. Postprocessing of NEP_{EC} (see Methods) permitted the estimation of GPP, indicating a total of 8025 g C m^{-2} over the 15-year observation period and, on average, an annual GPP flux of 553 ± 29 g C m^{-2} y^{-1}. In turn, the mean value of ecosystem respiration, Re, was estimated at 394 ± 17 g C m^{-2} y^{-1}; the C-use efficiency, NPP/GPP (CUE), was 0.42 on average. The annual NEP_{EC} and GPP values decreased in the drought years 2009, 2011 and 2013 (Fig. 2.2).

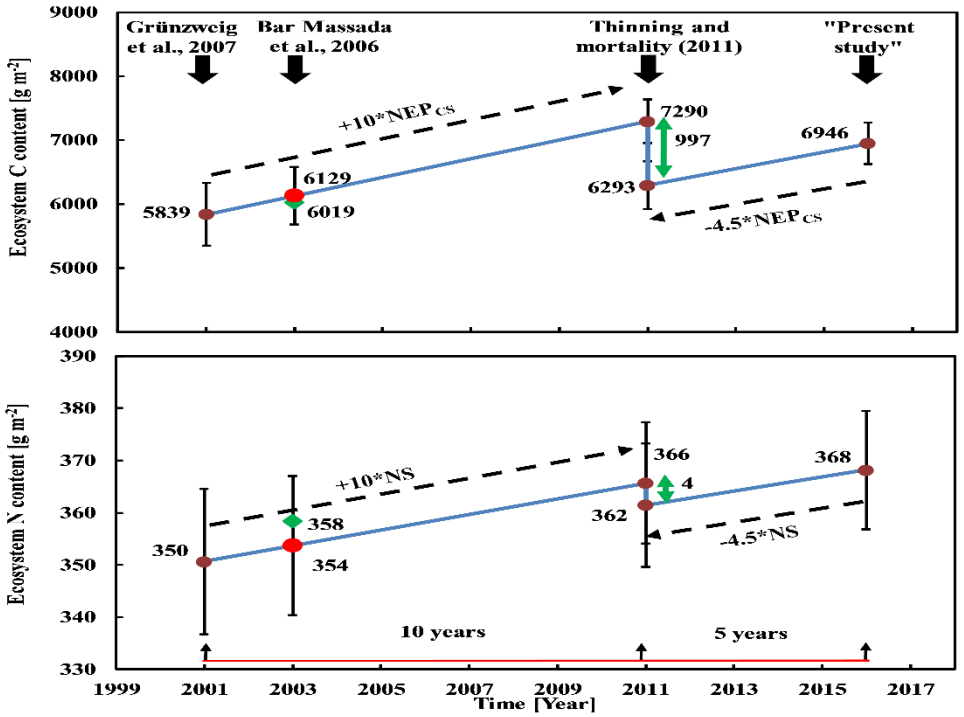

Figure 2.1 | Outline of the carbon and nitrogen evolution in the study site and across the observation period (2001–2016). The ecosystem C and N stocks in 2001 are based on Grünzweig et al., (2007) and the stocks in 2016 are based on the present study. The 2011 C stocks were estimated by either subtracting 4.5 years of mean NEP_{CS} from the 2016 values, or by adding 10 years of mean NEP_{CS} to the 2001 values. The difference between these two points is consistent with our independent C removal estimate (see Table 2.1; the exact agreement). The 2003 stocks are based on standing biomass in 10 plots across the forest by Bar Massada et al. (2006; green square) that was converted to total ecosystem C stocks using site-specific allometric equations, soil C with two-years of change, and two-years of understory as follows ($CS_{2003} = C_{tree\_2003}+[C_{soil\_2001}+2*\Delta C_{soil}]+2*C_u$); the ecosystem C stocks were then compared to the linear extrapolation for the same year (red circle). For the N stocks, the same procedure was applied as for the C stocks. Error bars represent ±SE among plots.

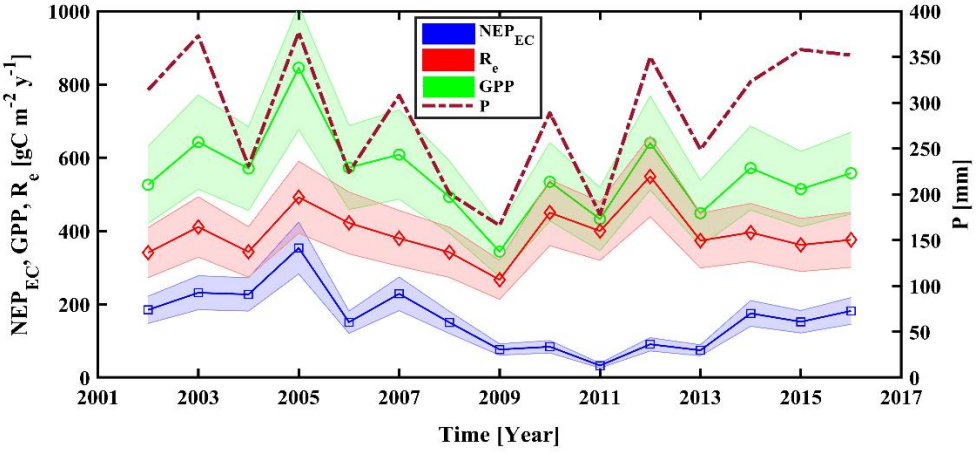

Figure 2.2 | Annual values of net ecosystem productivity estimated by eddy covariance measurements (NEP_{EC}) in the Yatir forest site during the study period of 2001–2016. Annual amounts of precipitation (P) were presented as well. Data points were set to the mid of the hydrological years (e.g. October 2001–September 2002). Fixed standard errors of ±20% are indicated as a guideline, based on the method comparison in this study and common literature values.

The NEP_{CS} values were lower by 9% on average than the NEP_{EC} estimates reported above (Fig. 2.3). However, this difference was within the uncertainties estimated for the two approaches. Moreover, the variations in the NEPs estimated by the two approaches indicated that NEP_{EC} was within the range observed in the inventory plots and that the mean NEP_{CS} value was well within the range of the interannual variations observed in NEP_{EC} (Fig. 2.3). The combined estimate of our long-term NEP estimate based on the two independent approaches is 152.5 ± 30.1 g C m^{-2} y^{-1} (i.e. ±20%; consistent with short term uncertainty assessments; Loescher et al., 2006).

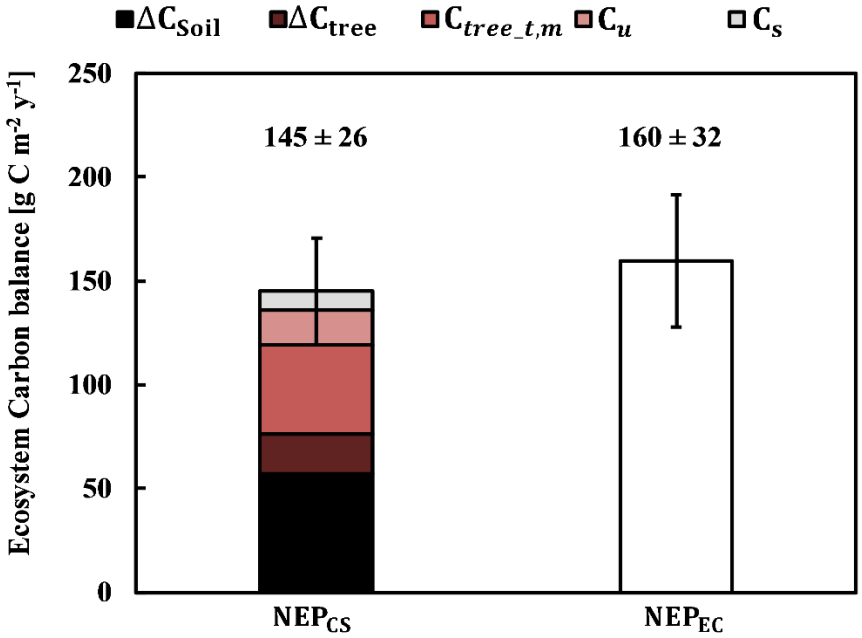

Figure 2.3 | Mean annual values of net ecosystem productivity (NEP) for the 2001–2016 study period based on the carbon stock (CS; 145 ± 26 g C m^{-2} y^{-1}) and eddy covariance (EC; 160 ± 32 g C m^{-2} y^{-1}) approaches. For NEP_{CS}, the different colors represent the contributions of the five components of NEP_{CS} as presented in Eq. 2.5 (from bottom to top): changes in soil organic carbon (ΔC_{soil}; 57 g C m^{-2} y^{-1}) and tree biomass (ΔC_{tree}; 19 g C m^{-2} y^{-1}), thinning and mortality ($C_{tree\_t,m}$; 43 g C m^{-2} y^{-1}), understory (C_u; 17 g C m^{-2} y^{-1}) and sanitation (C_s; 9 g C m^{-2} y^{-1}).

Table 2.2 | Mean carbon stocks (C), rate of accumulation (ΔC), and apparent turnover times, (τ), of the soil (soil), standing biomass (tree) and total ecosystem (eco) based on heterotrophic respiration (Rh), autotrophic respiration (Ra), and ecosystem respiration (Re). Carbon use efficiency, CUE, is indicated as the ratio of annual net primary productivity (NPP) and gross primary productivity (GPP) in %. Values from this study are mean (±SE) of n=5 plots.

Forest	C_{soil} [g m^{-2}]	C_{tree} [g m^{-2}]	C_{eco} [g m^{-2}]	ΔC_{soil} [g m^{-2} y^{-1}]	$\tau_{soil\_R_h}$ [y]	$\tau_{tree\_R_a}$ [y]	$\tau_{eco\_R_e}$ [y]	CUE [%]
Semi-arid[1]	4903	2043	6946	57	59	10	18	42
Europe, mean	15501	10313	25815	20	42	18	27	47
Boreal, global	15374	4749	20123	7	51	8	23	39
Temperate, global	7392	6076	13468	21	18	8	12	46
Tropical, global	7763	13448	21211	11	9	6	7	26

[1] This study. References for all other vegetation types appear in the SI.

2.4.4. CARBON TURNOVER

The simultaneous quantification of fluxes and stocks provided an opportunity to assess the ecosystem C turnover time, ($\tau_{eco\text{-}Re}$; years; Eq. 2.2; Table 2.2) and its two main components, the standing biomass, ($\tau_{tree\text{-}Ra}$), and soil ($\tau_{soil\text{-}Rh}$), which gives additional insights into the C storage capacity. As noted in the introduction, the available respiration fluxes were useful for estimating C turnover times without the need to assume that the ecosystem, which continuously accumulate carbon, is at steady-state (see Table A2.2 for additional turnover time estimates for comparison). As expected, the results show large differences in the carbon turnover time in the standing biomass (6 years) and the soil (59 years), resulting in overall ecosystem carbon turnover time of 18 years. The result also shows that most of the carbon is stored in the soil (71%, Table 2.1) and increasingly with depth (over 50% at the deepest layer; Table 2.1).

2.5. DISCUSSION

2.5.1. FLUX- AND STOCK-BASED NET ECOSYSTEM PRODUCTION

A mean NEP flux of 145 and 160 g C m^{-2} y^{-1} based on the EC and CS approaches confirms earlier estimates for this site (Grünzweig et al., 2003; Maseyk et al., 2008; Rotenberg and Yakir, 2010). The relatively small difference (~10%) between the two independent measures and the long-term perspective provide confidence in the widely used methodologies that yielded an overall mean and combined uncertainty of 152.5 ± 30.1 g C m^{-2} y^{-1} (indicating 20% uncertainty). There was also clear overlap between the spatial variation in NEP_{CS} and the range of interannual NEP_{EC} values, and we did not identify specific factor that could indicate which of the two approaches used here is more accurate. These results provide a relatively rare constraint on the widely used EC methodology on which much of the terrestrial C flux estimates rely, and may reflect its current level of uncertainty in estimating ecosystem NEP (i.e., ±20%; Campioli et al., 2016; Curtis et al., 2002; Gielen et al., 2013; see also short-term uncertainty analyses, such as Loescher et al., 2006). Nevertheless, long-term record of temporal changes in NEP are still rare, as is apparent in the Campioli et al. (2016) study, which identified only six sites (their Table S5) with temporal changes of 3–27 years. The potential for appreciable C uptake in semi-arid forests, such as Yatir, is therefore supported by our estimates of the carbon sink (NEP_{CS}) and the level of confidence in its estimate, when compared to the global mean NEP of ~200 g C m^{-2} y^{-1} (e.g., Luyssaert et al., 2010); and furthermore by considering the apparent high CUE (26–47%), compared to the reported global range of 15–20% (Campioli et al., 2016; Janssens et al., 2001; Luyssaert et al., 2010).

The potential for appreciable C uptake in semi-arid forests, such as Yatir, is therefore supported by our estimates of the carbon sink (NEP) and the level of confidence in its estimate, when compared to the global mean NEP of ~200 g C m^{-2} y^{-1} (e.g., Luyssaert et al., 2010); and furthermore by considering the apparent high CUE (26-47%), compared to the reported global range of 15-20% (Campioli et al., 2016; Janssens et al., 2001; Luyssaert et al., 2010).

Comparison of published data on the C sequestration efficiency with those in the present study provides another demonstration of its high efficiency in the semi-arid soils. Based on the published data from sites identified by Campioli et al., 2016, which provided repeated C inventories of ecosystem and soil, we calculated the ΔC_{soil}/NEP

ratio, where ΔC_{soil} and NEP represent annual mean values of soil and ecosystem C accumulation. Such comparison indicated a mean ΔC_{soil}/NEP value of 7% (in the range of 0-17%; n=7). A ΔC_{soil}/NEP value of 13% is obtained for 12 pine forests sites across Europe with mean soil sequestration of 20 g C m^{-2} yr^{-1} (Schulze et al., 2009) and mean NEP_{EC} of 200 g C m^{-2} yr^{-1} (Rotenberg and Yakir, 2010). The ΔC_{soil}/NEP value in the present study site is markedly higher, at 36% (with ΔC_{soil} of 57 g C m^{-2} and NEP of 160 gC m^{-2}) reflecting high efficiency of sequestration of C into SOC in this environment (Table 2.2). Ultimately, most carbon is sequestered as SOC (>70% of ecosystem C at our site), and the key to efficient C sequestration requires the entire sequence of high CUE, preferential partition of carbon to the soil pool (high ΔC_{soil}/NEP), and its long residence time (τ_{soil}, see below). The results demonstrate that such combination may be best achieved in semi-arid conditions, at least partly represented by the study site.

Comparison of published data on the C sequestration efficiency with those in the present study provides another demonstration of its high efficiency in the semi-arid soils. Based on the published data from sites identified by Campioli et al. (2016), which provided repeated C inventories of ecosystem and soil, we calculated the ΔC_{soil}/NEP ratio, where ΔC_{soil} and NEP represent annual mean values of soil and ecosystem C accumulation. Such a comparison indicated a mean ΔC_{soil}/NEP value of 7% (ranging 0–17%; n=7). A ΔC_{soil}/NEP value of 13% is obtained for 12 pine forests sites across Europe with mean soil sequestration of 20 g C m^{-2} y^{-1} (Schulze et al., 2009) and mean NEP_{EC} of 200 g C m^{-2} y^{-1} (Rotenberg and Yakir, 2010). The ΔC_{soil}/NEP value in the present study site is markedly higher, at 36% (with ΔC_{soil} of 57 g C m^{-2} and NEP of 160 g C m^{-2}), reflecting high efficiency of sequestration of C into SOC in this environment (Table 2.2). Ultimately, most C is sequestered as SOC (>70% of ecosystem C at our site), and the key to efficient C sequestration requires the entire sequence of high CUE, preferential partition of C to the SOC pool (high ΔC_{soil}/NEP), and its long residence time (τ_{soil}, see below). The results demonstrate that such a combination may be best achieved in semi-arid conditions, at least partly represented by the study site.

The high proportion of soil C (71%) is consistent with global model estimates (Carvalhais et al., 2014; Thompson and Randerson, 1999) but is higher than, for example, the 50% in a similarly aged ponderosa pine forest (Law et al., 2001). A high proportion of SOC could be expected in areas with dry conditions, low litter quality and, in turn, low decomposition rates (Gelfand et al., 2012; Hooker and Compton, 2003). The ΔSOC stock of 831 g C m^{-2} during the study period and the mean annual accumulation rate of 57 g C m^{-2} y^{-1} observed in Yatir Forest are within the ranges reported for other ecosystems following afforestation or along chronosequences (e.g., Hooker and Compton, 2003; Jackson et al., 2002; Paul et al., 2003; Post and Kwon, 2000). The relatively high accumulation rate may be related to the low initial background SOC (Grünzweig et al., 2007) and to the young age of the forest, considering that the forest was ≤50 years old and at a stage of near-linear C accumulation rate during the observation period (Fig. 2.1) in comparison to older ecosystems near SOC saturation (Gielen et al., 2013; Jackson et al., 2002; Trettin et al., 1999). Notably, the change in SOC with depth was complex, with a reduction in SOC stock in the top 5 cm but a large increase in the bottom layers.

Field-based measurements of changes in SOC are relatively scarce, especially in dry regions (Conen et al., 2005). Long-term monitoring of SOC at the plot scale throughout Europe showed a large range in both temporal trends and annual fluxes for different land use types (Schrumpf et al., 2011). In most cases, both forests and

grassland showed gains in SOC over time (Schrumpf et al., 2011; Johnson et al., 2007), while croplands showed SOC losses in most cases (Stevens and van Wesemael, 2008; Granier et al., 2008; Bellamy et al., 2005). Reports of differential changes in C storage with depth in dry regions are even more uncommon. Similar to what we have reported here, a decrease in SOC storage in the surface layers and a large increase in SOC storage in deeper layers were also reported for Alpine meadows (Ding et al., 2017). Such depth-dependent changes in SOC storage can be linked to shifts in allocation in root biomass towards deeper soil layers under a changing climate (Ding et al., 2017; Xu et al., 2016). Previous studies have also suggested that the surface soil is more sensitive than deeper horizons to climatic changes, nutrient availability and, in turn, enhanced C-turnover of accelerated decomposition rates (Mathieu et al., 2015; Ding et al., 2017; Gillabel et al., 2010; Schmidt et al., 2011; Garcia-Pausas et al., 2008).

Nitrogen (N) is considered one of the most significant nutrients limiting primary production and decomposition processes in dry ecosystems (Gebauer and Ehleringer, 2000; Turpin-Jelfs et al., 2019), with important implications for biogeochemical cycles at the global scale (Delgado-Baquerizo et al., 2013; Turpin-Jelfs et al., 2019). The small increase in soil N below the surface is consistent with estimates of small external N inputs from the combined contributions of deposition and biological N fixation observed at this site (Gelfand et al., 2012), and with a similar increase noted earlier at the upper level (10-20 cm) by Grünzweig et al., (2007). The changes observed in this study may therefore involve mainly shifting within the soil in the later period. The combination of a significant increase in C storage but negligible changes in N stock seems to be a consequence of the high N-use efficiency (NUE) in the semi-arid forest, which is consistent with the more comprehensive N budget study at our site by Gelfand et al. (2012). These results showed that the large increase in biomass following afforestation did not involve increase in N availability but, instead, increase in C/N ratio. For example, soil C/N ratio increased from 11.8 to 13.7 over the observation period. Overall, the present results showed continuing increase in the ecosystem C/N ratio, with 7% and 15% increase in above- and belowground ratio across the 15 years observation period, respectively. These results indicate increasing NUE, and possibly still marginal N limitation on C sequestration in this system (see also Paul et al., 2003). Carbon cannot accumulate independently of nutrients, in general, and primarily of N. But surprisingly (and perhaps indicative of the pine species studied here), there is no indication that our forest has yet reached that point after ~50 years (the age of the forest). So far, cumulative NEP has been almost linear with time (e.g. Fig. 2.1 and Bar-Massada et al. 2006), which is consistent with the high N remobilization, low litter N, and increasing NUE, as discussed in detail in Gelfand et al. (2012).

2.5.2. CARBON TURNOVER AND C SEQUESTRATION POTENTIAL

As noted above, τ in a non-steady-state, C accumulating system should be evaluated based on the outflux, i.e., R_e, R_a, or R_h. In the study site, the ecosystem is clearly a net C sink, with relatively large R_e (~71% of GPP). Consequently, R_e-based τ_{eco} are moderate (15–20 years; Table 2.2) and within the range reported for a wide range of ecosystems (10–255 years; Carvalhais et al. 2014; Thompson and Randerson 1999; Yan et al. 2017).

As expected, τ_{eco} is a combination of a short τ_{tree} and a much longer τ_{soil}. For τ_{soil}, the more appropriate term would include R_h as the relevant respiration flux, which show a long turnover time of 53–71 years (59 years on average, based on R_h; Table 2.2). These results indicate a relatively stable C sink, as expected in a dry environment

where microbial activity is limited and litter quality is low (Gelfand et al., 2012). The long C turnover time is particularly important for assessing the efficiency of the system for C storage considering that over 70% of the ecosystem C is stored in the soil (Table 2.2). Furthermore, the slow turnover is also consistent with the the large SOC stock in the deeper layers (>50%; Table 2.1). Note that in the present study, SOC was assessed in the top 0.5 m. This depth represents the maximum soil depth across most of the study forest but variations in this depth do exist, and C stored in deeper layers may result in some underestimation of τ_{soil} (Jobbagy and Jackson, 2000; Lal, 2018).

The non-steady-state status of the Yatir Forest, evident in continuous C uptake (Fig. 2.2) and the increased C stock (Table 2.2) clearly suggests that more C can be stored in the system than is currently present. Indeed, a preliminary assessment based on the soil clay content at the study site also indicated that the SOC pool is far from saturation, and, based on the current accumulation rate, could likely continue to accumulate C over the entire lifetime of the forest (See Table A2.3). This is consistent with other estimates of potentially high SOC saturation in 17 different types of desert regions of China (Feng et al., 2002). Clearly, such estimates ignore the effects of age, disturbance and climate change and is probably a poor predictor of the forest life-cycle. However, it does provide an indication that the semi-arid forest is a strong C sink at present, and is likely far from its potential capacity.

Assessing the C sequestration potential of afforestation in hot, semi-arid regions could be important to better assess the global potential for C storage in the land biosphere. Irrespective of other biogeophysical effects and disturbances (e.g. Betts, 2000; Rotenberg and Yakir, 2010), our study site provides robust quantitative data from 55 years old, ~30 km^2 semi-arid forest plantation (non-irrigated, non-fertilized) and likely represents at least some of the vast semi-arid environment. The observations of SOC sequestration are therefore interesting to consider, to a first approximation, in the larger perspective: The results indicate that afforestation of even 10% of the semi-arid lands (~$27*10^6$ km^2 or 18% of the land surface; Lal, 2004) can store ~9 Pg C, with even higher ultimate saturation potential, depending on clay content. While enhancing C storage in soils has been a contentious topic (Minasny et al., 2017; Schlesinger and Amundson, 2019; Amundson and Biardeau, 2018), we note that our study provides a distinct perspective not based on agricultural management or reduced benefits associated with energy-rich investments, supporting the idea that semi-arid afforestation could be important when considering climate mitigation strategies.

A2. APPENDIX

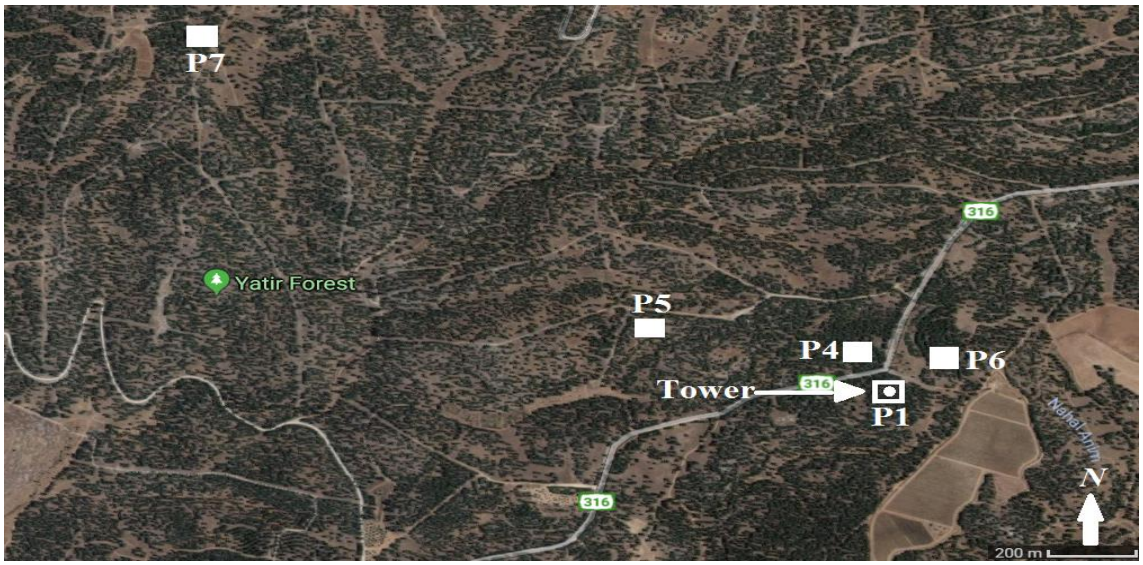

Figure A2.1 | Aerial picture of a section (about 2000 m across, see scale) of the *Pinus halepensis* Yatir forest in Southern Israel, indicating the location of the eddy covariance flux tower and the five sampling plots used in 2001 and re-visited in 2016.

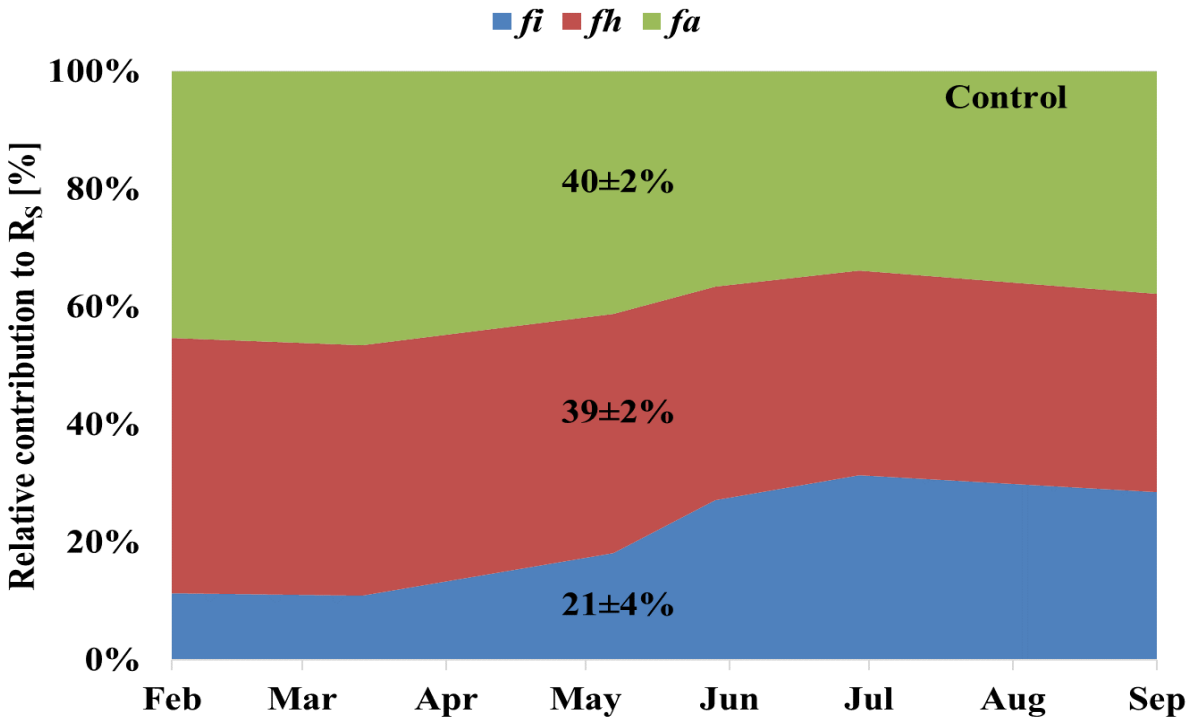

Figure A2.2 | Linear mixing models of $\delta^{13}C$ and $\Delta^{14}C$ in the soil CO_2 flux (R_S) were used to determine the relative contribution of the autotrophic (*fa*), heterotrophic (*fh*) and abiotic (*fi*) components in semi-arid Yatir forest during 8 campaigns (February-September) in 2017, using the soil profile CO_2 method (0, 30, 60, 90, and 120 cm soil depth). These results (Qubaja et al., 2019b) confirmed earlier estimates by Grünzweig et al. (2009) and Maseyk et al. (2008).

Table A2.1 | Annual net ecosystem productivity (NEP), gross primary productivity (GPP), net primary productivity (NPP), ecosystem respiration (R_e) and heterotrophic respiration (R_h) for the study period of 2001–2016 in the Yatir forest based on the carbon accounting (CS) and eddy-covariances (EC) approaches. EC estimates of NEP were partitioned to GPP and R_e based on nighttime values, R_h and NPP estimates are based on previous estimates (Maseyk et al 2008, Grünzweig et al., 2009). For the CS estimates, ratios of GPP/NEP and R_e/NEP identical to the ones obtained by EC were assumed.

	Eddy covariance (EC)				
Time	**NEP**	**GPP**	**Re**	**Rh**	**NPP**
yr			**gC m^{-2} y^{-1}**		
2001-2002	185	526	341	65	249
2002-2003	232	643	411	78	309
2003-2004	227	570	343	65	292
2004-2005	354	845	492	93	447
2005-2006	151	573	422	80	231
2006-2007	229	608	380	72	300
2007-2008	151	493	342	65	215
2008-2009	77	344	267	50	127
2009-2010	84	534	450	85	169
2010-2011	33	433	400	76	108
2011-2012	91	640	549	104	195
2012-2013	75	449	374	71	145
2013-2014	175	572	396	75	250
2014-2015	152	514	362	68	221
2015-2016	182	558	376	71	253
Mean(SE)	**160(32)**	**553(29)**	**394(17)**	**74(3)**	**234(22)**
CS (90% of EC)	**145(26)**	**503(27)**	**358(16)**	**68(3)**	**213(20)**

Table A2.2a | Carbon stocks used for turnover time (τ) calculations in Table 2.2, litter C stocks (C_l), soil (C_{soil}; LL-50 cm soil), standing biomass (C_{tree}), and total ecosystem C stocks for Yatir forest (means ± SE) of 5 plots have been presented.

	Litter layer	**Soil**	**Standing biomass**	**Ecosystem**
	C_l	C_{soil}	C_{tree}	C_{eco}
	[g m^{-2}]	**[g m^{-2}]**	**[g m^{-2}]**	**[g m^{-2}]**
Mean(SE)	**88(23)**	**4422(265)**	**2524(326)**	**6946(326)**

Table A2.2b | Tree characteristics (diameter at breast height, DBH, height, H) in 2016, and the change (Δ) relative to the 2001 survey.

	# trees	**Δtrees**	**DBH**	**ΔDBH**	**H**	**ΔH**
	[#]	**[#]**	**[cm]**	**[%]**	**[m]**	**[%]**
Mean	**21**	**-10**	**20**	**25**	**9**	**0**

Table A2.2c | Comparison of carbon and nitrogen stocks between standing biomass, soil, carbon and nitrogen removed from understory (u), thinning and mortality (tree_t,m) and sanitary (s), change in tree and total ecosystem carbon and nitrogen stocks (**Δ**), and mean annual change in total carbon stocks (NEP_{CS}) and total nitrogen stocks (NS) in Yatir forest for the period between the 2001 and 2016 surveys (15 years).

	Standing biomass		Soil		Removed			Ecosystem	
	C_{tree_2016}	ΔC_{tree}	C_{soil_2016}	ΔC_{soil}	$C_{tree\_t,m}$	C_u	C_s	ΔC_{total}	NEP_{CS}
	[g m^{-2}]		[g m^{-2}]		[g m^{-2}]			[g m^{-2}]	[g m^{-2} y^{-1}]
Mean (SE)	**2043 (341)**	**276 (220)**	**4903 (297)**	**831 (432)**	**620 (123)**	**240 (48)**	**137**	**2104 (375)**	**145 (26)**

	N_{tree_2016}	ΔN_{tree}	N_{soil_2016}	ΔN_{soil}	$N_{tree\_t,m}$	N_u	N_s	ΔN_{total}	NS
	[g m^{-2}]		[g m^{-2}]		[g m^{-2}]			[g m^{-2}]	[g m^{-2} y^{-1}]
Mean (SE)	**9.0 (1.2)**	**1.1 (1.0)**	**359 (10.5)**	**16.4 (6.6)**	**3.0 (0.7)**	**0.60 (0.1)**	**0.7**	**22 (7)**	**1.5 (0.5)**

Table A2.2d | Mean carbon turnover times, (τ, years), calculated as $\tau = C_{stock}/F_{in}$ or $\tau = C_{stock}/F_{out}$. C_{stock} is the carbon stock (g C m^{-2}) in the litter, soil, standing biomass, or total ecosystem. F_{in} is the carbon influx (GPP, NPP, or P_l), F_{out} is the outflux (R_e and R_h; g C m^{-2} y^{-1}). P_l is the annual litter carbon production (g C m^{-2} y^{-1}).

	Litter layer	Soil		Standing biomass			Ecosystem		
	$\tau_{litter\_P_l}$	τ_{soil_NPP}	$\tau_{soil\_R_h}$	τ_{tree_GPP}	τ_{tree_NPP}	$\tau_{tree\_R_e}$	τ_{eco_GPP}	τ_{eco_NPP}	$\tau_{eco\_R_e}$
	[y]	[y]	[y]	[y]	[y]	[y]	[y]	[y]	[y]
Mean(SE)	**1.5(0.4)**	**19(1)**	**59(4)**	**4.6(0.6)**	**11(1)**	**6(1)**	**13(1)**	**30(1)**	**18(1)**
CS(110% of EC)		**21(1)**	**65(4)**	**5.0(0.6)**	**12(2)**	**7(1)**	**14(1)**	**33(2)**	**19(1)**

Table A2.3 | Carbon Saturation: Published algorithms used to estimate the soil C sequestration potentials in different soils. Input parameters from the present study site, including current C content (7.0 g kg^{-1}) and the soil properties, were used to estimate the soil C saturation concentration (C_{sat}) of the local soil profile (0–50 cm), and from it, the relative soil C saturation ($C_{sat\%} = C_{sat}$-7/C_{sat}), the saturation deficit concentration ($C_{satdef} = C_{sat}$-7), and the potential C sequestration stock (C_{seq}; g m^{-2}; eq. SI1). The time to reach C_{sat} (T_{sat}; years) was calculated based on the mean carbon accumulation rate in the study period. x is % particles <20 µm. *See additional notes below.

	Model	r	Size class	C_{sat} [g kg^{-1}]	$C_{sat\%}$ [%]	C_{satdef} [g kg^{-1}]	C_{seq} [g m^{-2}]	T_{sat} [y]
Model[1]	0.375*x+21.1		Clay only	37	19	30	18971	331
Grassland[2]	0.29*x+6.9	0.91	<20 µm	25	28	18	11261	196
Temperate and tropical[3]	0.37*x+4.09	0.80	<20 µm	27	26	20	12607	220
Various soils[4]	0.21*x+14.76	0.26	<20 µm	28	25	21	13109	229
Forest[4]	0.24*x+16.24	0.59	<20 µm	31	23	24	15216	265
Forest[4]	0.63*x-2.51	0.74	<20 µm	36	19	29	18583	324
Various soils[4]	0.41*x+3.86	0.62	<20 µm	29	24	22	14023	245
Semi-arid soils[5]	0.36*x-0.23	0.98	<20 µm	22	32	15	9485	165
Dryland soils[6]	0.24*x+6.9	0.73	<20 µm	22	32	15	9200	160
				29(2)	**25(2)**	**22(2)**	**13606 (1175)**	**237(20)**

[1] Hassink and Whitmore (1997); [2] Hassink et al. (1997); [3] Hassink (1997); [4] Six et al. (2002); [5] Wiesmeier et al. (2015); [6] Gil and Grossman (1979)

*The carbon sequestration potential of an ecosystem ultimately depends on its soil C saturation, C_{sat} (g C kg^{-1} soil), which was suggested to be a function of the soil clay only (*x*, 42% at our site) or clay and silt contents together (62% at our site, based on Klein et al. 2014) (Hassink et al., 1997; Six et al., 2002; Wiesmeier et al., 2015). Several empirical

algorithms have been proposed to estimate the C sequestration potential in different environments (e.g., Kemanian and Stöckle, 2010; Lal, 2004; Stewart et al., 2009). We used various models that are based on soil particle size to compute the C_{sat} for semi-arid ecosystems. Estimates of the clay and silt fraction at our site at the root depth were obtained from Klein et al. (2014). The organic C sequestration potential of a specific soil (C_{seq}, kg C m^{-2}) was calculated according to Wiesmeier et al. (2015) as:

$$C_{seq}=(C_{satdef}/1000)\cdot BD\cdot(1\text{-}RF)\cdot T \quad (A2.1)$$

where BD is the bulk density (1387 kg m^{-3}), RF is the volumetric fraction of rock fragments >2 mm (8.8%), and T is the topsoil thickness (0.5 m on average) (see Sec. 2.2). C_{satdef}, the saturation deficit, is the difference between C_{sat} and the current SOC concentration. Finally, the time remaining to reach C saturation, T_{sat} (years), was estimated as:

$$T_{sat}=C_{seq}/(\Delta C_{soil}/t) \quad (A2.2)$$

where t is the observation period (15 years). To assess the SOC saturation deficit, the current soil C estimated in the present study was subtracted from the estimated soil C saturation (C_{sat}; Table A2.3); this approach was based on published empirical relationships and our site-specific soil analyses (see Methods). In general, the current SOC concentration was approximately 25 ± 2% of C_{sat} (Table A2.3; Mean value). The SOC concentration reflected a SOC saturation deficit between 15 and 30 g kg^{-1} and corresponded to a soil C sequestration potential of 9200–18971 g C m^{-2} (13606 ± 1175) at our semi-arid study site and a total soil C sequestration of 18028 g C m^{-2} (considering the current soil stock) at the T_{sat}. Due to the relatively small fluxes, the additional time required to reach SOC saturation, T_{sat}, is very long (estimated at ~237 ± 20 y). Note that the life-cycle time for the semi-arid forest at Yatir is not known, although it still accumulates C at a nearly constant rate after more than 50 years.

Table A2.4 | A convenience copy of the Allometric equations coefficients for biomass (kg d.m.) of *P. halepensis* trees in Yatir forest from Grünzweig et al., 2007.

	n	Equations form[z]	a	b	r^2
1. Standing biomass					
Total aboveground biomass	28	$a\,(d^2 h)^b$	0.030553	1.031064	0.987
Stem	28	$a\,(d^2 h)^b$	0.039508	0.918943	0.995
Branches, twigs, cones	28	$a\,(d^2 h)^b$	0.001348	1.291356	0.956
Foliage	28	$a\,(d^2 h)^b$	0.031062	0.741424	0.941
Belowground					
Stem-root transition section	5	$a\,(d^2 h)^b$	0.219842	0.539662	0.997
2. Harvested biomass					
Aboveground biomass	28	$a\,d^b$	0.082228	2.540675	0.988
Stem	28	$(a + b\,d)^2$	-0.925181	0.505739	0.990
Branches, twigs, cones	28	$a\,d^b$	0.005591	3.125069	0.961
Foliage	28	$(a + b\,d)^2$	0.333570	0.175186	0.933

[z] ***a*** and ***b*** are regression coefficients, ***d*** is stem diameter at 1.3 m height (cm), ***h*** is tree height (m), n is the number of trees used for the generation of the equation.

3

PARTITIONING OF CANOPY AND SOIL CO_2 FLUXES IN A PINE FOREST AT THE DRY TIMBERLINE ACROSS A 13-YEAR

Partitioning carbon fluxes is key to understanding the process underlying ecosystem response to change. This study used soil and canopy fluxes with stable isotopes (^{13}C) and radiocarbon (^{14}C) measurements in an 18 km^2, 50-year-old dry (287 mm mean annual precipitation; non-irrigated) Pinus halepensis forest plantation in Israel to partition the net ecosystem's CO_2 flux into gross primary productivity (GPP) and ecosystem respiration (Re) and (with the aid of isotopic measurements) soil respiration flux (Rs) into autotrophic (Rsa), heterotrophic (Rh), and inorganic (Ri) components. On an annual scale, GPP and Re measured 655 and 488 g C m^{-2}, respectively, with a net primary productivity (NPP) of 282 g C m^{-2} and carbon-use efficiency (CUE=NPP/GPP) of 0.43. Rs made up 60% of the Re and comprised 24 ± 4%, 23 ± 4%, and 13 ± 1% from Rsa, Rh, and Ri, respectively. The contribution of root and microbial respiration to Re increased during high productivity periods, and inorganic sources were more significant components when the soil water content was low. Comparing the ratio of the respiration components to Re of our mean 2016 values to those of 2003 (mean for 2001–2006) at the same site indicated a decrease in the autotrophic components (roots, foliage, and wood) by about -13%, and an increase in the heterotrophic component (Rh/Re) by about +18%, with similar trends for soil respiration (Rsa/Rs decreasing by -19% and Rh/Rs increasing by +8%, respectively). The soil respiration sensitivity to temperature (Q_{10}) decreased across the same observation period by 36% and 9% in the wet and dry periods, respectively. Low rates of soil carbon loss combined with relatively high belowground carbon allocation (i.e., 38% of canopy CO_2 uptake) and low sensitivity to temperature help explain the high soil organic carbon accumulation and the relatively high ecosystem CUE of the dry forest.

Key words: *Carbon balance; Soil respiration; Autotrophic; Heterotrophic; Inorganic flux; Temperature response; Semi-arid ecosystem; Pine forest; Canopy cover; Soil chamber*

This chapter is published as: Qubaja, R., Tatarinov, F., Rotenberg, E., & Yakir, D.: Partitioning of canopy and soil CO_2 fluxes in a pine forest at the dry timberline across a 13-year observation period, Biogeosciences. doi:10.5194/bg-2019-291.

3.1. ITRODUCTION

The annual net storage of carbon in the land biosphere, known as net ecosystem production (NEP), is the balance between carbon uptake during gross primary productivity (GPP) and carbon loss during growth, maintenance respiration by plants (i.e., autotrophic respiration, Ra), and decomposition of litter and soil organic matter (i.e., heterotrophic respiration, Rh; Bonan, 2008). The difference between GPP and Ra expresses the net primary production (NPP) and is the net carbon uptake by plants that can be used for new biomass production. Measurements from a range of ecosystems have shown that total plant respiration can be as large as 50% of GPP (e.g., Etzold et al., 2011) and together with Rh comprises total ecosystem respiration (Re, Re=Ra+Rh). The partitioning of the ecosystem carbon fluxes can therefore be summarized as:

$$GPP = NPP + Ra = NEP + Rh + Ra \quad (3.1)$$

Earlier campaign-based measurements carried out by Maseyk et al. (2008a) and Grünzweig et al. (2009) in the semi-arid *Pinus halepensis* (Aleppo pine) Yatir forest indicated that GPP at this site was lower than among temperate coniferous forests (1,000–1,900 g C m^{-2} y^{-1}) but within the range estimated for Mediterranean evergreen needle-leaf and boreal coniferous forests (Falge et al., 2002; Flechard et al., 2019b), and had a high carbon-use efficiency of 0.4 (CUE = NPP/GPP; DeLucia et al., 2007). The total flux of CO_2 released from the ecosystem (Re) can be partitioned into aboveground autotrophic respiration (i.e., foliage and sapwood, Rf) and soil CO_2 flux (Rs). Rs, in turn, is a combination of three principal components and can be further partitioned into the components originating from roots or rhizospheres and mycorrhizas (i.e., belowground autotrophic, Rsa), from carbon respired during the decomposition of dead organic matter by soil microorganisms and macrofaunal (heterotrophic respiration, Rh; Bahn et al., 2010; Kuzyakov, 2006), and pedogenic or anthropogenic acidification of soils containing $CaCO_3$ (Ri; Joseph et al., 2019; Kuzyakov, 2006), which is expressed as:

$$Re = Rs + Rf = [Rsa + Rh + Ri] + Rf \quad (3.2)$$

Previously published results show that the contribution of Rsa and Rh to Rs ranges from 24 to 65% and from 29 to 74%, respectively, in forest soils in different biomes and ecosystems (Binkley et al., 2006; Chen et al., 2010; Flechard et al., 2019a; Frey et al., 2006; Hogberg et al., 2009; Subke et al., 2011). Some studies reported significant proportions of abiotic contribution to Rs, ranging between 10 and 60% (Martí-Roura et al., 2019; Ramnarine et al., 2012; Joseph et al., 2019). However, most of these experiments were performed in boreal, temperate, or subtropical forests, and there is a general lack of information on water-limited environments, such as dry Mediterranean ecosystems. Using both ^{13}C and CO_2/O_2 ratios also showed that abiotic processes, such as CO_2 storage, transport, and interactions with sediments, can influence Rs measurements at such sites (Angert et al., 2015; Carmi et al., 2013). Furthermore, root-respired CO_2 can also be dissolved in the xylem water and carried upward with the transpiration stream (Etzold et al., 2013).

Rates of the soil-atmosphere CO_2 flux (Rs) have been altered owing to global climatic change, particularly through changes in soil temperature (Ts) and soil

moisture (SWC; Bond-Lamberty and Thomson, 2010; Buchmann, 2000; Carvalhais et al., 2014; Hagedorn et al., 2016; Zhou et al., 2009), which could account for 65–92% of the variability of Rs in a mixed deciduous forest (Peterjohn et al., 1994). Soil moisture impacts on Rs have been observed in arid and Mediterranean ecosystems, where Ts and SWC are negatively correlated (e.g., Grünzweig et al., 2009). CO_2 efflux generally increases with increasing soil temperatures (Frank et al., 2002), which can produce positive feedback on climate warming (Conant et al., 1998), converting the biosphere from a net carbon sink to a carbon source (IPCC-AR5 2014). A range of empirical models have been developed to relate Rs rate and temperature (Balogh et al., 2011; Lellei-Kovács et al., 2011), and the most widely used models rely on the Q_{10} approach (Bond-Lamberty and Thomson, 2010), which quantifies the sensitivity of Rs to temperature and can integrate it with physical processes, such as the rate of O_2 diffusion into and CO_2 diffusion out of soils and the intrinsic temperature dependency of enzymatic processes (Davidson and Janssens, 2006). Soil moisture (SWC) may be of greater importance than temperature in influencing Rs in water-limited ecosystems (Hagedorn et al., 2016; Grünzweig et al., 2009; Shen et al., 2008). In general, the Rs rate increases with the increase of SWC at low levels but decreases at high levels of SWC (Deng et al., 2012; Hui and Luo, 2004; Jiang et al., 2013). Several studies highlight the sensitivity of carbon fluxes in semi-arid Mediterranean ecosystems to the irregular seasonal and interannual distribution of rain events (Poulter et al., 2014; Ross et al., 2012). While Rs is generally constrained by low SWC during summer months, abrupt and large soil CO_2 pulses have been observed after rewetting the dry soil (Matteucci et al., 2015).

The objectives were twofold. First, to obtain detail on partitioning of the carbon fluxes in a semi-arid pine forest to help explain the high productivity and carbon use efficiency recently reported for this ecosystem (Qubaja et al., in press), and provide process-based information to assess the carbon sequestration potential of such a semi-arid afforestation system. Second, to combine this 2016 study with the results of a similar one at the same site in 2003 (mean values for 2001–2006; Grünzweig et al., 2007, 2009) to obtain a long-term perspective across 13 years on soil respiration and its partitioning. We hypothesized that the high carbon use efficiency of the dry forest ecosystem is associated with high belowground carbon allocation and relatively low decomposition rates, and that the long-term trend associated with warming may be suppressed by the dry conditions.

3.2. MATERIALS AND METHODS

3.2.1. SITE DESCRIPTION

The Yatir forest (31°20'49" N; 35°03'07" E, 650 m a.s.l.) is situated in the transition zone between sub-humid and arid Mediterranean climates (Fig. A3.1) on the edge of the Hebron mountain ridge. The ecosystem is a semi-arid pine afforestation established in the 1960s and covering approximately 18 km^2. The average air temperatures for January and July are 10.0 ºC and 25.8 ºC, respectively. Mean annual potential evapotranspiration (ET) is 1,600 mm, and mean annual precipitation is 287 mm. Only winter (December to March) precipitation occurs in this region, creating a distinctive wet season, while summer (June to October) is an extended dry season. There are short transition periods between seasons, with a wetting season (i.e., autumn) and a drying season (i.e., spring). The forest is dominated by Aleppo pine (*Pinus halepensis* Mill.), with smaller proportions of other pine species and cypress and little understory

vegetation. Tree density in 2007 was 300 trees ha^{-1}; mean tree height was 10.0 m; diameter at breast height (DBH) was ~15.9 cm; and the leaf area index (LAI) was ~1.5. The native background vegetation was sparse shrubland, which is dominated by the dwarf shrub *Sarcopoterium spinosum* (L.) Spach, with patches of herbaceous annuals and perennials reaching a total vegetation height of 0.30–0.50 m (Grünzweig et al., 2003, 2007). The root density range is 30–80 roots m^{-2} at the upper 0.1 m soil depth, falling to the minimum value (~0 roots m^{-2}) at 0.7 m soil depth (Preisler et al., 2019). Biological soil crust (BSC) is evident in the forest but is less than in the surrounding shrub by ~40% (Gelfand et al., 2012).

The soil at the research site is shallow (20–40 cm), reaching only 0.7–1.0 m; the stoniness fraction for the soil depth (0–1.2 m) is 15–60%, and the rock cover of the surface ranges between 9 and 37%, as recently described in detail (Preisler et al., 2019); the soil is eolian-origin loess with a clay-loam texture (31% sand, 41% silt, and 28% clay; density: 1.65 ± 0.14 g cm^{-3}) overlying chalk and limestone bedrock. Deeper soils (up to 1.5 m) are sporadically located at topographic hollows. While the natural rocky hill slopes in the region are known to create flash floods, the forested plantation reduces runoff dramatically to less than 5% of annual rainfall (Shachnovich et al., 2008). Groundwater is deep (>300 m), reducing the possibility of groundwater recharge due to negative hydraulic conductivity or of water uptake by trees from the groundwater.

3.2.2. FLUX AND METEOROLOGICAL MEASUREMENTS

An instrumented eddy covariance tower was erected in the geographical center of Yatir forest, following the EUROFLUX methodology (Aubinet et al., 2000). The system uses a three-dimensional (3D) sonic anemometer (Omnidirectional R3, Gill Instruments, Lymington, UK) and a closed path LI-COR 7000 CO_2/H_2O gas analyzer (LI-COR Inc., Lincoln, NE, USA) to measure the evapotranspiration flux (ET) and net CO_2 flux (NEE). EC flux measurements were used to estimate the annual scale of NEP by integrating half-hour NEE values. The long-term operation of our EC measurement site (since 2000; see Rotenberg and Yakir, 2010) provides continuous flux and meteorological data with about 80% coverage, which are subjected to U* night-time correction and quality control, and gap filling is based on the extent of the missing data, as recently described in more detail in Tatarinov et al. (2016). A site-specific algorithm was used for flux partitioning into Re and GPP. Daytime ecosystem respiration (Re-d, in µmol m^{-2} s^{-1}) was estimated based on measured night-time values (Re-n; i.e., when the global radiation was <5 W m^{-2}), averaged for the first three half-hours of each night. The daytime respiration for each half-hour was calculated according to Eq. 3.3 (Maseyk et al., 2008a; Tatarinov et al., 2016):

$$R_{e-d} = R_{e-n}(\alpha_1\beta_s^{dT_s} + \alpha_2\beta_w^{dT_a} + \alpha_3\beta_f^{dT_a}) \quad (3.3)$$

where βs, βw, and βf are coefficients that correspond to soil, wood, and foliage, respectively; dTs and dTa are soil and air temperature deviations from the values at the beginning of the night; and α1, α2, and α3 are partitioning coefficients fixed at 0.5, 0.1, and 0.4, respectively. The βs, βw, and βf coefficients were calculated as follows: βs values were based on Q_{10} from the Grünzweig et al. (2009) study at the same site; where βs = 2.45 for wet soil (i.e., SWC in the upper 30 cm above 20% vol); βs = 1.18 for dry soil (i.e., SWC in the upper 30 cm equal to or below 20% vol); βf = 3.15–0.036

Ta; and βw = 1.34+0.46 exp (-0.5((DoY–162)/66.1)^2), where DoY is the day of the hydrological year starting from 1 October. Finally, GPP was calculated as GPP =NEE–Re. Negative values of the NEE and GPP indicated that the ecosystem was a CO_2 sink.

Half-hour auxiliary measurements used in this study included photosynthetic activity radiation (PAR mol m^{-2} s^{-1}), vapor pressure deficit (VPD, kPa), wind speed (m s^{-1}), and relative humidity (RH, %), with additional measurements as described elsewhere (Tatarinov et al., 2016). Furthermore, the soil microclimatology half-hour measurements were measured and calculated with soil chamber measurements, using the LI-8150-203 (LI-COR, Lincoln, NE), as described below, namely air temperature (Ta, °C) and relative humidity (RH, %) at 20 cm above the soil surface and soil temperature (Ts, °C) at a 5 cm soil depth using a soil temperature probe, as well as volumetric soil water content (SWC_{0-10}, m^3 m^{-3}) in the upper 10 cm of the soil near the chambers, using the ThetaProbe model ML2x (Delta-T Devices Ltd., Cambridge, UK), which was calibrated to the soil composition based on the manufacturer's equations.

3.2.3. SOIL CO_2 FLUX

Soil CO_2 fluxes (Rs) were measured with automated non-steady-state systems, using 20 cm diameter opaque chambers and a multiplexer to allow for simultaneous control of several chambers (LI -8150, -8100-101, -8100-104; LI-COR, Lincoln, NE). The precision of CO_2 measurements in the chambers' air is ±1.5% of the measurements' range (0–20,000 ppm). The chambers were closed on preinstalled PVC collars 20 cm diameter, allowing for short measurement time (i.e., 2 min), and positioned away from the collars for the rest of the time. Data were collected using a system in which air from the chambers was circulated (2.5 l min^{-1}) through an infrared gas analyzer (IRGA) to record CO_2 (µmol CO_2/mol air) and H_2O (mmol H_2O/mol air) concentrations in the system logger (1 s^{-1}). Gap filling of missing data due to technical problems (i.e., 27 % of the data across the study period between November 2015 and October 2016) was based on the average diurnal cycle of each month.

The rates of soil CO_2 flux, Rs (µmol CO_2 m^{-2} s^{-1}), were calculated from chamber data using a linear fit of change in water-corrected CO_2 mole fraction using Eq. 3.4 (LiCor Manual, 2015) as follows:

$$R_s = \frac{dC}{dt} \cdot \frac{v\,P}{s\,T_a R} \quad . \tag{3.4}$$

where dC/dt is the rate of change in the water-corrected CO_2 mole fraction (µmol CO_2 mol^{-1} air s^{-1}), v is the system volume (m^3), P is the chamber pressure (Pa), s is the soil surface area within the collar (m^2), Ta is the chamber air temperature (K), and R is the gas constant (J mol^{-1} K^{-1}). A measurement period of 2 minutes was used, based on preliminary tests to obtain the most linear increase of CO_2 in the chambers with the highest R^2.

Soil CO_2 fluxes in the experimental plot were measured between November 2015 and October 2016 by means of three measurement chambers using 21 collars grouped in seven sites in the forest stand, with three locations (i.e., three collars) per site, based on different distances from the nearest tree (Dt). The collars were inserted 5 cm into the soil. Data were recorded on a half-hour basis (48 daily records). The three chambers were rotated between the seven sites every 1–2 weeks to cover all sites and to assess spatial and temporal variations.

Upscaling of the collar measurements to plot-scale soil CO_2 flux was carried out by grouping collars based on three locations (i.e., under trees [<1 m from nearest tree; UT], in gaps between trees [1–2.3 m; BT], and in open areas [>2.3 m; OA]), with one chamber taking measurements at each location, and estimating the fractional areas (Ø) of the three locations based on mapping the sites according to the distances noted above, as previously done by Raz-Yaseef et al. (2010):

$$Rs = Rs_{OA} * Ø_{OA} + Rs_{BT} * Ø_{BT} + Rs_{UT} * Ø_{UT} \quad (3.5)$$

$$Ø_{OA} + Ø_{BT} + Ø_{UT} = 1 \quad (3.6)$$

The annual scale of Rs was derived from the upscaled chamber measurements (Eq. 3.5) based on daily records (48 half-hourly values) of spatial upscaled Rs.

Estimating the temperature sensitivity of Rs (Q_{10}) was performed as described by Davidson and Janssens (2006) using a first-order exponential equation (see also Xu et al., 2015).

$$Rs = ae^{bTs}, \quad (3.7)$$

where Rs represents the half-hour spatial upscaled time series of soil respiration flux (μmol m^{-2} s^{-1}), Ts (°C) is soil temperature at a 5 cm depth (upscaled spatially and temporally using the same method as for Rs), and a and b are fitted parameters. The b values were used to calculate the Q_{10} value according to the following equation:

$$Q_{10} = e^{10b}. \quad (3.8)$$

3.2.4. SOIL CO_2 FLUX PARTITIONING

Determination of different sources of soil CO_2 efflux was based on linear mixing models (Lin et al., 1999) to estimate proportions for three main sources (autotrophic, heterotrophic, and abiotic), using isotopic analysis of soil CO_2 profiles and soil incubation data from eight campaigns (January to September) during 2016, according to Equations 3.9–3.11. Partitioning of the monthly Rs values into components was done using a 3-endmember triangular model for interpreting the $\delta^{13}C$ and $\Delta^{14}C$ values of CO_2 flux; the 3-endmember triangular corners are the autotrophic (Rsa), heterotrophic (Rh), and abiotic (Ri) sources of Rs. The $\delta^{13}C$ and $\Delta^{14}C$ isotope signatures of monthly Rs locate it inside the triangle (Fig. A3.2):

$$\delta^{13}C_{Rs} = f_{sa} * \delta^{13}C_{sa} + f_h * \delta^{13}C_h + f_i * \delta^{13}C_i \quad (3.9)$$

$$\Delta^{14}C_{Rs} = f_{sa} * \Delta^{14}C_{sa} + f_h * \Delta^{14}C_h + f_i * \Delta^{14}C_i \quad (3.10)$$

$$1 = f_{sa} + f_h + f_i \quad (3.11)$$

where f indicates the fraction of total soil flux (e.g., $f_h=R_h/R_s$), while subscripts sa, h, and i indicate autotrophic, heterotrophic, and inorganic components, respectively. The three-equations system was used to solve the three unknown f fractions of the total soil flux based on empirical estimates of the isotopic endmembers. Additionally, $\delta^{13}C$ and $\Delta^{14}C$ are the stable and radioactive carbon isotopic ratios, where $\delta^{13}C$ =

$[([^{13}C/^{12}C]_{sample}/[^{13}C/^{12}C]_{reference})-1]*1000‰$ and the reference is the Vienna international standard (VPDB). Radiocarbon data are expressed as $\Delta^{14}C$ in parts per thousand or per mil (‰), which is the deviation of a sample $^{14}C/^{12}C$ ratio relative to the OxI standard in 1950 (see Taylor et al., 2015), that is, $\Delta^{14}C = [([^{14}C/^{12}C]_{sample}/(0.95*[^{14}C/^{12}C]_{reference}*\exp[(y-1950)/8267]))-1]*1000‰$, where y is the year of sample measurements.

The $\delta^{13}C_{Rs}$ was estimated monthly using the Keeling plot approach (Figs A3.3 and A3.4; Pataki et al., 2003; Taneva and Gonzalez-Meler, 2011). Soil air was sampled using closed-end stainless steel tubes (6 mm diameter) perforated near the tube bottom at four depths (30, 60, 90, and 120 cm). Samples of soil air were collected in pre-evacuated 150 mL glass flasks with high-vacuum valves, the dead volume in the tubing and flask necks having been purged with soil air using a plastic syringe equipped with a three-way valve.

Note that the Keeling plot approach is based on the 2-endmembers mixing model (see Review of Pataki et al., 2003), which often does not hold in soils because of variations in the $\delta^{13}C$ values of source material with depth (see a recent example in Joseph et al., 2019). However, probably because of the very dry conditions at our study site, no change in $\delta^{13}C$ with depth in the root zone is observed (±0.1‰ across the 35 cm depth profiles; Fig. A3.5), providing an opportunity to avoid this caveat. The soil CO_2 samplings carried out therefore represented predominantly the mixing of atmospheric CO_2 with a single integrated soil source signal, consistent with the Keeling plot approach.

The autotrophic ($\delta^{13}C_{sa}$) endmember was estimated based on incubations during the sampling periods of excised roots, following Carbone et al. (2008). Fine roots (<2 mm diameter) were collected, rinsed with deionized water, and incubated for 3 hours in 10 mL glass flasks connected with Swagelok Ultra-Torr tee fittings to 330 mL glass flasks equipped with Louwers high-vacuum-valves. The flasks were flushed with CO_2-free air at room temperature close to field conditions. The CO_2 was allowed to accumulate to at least 2,000 ppm (~2 h).

The heterotrophic ($\delta^{13}C_h$) endmember was estimated as in Taylor et al. (2015), and, similar to the root-incubation experiment, soil samples from the top 5 cm of the litter layer or 10 cm below the soil surface were collected, and roots were carefully removed to isolate heterotrophic components. Root-free soils were placed in 10 mL glass flasks and allowed to incubate for 24 hours before being transferred to evacuated 330 mL glass flasks. The inorganic source ($\delta^{13}C_i$) endmember was estimated using one gram of dry soil (ground to pass through a 0.5 mm mesh) placed in a 10 mL tube with a septum cap; then, 12 mL of 1M HCl was added to dissolve the carbonate fraction, and the fumigated CO_2 withdrawn from each tube was collected using a 10 mL syringe and injected into a 330 mL evacuated flask for isotopic analysis.

Radiocarbon estimates were based on the work of Carmi et al. (2013) at the same site, adjusted to the measured atmospheric ^{14}C values during the study period (49.5‰; Carmi et al., 2013). The $\Delta^{14}C_{sa}$ and $\Delta^{14}C_h$ endmembers were estimated based on the assumption that they carry the ^{14}C signatures of 4 and 8.5 years, respectively, older than the ^{14}C signature of the atmosphere at the time of sampling, based on mean ages previously estimated (Graven et al., 2012; Levin et al., 2010; Taylor et al., 2015). $\Delta^{14}C_i$ was obtained from Carmi et al. (2013). Monthly values of $\Delta^{14}C_{Rs}$ were obtained using the linear equation of the regression line of the measured $\delta^{13}C$ values of Rsa, Rsh, and Ri and the corresponding estimated $\Delta^{14}C$ values (Fig. A3.2) and monthly $\delta^{13}C$ values of Rs.

3.2.5. ISOTOPIC ANALYSIS

Isotopic analysis followed the methodology described in Hemming et al. (2005). The $\delta^{13}C$ of CO_2 in the air was analyzed using a continuous flow mass spectrometer connected to a 15-flask automatic manifold system. An aliquot of 1.5 mL of air was expanded from each flask into a sampling loop on a 15-position valve (Valco Houston, TX, USA). CO_2 was cryogenically trapped from the air samples using helium as a carrier gas; it was then separated from N_2O with a Carbosieve G (Sigma Aldrich) packed column at 70°C and analyzed on a Europa 20-20 Isotope Ratio Mass Spectrometer (Crewe, UK). $\delta^{13}C$ results were quoted in parts per thousand (‰) relative to the VPDB international standard. The analytical precision was 0.1%. To measure [CO_2], an additional 40.0 mL subsample of air from each flask was expanded into mechanical bellows and then passed through an infrared gas analyzer (LICOR 6262; Lincoln, NE, USA) in an automated system. The precision of these measurements was 0.1 ppm. Flasks filled with calibrated standard air were measured with each batch of 10 sample flasks; five standards were measured per 10 samples for $\delta^{13}C$ analyses and four standards per 10 samples for [CO_2] analyses.

Organic matter samples were dried at 60°C and milled using a Wiley Mill fitted with size 40 mesh, and soil samples were ground in a pestle and mortar. Soils containing carbonates were treated with 1M hydrochloric acid. Between 0.2 and 0.4 mg of each dry sample was weighed into tin capsules (Elemental Microanalysis Ltd., Okehampton, UK), and the $\delta^{13}C$ of each was determined using an elemental analyzer linked to a Micromass Optima IRMS (Manchester, UK). Three replicates of each sample were analyzed, and two samples of a laboratory working standard cellulose were measured for every 12 samples. Four samples of the acetanilide (Elemental Microanalysis Ltd.) international standard were used to calibrate each run, and a correction was applied to account for the influence of a blank cup. The precision was 0.1%.

3.2.6. TOTAL BELOWGROUND CARBON ALLOCATION (TBCA)

TBCA (g C m^{-2} y^{-1}) was calculated following Giardina and Ryan (2002) for the study year (November 2015–October 2016) as follows:

$$TBCA = Rs - Rl + \Delta C_{soil}\ , \qquad (3.12)$$

where R_l is the annual aboveground litter production between November 2014 and October 2015, and ΔC_{soil} is the annual change in belowground total soil organic C. Litter production, not measured during the present study, was estimated based on values obtained by Masyk et al. (2008b) for 2000–2006 (56 g C m^{-2} y^{-1}) and assumed to have increased in the study period (2014–2015) proportionally to the measured increase in leaf area index (LAI; 1.31 to 1.9; i.e., R_l = [(1.9*56)/1.31] = 83 g C m^{-2} y^{-1}). For herbaceous litter production, three plots of 25 m^2 were randomly selected in 2002 and harvested at the end of the growing season, total fresh biomass was weighed, and subsamples were used to determine dry weight and C content. Grünzweig et al. (2007) found that herbaceous litter production was close to the average rainfall for the specific year; this method was adapted in the current study for the period between November 2014 and October 2015. Since aboveground litter (Rl; the sum of tree litter and herbaceous litter production) of a given year was mainly produced during that year but decayed during the following hydrological year, TBCA was on the current year's

Rs (2015–2016) and the previous year's Rl (2014–2015). ΔC_{soil} was set constant as the average annual belowground carbon increase since afforestation (Qubaja et al., in press).

3.2.7. STATISTICAL ANALYSES

Tow-way ANOVA tests were performed at a significance level set at $p = 0.001$ to detect significant effects of locations (OA, BT, and UT), sites, and their interactions on Rs and metrological parameters. Pearson correlation analysis (r) was used to detect the correlation between Rs and meteorological parameters. To quantify spatio-temporal variability in Rs, the coefficient of variation (CV%) was calculated as [(STDEV/Mean)*100%]. Heterogeneity was considered weak if CV% ≤ 10%, moderate if 10% < CV% ≤ 100%, and strong if CV% > 100%. All the analyses were performed using Matlab software, Version R2017b (MathWorks, Inc., MA, USA).

3.3. RESULTS

3.3.1. SPATIAL VARIATIONS

The spatial variations in Rs across locations (distance from nearest tree) and sites (across the study area) are reported in Table 3.1, together with other measured variables. The results indicated an overall mean Rs value of 0.8 ± 0.1 μmol m^{-2} s^{-1}, with distinct values for the three locations. Rs was greater at UT locations than at the BT and OA locations by a factor of ~2. The spatial variability among the locations was also apparent in the Rs daily cycle (Fig. 3.1), with clear differences between the wet season (November to April), when the UT showed consistently higher Rs values than at other locations by a factor of about 1.6 and the dry season by a factor of approximately 2.6. Note that the daily peak in Rs remained at midday in both the wet and dry seasons. Overall, the 21 collars showed moderate variations (CV = 55%; Table 3.1), Rs was negatively correlated with distance from trees (Dt; $r = 0.62$; $p < 0.01$) and with soil and air temperatures (Ts and Ta; $r = 0.45$; $p < 0.05$), and positively correlated with soil water content and relative humidity (SWC and RH; $r = 0.50$; $p < 0.05$). The inverse correlation between Rs and distance from the nearest tree could be useful in considering the expected decline in stand density due to thinning and mortality (e.g., associated with a drying climate). For a first approximation, the results indicate that decreasing from the present stand density of 300 trees ha^{-1} to 100 trees ha^{-1} and the resulting increase in mean distance among trees could result in decreasing ecosystem Rs by 11%.

3.3.2. TEMPORAL DYNAMICS

On the diurnal timescale, CO_2 fluxes showed typical daily cycles (Fig. 3.1). As expected, on average, all CO_2 fluxes were higher during the wet period compared to the dry season by a factor of ~2. However, Rs and Re peaked around midday in both the wet and dry seasons, while the more physiologically controlled NEE and GPP showed a shift from midday (around 11:00–14:00) to early morning (08:00–11:00) in the dry season, with a midday depression and a secondary afternoon peak (Fig. 3.1d).

The temporal variations across the seasonal cycle are reported in Fig. 3.2, based on monthly mean values, exhibiting sharp differences between the wet and dry seasons.

As previously observed in this semi-arid site, all CO_2 fluxes peak in early spring between March and April. The corresponding high-resolution data are reported in Fig. A3.6, which show also that the high winter (February) Rs rates were associated with clear days when photosynthetic active radiation (PAR) increased with air temperature, Ta. These data also show that, following rainy days, daily Rs values could reach 6.1 µmol m^{-2} s^{-1}, although the average was 1.1 ± 0.2 µmol m^{-2} s^{-1} during the wet period, which diminished by ~55% in the dry season to mean daily values of 0.5 ± 0.1 µmol m^{-2} s^{-1}. In spring (April), all CO_2 fluxes peaked during the crossover trends of decreasing soil moisture content and increasing both temperature and PAR (Fig. A3.6).

Table 3.1 | Annual mean of half-hour values across locations (OA, open area; BT, between trees; UT, under tree) in seven sites in the forest during the study period, of soil respiration flux rates (Rs) together with the soil water content at 10 cm depth (SWC), minimum distances from nearby tree (Dt), soil temperature at 5 cm depth (Ts), and air temperature (Ta) and relative humidity (RH) at the soil surface (numbers in parenthesis indicate ±se).

Locations	Sites	Rs [µmol m^{-2} s^{-1}]	SWC [x100 m^3 m^{-3}]	Dt [m]	Ts [ºC]	Ta [ºC]	RH [%]
OA	1	1.64 (0.02)	16.5 (0.2)	2.9	15.6 (0.1)	15.4 (0.2)	59.7 (0.5)
	2	0.72 (0.01)	14.5 (0.2)	3.6	15.9 (0.2)	15.0 (0.2)	58.4 (0.6)
	3	1.23 (0.02)	19.3 (0.2)	7.0	20.6 (0.3)	18.2 (0.2)	53.5 (0.5)
	4	0.38 (0.01)	11.3 (0.2)	3.0	22.6 (0.2)	20.8 (0.1)	58.9 (0.4)
	5	0.38 (0.01)	5.8 (0.2)	3.0	25.5 (0.1)	24.0 (0.1)	43.1 (0.4)
	6	0.31 (0.01)	5.7 (0.4)	2.8	30.0 (0.3)	26.2 (0.3)	51.8 (0.9)
	7	0.14 (0.01)	6.1 (0.3)	3.5	25.5 (0.2)	23.2 (0.3)	44.5 (0.9)
	Average	**0.68 (0.21)**	**11 (0)**	**3.7 (0.6)**	**22.3 (2.0)**	**20.4 (1.6)**	**52.8 (2.6)**
	CV [%]	**81 %**	**50%**	**41%**			**13 %**
BT	1	0.77 (0.01)	10.5 (0.2)	1.8	16.1 (0.1)	15.2 (0.2)	60.5 (0.5)
	2	0.88 (0.01)	12.1 (0.2)	1.5	14.8 (0.2)	14.7 (0.2)	59.5 (0.6)
	3	0.84 (0.01)	20.4 (0.2)	2.7	20.1 (0.3)	18.4 (0.2)	54.1 (0.6)
	4	0.91 (0.01)	14.4 (0.2)	2.7	23.3 (0.2)	21.3 (0.2)	58.5 (0.4)
	5	0.41 (0.00)	3.9 (0.2)	2.0	24.6 (0.1)	24.0 (0.1)	43.2 (0.4)
	6	0.41 (0.01)	3.3 (0.4)	2.5	29.1 (0.2)	26.0 (0.3)	52.5 (0.8)
	7	0.46 (0.01)	5.5 (0.3)	1.2	23.9 (0.1)	22.8 (0.3)	45.7 (0.9)
	Average	**0.67 (0.09)**	**10 (0)**	**2.0 (0.2)**	**21.7 (1.9)**	**20.3 (1.6)**	**53.4 (2.6)**
	CV [%]	**35 %**	**63%**	**29%**			**13 %**
UT	1	1.22 (0.02)	9.3 (0.2)	0.2	15.7 (0.1)	15.2 (0.2)	60.0 (0.5)
	2	1.42 (0.01)	14.0 (0.2)	0.3	14.8 (0.2)	14.8 (0.2)	59.4 (0.6)
	3	1.64 (0.01)	19.8 (0.2)	0.5	19.0 (0.2)	18.0 (0.2)	54.5 (0.6)
	4	1.90 (0.02)	11.3 (0.2)	0.6	22.0 (0.1)	20.8 (0.1)	59.0 (0.4)
	5	1.16 (0.01)	4.0 (0.2)	0.4	23.9 (0.1)	23.7 (0.1)	44.1 (0.4)
	6	1.29 (0.01)	4.5 (0.4)	0.2	29.5 (0.3)	25.9 (0.3)	52.7 (0.9)
	7	0.89 (0.01)	5.2 (0.3)	0.2	25.0 (0.1)	23.0 (0.3)	45.5 (0.9)
	Average	**1.36 (0.13)**	**10 (0)**	**0.3 (0.1)**	**21.4 (2.0)**	**20.2 (1.6)**	**53.6 (2.5)**
	CV [%]	**25 %**	**60%**	**46%**			**12 %**
All	**Average (SE)**	**0.8 (0.1)**	**11 (0)**	**2.0 (0.4)**	**21.8 (1.1)**	**20.3 (0.9)**	**53.3 (1.4)**
	Max	**1.90**	**20**	**7.0**	**30.0**	**26.2**	**60.5**
	Min	**0.14**	**3**	**0.2**	**14.8**	**14.7**	**43.1**
	CV [%]	**55 %**	**55%**	**82%**			**12 %**
Two-way ANOVA (*P* value)	**Site**	**0.000**	**0.000**		**0.000**	**0.000**	**0.000**
	Location	**0.000**	**0.000**		**0.000**	**0.220**	**0.074**
	Site x Location	**0.000**	**0.000**		**0.000**	**0.645**	**0.961**
Pearson Correlation with Rs			**.50***	**-.62****	**-.45***	**-.45***	**.50***

**. Correlation is significant at the 0.01 level (two-tailed).

*. Correlation is significant at the 0.05 level (two-tailed).

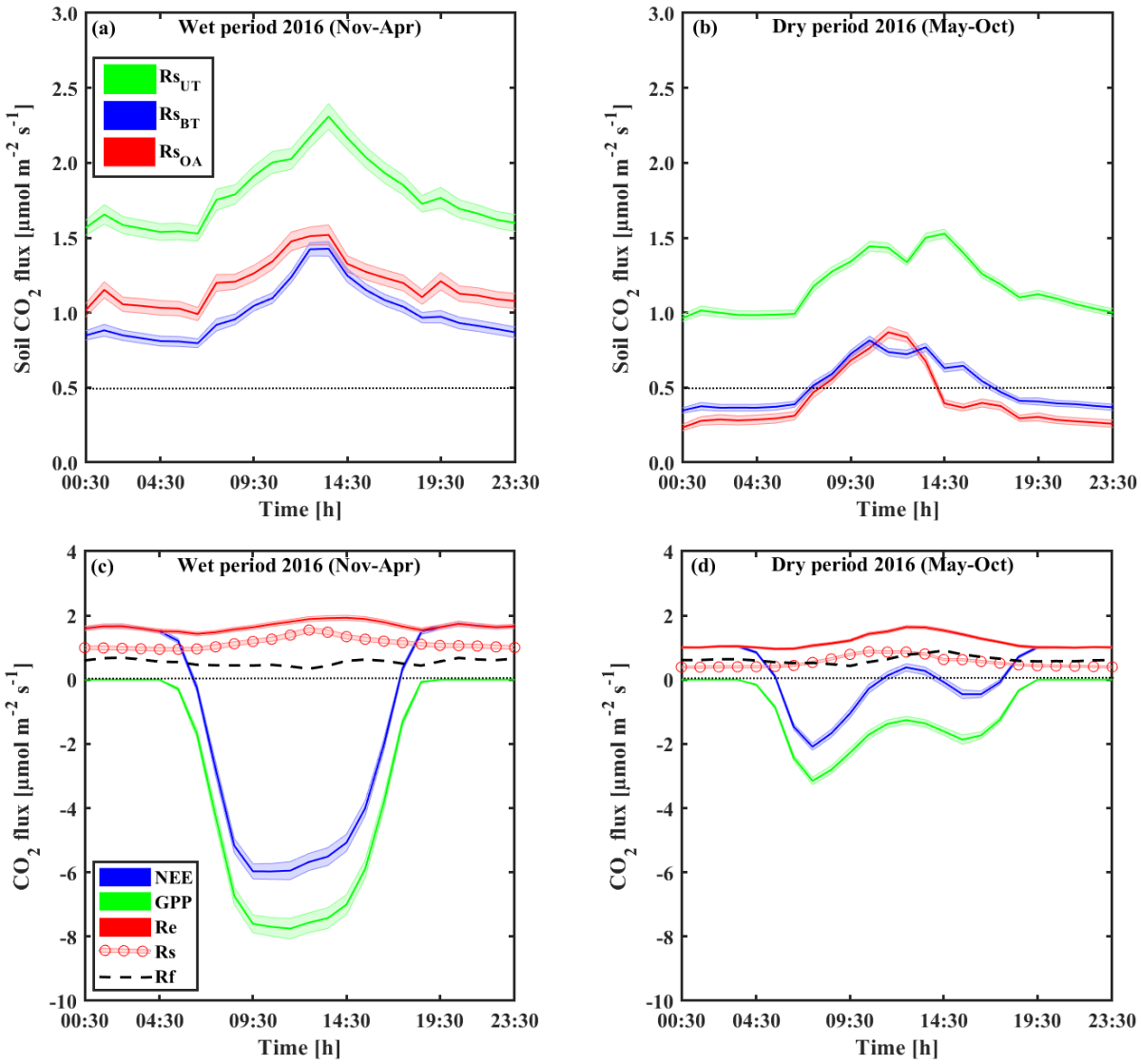

Figure 3.1 | Representative diurnal cycles of soil respiration (Rs; using soil chambers across locations: open area, OA; between trees, BT; under trees, UT) and sites in panels a and b, of net ecosystem exchange (NEE; canopy scale eddy covariance) and gross primary production (GPP), and ecosystem respiration (Re) and its partitioning to soil respiration (Rs) and aboveground tree respiration (Rf) in panels c and d, during the wet (Nov–Apr) and dry (May–Oct) periods. Based on half-hour values over the diurnal cycle; shaded areas indicate ±se; Rf was estimated as the residual as Rf = Re-Rs and was presented as a dashed line.

The temporal variations in the half-hour values of Rs reflected changes in soil moisture at 0–5 cm depth and PAR (r = 0.5 and 0.2, respectively; p < 0.01) and negative correlations with Ts and RH (r = 0.2 and 0.1, respectively; p < 0.01). The variations in the integrated Rs showed a CV of 71%, with the temporal variations dominated strongly by PAR (CV > 100%), moderately by SWC (CV~85%), and weakly by RH (CV~40%). Repeating the models applied by Grünzweig et al. (2009), the potential climatic factors that best predicted daily Rs shifted from SWC and PAR in the dry season to Ts and PAR in the wet season (Table A3.2). These equations explained 43% and 70% of the variation in Rs in the dry and wet seasons, respectively (Table A3.2). A reasonable forecast of the temporal variations in Rs (µmol m^{-2} s^{-1}) at half-hour values (R^2 = 0.60, p < 0.0001) was obtained based on $SWC_{0\text{-}10}$ and Ts values across the entire seasonal cycle, based on:

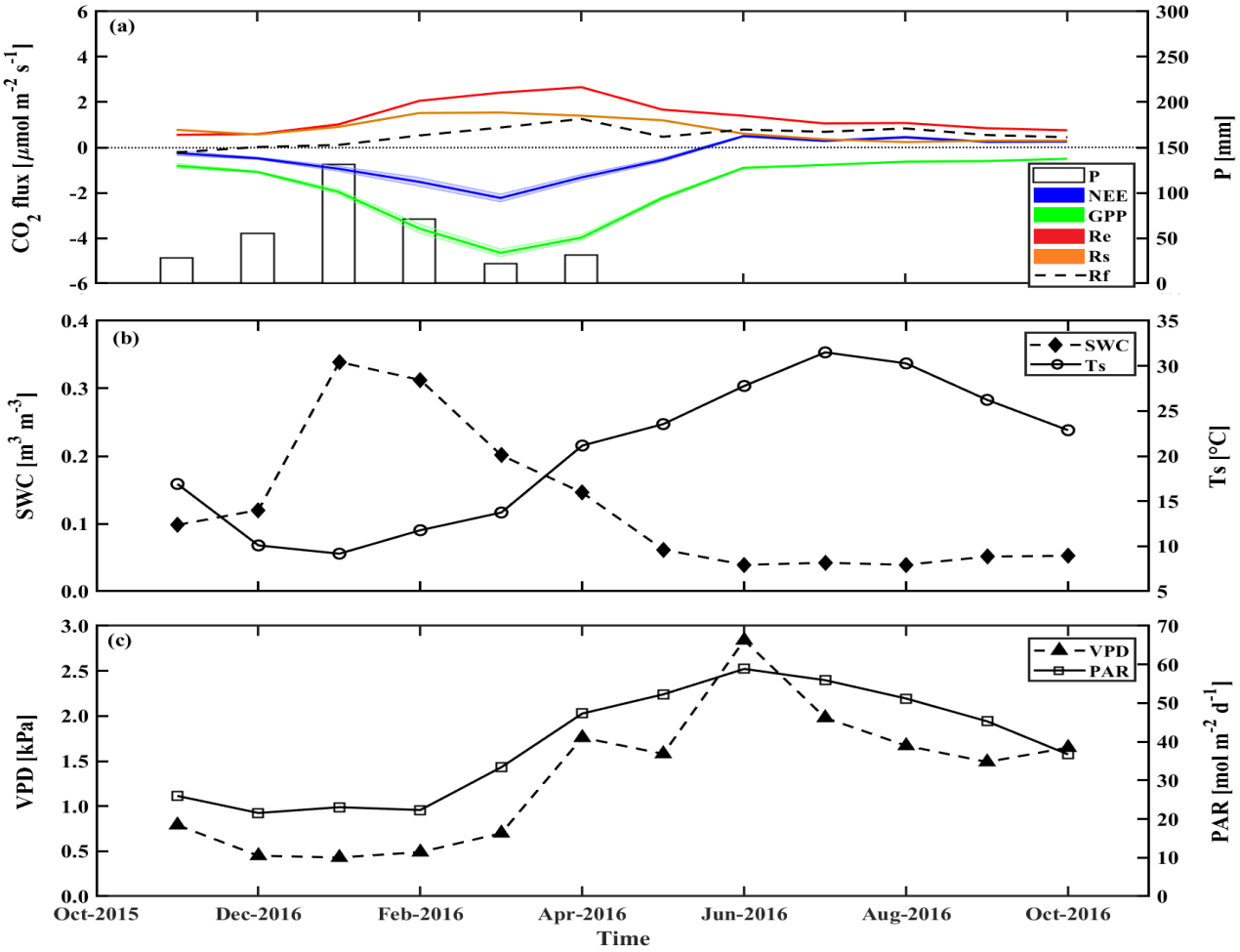

Figure 3.2| Seasonal trends of monthly mean values during the research period of a) the fluxes of net ecosystem exchange (NEE), gross primary production (GPP), and ecosystem respiration (Re) and its components, soil respiration (Rs) and aboveground tree respiration (Rf); and monthly mean of key environmental parameters, b) soil water content at the top 10 cm ($SWC_{0\text{-}10}$) and soil temperature at 5 cm (Ts), and c) vapor pressure deficit (VPD) and photosynthetic activity radiation (PAR). Rf is obtained from the Re-Rs.

$$Rs = 0.05126 * \exp(0.04274 * Ts + 28.51 * SWC - 74.44 * SWC^2) \quad (3.14)$$

At the ecosystem scale, Re was characterized by high fluxes in the wet season and peak values of ~2.4 µmol m^{-2} s^{-1} in February to April (Fig. 3.2; Table A3.1). Refluxes rapidly decreased after the cessation of rain and reached the lowest values in the fall (September to October), with mean dry period values of 0.5 ± 0.1 µmol m^{-2} s^{-1} (Fig. 3.2, Table A3.1). GPP had a mean value of -1.8 ± 0.4 µmol m^{-2} s^{-1}, and daily NEE had a mean value of -0.5 ± 0.3 µmol m^{-2} s^{-1} (Table A3.1 and Fig. A3.6), with the same seasonality (Fig. 3.2).

Figure 3.3 (see also Table 3.2) summarizes the seasonal variations in Rs and Re partitioning. The monthly Rsa and Rh were not significantly different but were significantly different from Ri ($p < 0.05$). The Rsa/Rs ratios ranged from 0.32 to 0.46, the largest contribution occurring in early spring from February to April. The Rh/Rs fraction ranged between 0.33 and 0.45, being highest during the wet season. The Ri/Rs – the fraction of inorganic sources from the total soil respiration – ranged from 0.09 to 0.35, the largest contribution being in the driest period. The mean relative

contributions of these components to Rs over the sampling campaigns are presented in Figure 3.3a, but, on average, soil biotic fluxes were higher than abiotic fluxes by a factor of ~4. Repartitioning showed an average increase in Rf/Re from 25% in the wet season to 54% in the dry season and a decline in Rs/Re from 75% to 46% on average in the wet and the dry seasons, respectively, which reflected a seasonal change of Rf in the wet season to peak values in the dry season (Fig. 3.3b). Both the highest and lowest Rs fractions (~0.74 and nearly 0.34) along the seasonal cycle were associated with low total Re fluxes, that is, in the fall before the Rf peak in the spring and in the summer, when physiological controls limited water loss.

Table 3.2 | $\delta^{13}C$ and $\Delta^{14}C$ signature of soil respiration (Rs) and its partitioning to autotrophic (Rsa), heterotrophic (Rh), and abiotic (Ri), together with the relative contribution of each to the soil and ecosystem respiration for Yatir forest during eight campaigns of measurements from January to September 2016 (numbers in parenthesis indicate ±se) in comparison to results obtained previously in the same forest (2001–2006 mean values). The monthly contribution of Rsa, Rh, and Ri to Rs or Re is presented in Fig. 3.3a and b, respectively.

Signature	**Rsa**	**Rh**	**Ri**	**Rs**
			[‰]	
$\delta^{13}C$	-23.7 (0.5)[1]	-24.3 (0.0)[1]	-6.5 (0.0)[1]	-20.8 (±0.6)[1]
$\Delta^{14}C$	30[3]	50[3]	-900[2]	-134 (34)[4]
Relative contribution to Rs (2015–2016)	**0.40 (0.02)**	**0.39 (0.02)**	**0.21 (0.04)**	
Relative contribution to Re (2015–2016)	**0.24 (0.04)**	**0.23 (0.04)**	**0.13 (0.01)**	**0.60 (0.06)**

[1] Measured in the present study; [2] measured by Carmi et al., (2013); [3] calculated based on the measured atmospheric value by Carmi et al. (2013); and [4] calculated based on the best fit regression equation in Fig. A3.2.

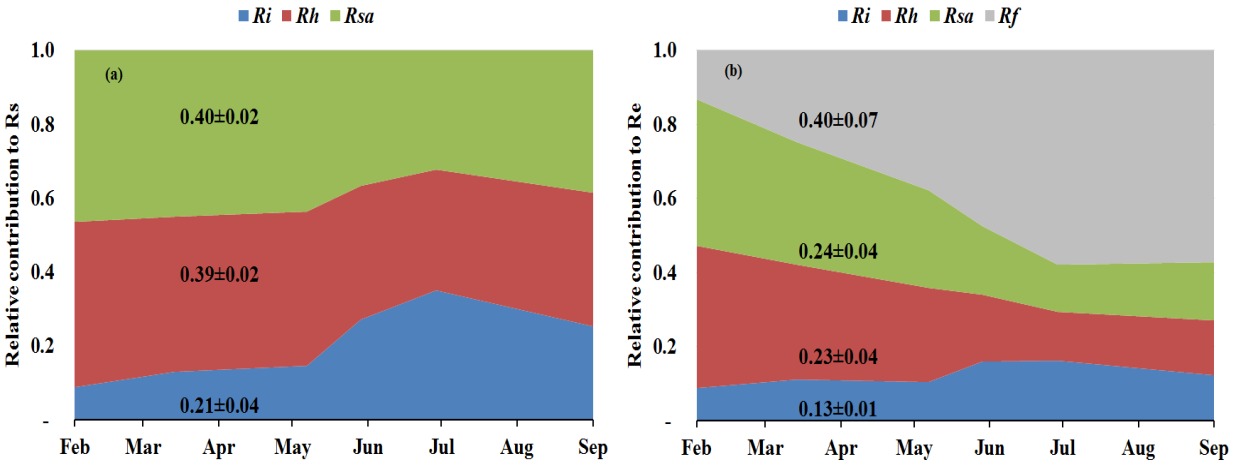

Figure 3.3 | a) Linear mixing models $\delta^{13}C$ and $\Delta^{14}C$ of soil respiration (Rs) isotope signatures (from soil CO_2 profile method at 0, 30, 60, 90, and 120 cm soil depth) were used to determine the seasonal variations in the relative contribution of soil autotrophic (Rsa), heterotrophic (Rh), and abiotic (Ri) components to Rs, and b) seasonal variations in the relative contribution of soil autotrophic (Rsa), heterotrophic (Rh), abiotic (Ri), and foliage and stem respiration (Rf is obtained from the Re-Rs) components to ecosystem respiration (Re) during eight campaigns (Jan–Sep) in 2016. These results confirmed earlier estimates of Grünzweig et al. (2009) and Maseyk et al. (2008a).

3.3.3. ANNUAL-SCALE

On an annual timescale, estimates of CO_2 flux components based on EC measurements resulted in annual values of GPP, NPP, Re, and NEP of 655, 282, 488, and 167 g C m^{-2} y^{-1}, respectively (Tables 3.3 and A3.1). On average across the measurement period,

Rs was the main CO_2 flux to atmosphere, making up 60 ± 6% of Re (295 ± 4 g C m^{-2} y^{-1}; Tables 3.3 and A3.1), and Rf was another significant component accounting for 40 ± 6% of Re (Fig. 3.3b), which reflected the low density (300 trees ha^{-1}) nature of the semi-arid forest. As indicated above, Re partitioning showed a decrease in Rs/Re and an increase in Rf/Re from winter to summer, which is clearly apparent in Fig. 3.3b. On an annual scale, during the study period, estimates of Rf, Rsa, Rh, and Ri values were 194 ± 36, 119 ± 21, 115 ± 20, and 61 ± 6 g C m^{-2} y^{-1}, respectively. Despite relatively high rates of respiration fluxes, the CUE of the ecosystem remained high at 0.43.

Using the site records of nearly 20 years, long-term trends in GPP, NPP, Re, and NEP were obtained. Soil respiration and its partitioning could not be similarly monitored continuously, but combining the present results with the 2001–2006 values obtained by Grünzweig et al. (2009) and Maseyk et al. (2008a) provided a basis for estimating the long-term trends in soil respiration. Notably, no clear or significant trend over time was observed in any of the canopy-scale continuously monitored fluxes, but, because of relatively large interannual variations, associated mainly with those in precipitation (see Qubaja et al., in press), it is likely that the relative contributions of the different fluxes, expressed as ratios in Table 3.3, provide a more robust perspective of the long-term temporal changes in the ecosystem functioning. The results presented n Table 3.3 reflect the long-term growth of the forest, with a relatively large increase in LAI, but the belowground allocation remained around 40%. The ratio of the respiration components to total ecosystem respiration, Re, or to GPP indicated little change in the total soil respiration, Rs, component, but a general shift from the autotrophic components Rsa, Rl, and Rw to the heterotrophic component, Rh, across the 13-year observation period noted above (with the mean values for 2011–2005 assigned to 2003 and the new data to 2016).

Table 3.3 | Mean annual values of ecosystem respiration (Re), its components and associated ratios, net ecosystem exchange (NEE; from eddy covariance), net primary productivity (NPP), gross primary productivity (GPP), carbon-use efficiency (CUE), leaf area index (LAI), and ratio of total belowground carbon allocation (TBCA) to GPP (TBCA/GPP) in the present study (mean of Nov 2015 to Oct 2016) and in comparison to results obtained previously in the same forest (2001–2006 mean values). Ri, Rh, Rsa, Rs, Rl and Rw denote abiotic, heterotrophic, soil autotrophic, soil, foliage, and wood CO_2 flux, respectively. Q_{10} is derived during the two studies for the wet and dry season.

Study	Rs	Rh	Rsa	Rl	Rw	Ri	Re	NEE	NPP	GPP
					[g m^{-2} y^{-1}]					
Mean (2001–2006)	406	147	203	260	70	56	735	-211	-358	-880
x/Rs		0.36	0.50			0.14				
x/Re	0.55	0.20	0.28	0.35	0.10	0.07				
Mean (2015–2016)	295	115	119	155	39	61	488	-167	-282	-655
x/Rs		0.39	0.40			0.21				
x/Re	0.60	0.23	0.24	0.32	0.08	0.13				
Ratio of $(x/Rs)_{2016}/(x/Rs)_{2003}$		**1.08**	**0.81**			**1.50**				
Ratio of $(x/Re)_{2016}/(x/Re)_{2003}$	**1.09**	**1.18**	**0.88**	**0.90**	**0.84**	**1.64**				

Study	Q_{10}		CUE	TBCA/GPP[3]	LAI
	SWC[1]	SWC[2]			[m^2 m^{-2}]
Mean (2001–2006)	2.5	1.2	0.40	0.41	1.3
Mean (2015–2016)	1.6	1.1	0.43	0.38	2.1
Ratio of x_{2016}/x_{2003}	**0.64**	**0.92**	**1.06**	**0.93**	**1.62**

[1] SWC ≥ 0.2 [m^3 m^{-3}] and [2] SWC < 0.2 [m^3 m^{-3}]; [3] and the mean of GPP used by Grünzweig et al., 2009 to estimate the TBCA/GPP was 834 g m^{-2} y^{-1}.

3.4. DISCUSSION

Partitioning ecosystem carbon fluxes and long-term observational studies are key to understanding ecosystem carbon dynamics and their response to change. Overall, the results support our research hypothesis that the observed high CUE at our site is at least partly due to the characteristics of the carbon flux partitioning that can be associated with the semi-arid conditions. Compared to other sites and climates (see comparative compilation in Table A3.3), the results reflect several key points: 1) relatively high belowground allocation; 2) low soil respiration in general, and low heterotrophic respiration in particular; 3) combining the results for 2016 and those of our earlier study offered a long-term perspective across 13 years, indicating that the low Rs in this ecosystem is robust and exhibits reduced sensitivity to temperature, and 4) there is a general long-term shift from autotrophic to heterotrophic respiration.

Comparing CO_2 fluxes in this forest with fluxes in a range of European forests showed that mean NEP in the semi-arid forest (167 g C m^{-2} y^{-1}) is similar to the mean NEP in other European forests (150 g C m^{-2} y^{-1}; FLUXNET).

Carbon partitioning belowground (TBCA/GPP) was relatively high (~38%), with little change across the long-term observation period. It is, however, within the range of mean value for forests in different biomes (Litton et al., 2007). High belowground allocation helps explain the high rate of SOC accumulation observed over the period since afforestation (Grünzweig et al., 2007; Qubaja et al., in press). Note that, irrespective of the soil carbon accumulation, the abiotic component to the CO_2 flux seems to be significant in dry environments (Table 3.3) and in particular in the dry seasons, when biological activities drastically decrease (Kowalski et al., 2008; Lopez-Ballesteros et al., 2017; Serrano-Ortiz et al., 2010; Martí-Roura et al., 2019). The results show that considering the abiotic effects on estimating soil respiration and, in turn, on estimating the carbon budget in dry calcareous soils can play an important part in estimating soil and ecosystem respiration fluxes (Angert et al., 2015; Roland et al., 2012).

The soil CO_2 efflux in the semi-arid forest (295 g C m^{-2} y^{-1}) is at the low end of Rs values across the range of climatic regions, from 50 to 2,750 g C m^{-2} y^{-1} (Adachi et al., 2017; Chen et al., 2014; Grünzweig et al., 2009; Hashimoto et al., 2015). This is clearly lower than the mean Rs value for global evergreen needle forests, which is estimated at 690 g C m^{-2} y^{-1} (Chen et al., 2014), and between estimates for desert scrub and Mediterranean woodland (224–713 g C m^{-2} y^{-1}; Raich and Schlesinger, 1992) or for Mediterranean forests (561–1,015 g C m^{-2} y^{-1}; Casals et al., 2011; Luyssaert et al., 2007; Matteucci et al., 2015; Misson et al., 2010; Rey et al., 2002; Rodeghiero and Cescatti, 2005). The mean instantaneous rate of Rs, 0.8 µmol m^{-2} s^{-1}, is also in the range reported for unmanaged forest and grassland in the dry Mediterranean region (0.5 and 2.1 µmol m^{-2} s^{-1}; Correia et al., 2012).

The observed low Rs values were associated with a relatively high fraction of autotrophic and a lower fraction of heterotrophic respiration. The mean annual-scale Rsa/Rs ratio of 0.40 was at the high end of the global range of 0.09 to 0.49 (Chen et al., 2014; Hashimoto et al., 2015). In contrast, heterotrophic respiration showed an annual-scale Rh/Rs ratio of 0.39 ± 0.02 (Table 3.2 and Fig. 3.3), which is lower than the estimated global mean Rh/Rs value of 0.56 (Hashimoto et al., 2015), but within the range of Mediterranean region forest, which varies between 0.29 to 0.77 (Casals et al., 2011; Luyssaert et al., 2007; Matteucci et al., 2015; Misson et al., 2010; Rey et al., 2002; Rodeghiero and Cescatti, 2005). The relatively low annual scale of the heterotrophic respiration to Rs is consistent with the dry soil over much of the year in

this forest (Figs 3.2 and A3.6) and the observed low decomposability of plant detritus and high mean SOC accumulation rate (Grünzweig et al., 2007).

The long-term perspective from the 13-year observation period indicates emerging trends that can be a basis for assessing the effects of forest age and the marked increase in LAI (Table 3.3) and changes in environmental conditions (generally warming and drying; see, e.g., Lelieveld et al., 2012). As noted above, comparing the non-continuous data from the present (2016) and earlier (2001–2006) studies is sensitive to the large interannual variations in the ecosystem activities and fluxes (Qubaja et al., in press), and we therefore focused on the more robust changes in the ratio of the respiration components to the overall fluxes (Re) (Table 3.3). This shows a shifting trend from the autotrophic components to the heterotrophic, with little change in the contribution of Rs to the overall efflux. The ratios of Rsa, Rl, and Rw to Re tended to decrease by about 13%, while that of Rh increased by about 18%; similar trends were seen in soil respiration, with Rsa/Rs decreasing by -19% and Rh/Rs increasing by +8% (Table 3.3). The relatively low Rs under conditions of high temperature in the semi-arid ecosystem implies reduced sensitivity of respiration to temperature. This is partly imposed by low SWC conditions during extended parts of the year (Grünzweig et al., 2009; cf. Rey et al., 2002; Xu and Qi, 2001). Accordingly, Rs showed greater sensitivity to Ts in the wet period, but during the 8–9 months of the year when SWC was below ~0.2 m^3 m^{-3}, Rs varied predominantly with water availability. The long-term perspective reported in Table 3.3 indicates a further decrease in temperature sensitivity, with mean Q_{10} values in the dry season decreasing from 1.6 to 1.1. These estimated Q_{10} values are generally consistent with published values for different ecosystems (1.4 to 2.0; Hashimoto et al., 2015; Zhou et al., 2009) and with low values under low SWC (Reichstein et al., 2003; Tang et al., 2005). This is also consistent with soil warming experiments by 0.76°C in Mediterranean ecosystems, which decreased the Rs by 16%, and Q_{10} by 14% (Wang et al., 2014). Note also that the low temperature sensitivity in the dry season is likely to be related to reduced microbial activity, but may also involve downregulation of plant activity (Maseyk et al., 2008a) and drought-induced dormancy of shallow roots (Schiller, 2000). Finally, we also note that the greater importance of moisture availability in influencing respiration is clearly apparent from the observed relationships of Rs and Rh to mean annual precipitation (MAP) in European evergreen needle forests (Fig. A3.8; see also Grünzweig et al., 2007), which are not observed with respect to mean annual temperature.

A3. APPENDIX

Table A3.1 | Monthly mean values of net ecosystem exchange (NEE), gross primary production (GPP), and ecosystem respiration (Re) and soil respiration (Rs) during study period. Note: the numbers in parenthesis is the ±se.

Season	Month	NEE	GPP	Re	Rs
		[µmol m^{-2} s^{-1}]			
Wet season (Nov-Apr)	Nov	-0.25 (0.10)	-0.81 (0.10)	0.56 (0.03)	0.78 (0.01)
	Dec	-0.48 (0.05)	-1.08 (0.04)	0.59 (0.01)	0.57 (0.01)
	Jan	-0.94 (0.11)	-1.96 (0.11)	1.02 (0.02)	0.91 (0.01)
	Feb	-1.52 (0.19)	-3.58 (0.20)	2.06 (0.03)	1.52 (0.02)
	Mar	-2.23 (0.17)	-4.65 (0.17)	2.42 (0.02)	1.54 (0.01)
	Apr	-1.32 (0.13)	-3.98 (0.13)	2.66 (0.02)	1.40 (0.01)
	Average [µmol m^{-2} s^{-1}]	**-1.12 (0.30)**	**-2.68 (0.66)**	**1.55 (0.38)**	**1.12 (0.17)**
	Season sum [g C m^{-2}]	**-203 (9)**	**-482 (20)**	**279 (11)**	**202 (5)**
	Rs/Re [%]				**72 (13)**
Dry season (May-Oct)	May	-0.55 (0.08)	-2.23 (0.08)	1.67 (0.02)	1.20 (0.01)
	Jun	0.50 (0.04)	-0.90 (0.04)	1.40 (0.02)	0.61 (0.01)
	Jul	0.29 (0.04)	-0.77 (0.03)	1.06 (0.01)	0.36 (0.01)
	Aug	0.45 (0.05)	-0.63 (0.04)	1.08 (0.02)	0.24 (0.01)
	Sep	0.25 (0.04)	-0.60 (0.04)	0.85 (0.02)	0.30 (0.01)
	Oct	0.26 (0.03)	-0.50 (0.02)	0.76 (0.01)	0.30 (0.01)
	Average [µmol m^{-2} s^{-1}]	**0.20 (0.16)**	**-0.94 (0.26)**	**1.14 (0.14)**	**0.50 (0.15)**
	Season sum [g C m^{-2}]	**36 (5)**	**-173 (8)**	**209 (4)**	**93 (5)**
	Rs/Re [%]				**44 (7)**
Annual	**Average (SE) [µmol m^{-2} s^{-1}]**	**-0.46 (0.26)**	**-1.81 (0.43)**	**1.34 (0.20)**	**0.8 (0.1)**
	Annual sum (SE) [g C m^{-2} y^{-1}]	**-167 (8)**	**-655 (13)**	**488 (6)**	**295 (4)**
	Rs/Re [%]				**60 (10)**

Table A3.2 | Exponential and linear relationships between soil respiration rate (Rs; µmol m^{-2} s^{-1}) and abiotic factors during 2015-2016. Ts (°C): soil temperature; SWC (m^3 m^{-3}): soil water content; PAR (µmol m^{-2} s^{-1}): incoming photosynthetic activity radiation above canopy. The best-fit model parameters (β_0, β_1, β_2, and β_3) are reported for each model together with the squared coefficient of regression (R^2), and the root mean squared error (RSME).

a) Up-scaled daily time series (the models that used during Grünzweig et al., 2009)

Model	Study	β_0	β_1	β_2	β_3	β_4	R^2
$\beta_0 + \beta_1\theta + \beta_2 PAR$	2000-2006	-2.306	25.39	0.000545			0.83
<0.2 m^3 H_2O m^{-3} soilθ	2015-2016	-0.7313	11.14	0.000564			0.43
$\beta_0 + \beta_1 e^{\beta_2 Ts} + \beta_3 e^{\beta_4 PAR}$	2000-2006	1.394	0.1463	0.151	0.008408	0.003154	0.86
<0.2 m^3 H_2O m^{-3} soilθ	2015-2016						0.70

b) Up-scaled half-hour time series

Model	β_0	β_1	β_2	β_3	R^2	SSE
$\beta_0 + \beta_1 Ts$	1.264	-0.02			0.07	0.556
$\beta_0 e^{\beta_1 Ts}$	1.309	-0.02			0.07	0.558
$\beta_0 + \beta_1\theta$	0.2934	5.57			0.35	0.4667
$\beta_0 + \beta_1\theta + \beta_2\theta^2$	-0.2175	17.47	-48.35		0.42	0.4388
$e^{\beta_0 + \beta_1\theta + \beta_2\theta^2}$	-1.68	23.49	-67.3		0.44	0.4378
$\beta_0 + \beta_1 PAR$	0.7121	0.0002			0.05	0.5603
$\beta_0 + \beta_1\theta + \beta_2 Ts$	-0.4213	7.626	0.02473		0.40	0.4499
$\beta_0 + \beta_1\theta + \beta_2 PAR$	0.1162	5.989	0.00028		0.44	0.4295
$\beta_0 \beta_1^{((Ts-10)/10)} \theta^{\beta_2}$	6.714	1.655	1.083		0.52	0.4151
$(\beta_0/(1 + e^{\beta_1 * (\beta_2 - Ts)})) * \theta^{\beta_3}$	11.91	0.267	12.04	0.9908	0.54	0.3914
$(\beta_0/(1 + e^{\beta_1 * (\beta_2 - PAR)})) * \theta^{\beta_3}$	90.12	0.0004	8625	0.6838	0.50	0.4169
$\beta_0 e^{\beta_1 Ts} e^{\beta_2\theta + \beta_3\theta^2}$	0.05126	0.04274	28.51	74.44	0.60	0.3932

Table A3.3 | Annual heterotrophic respiration (Rh), autotrophic respiration (Ra), soil respiration (Rs), ecosystem respiration (Re), gross primary productivity (GPP), net primary productivity (NPP), net ecosystem production (NEP; from eddy covariance), respectively. The relative contribution of Rh, and Ra and Rs to Re, and the ecosystem and soil carbon sequestration efficiency as CSE (NEP/GPP) and SCSE (ΔC_{soil}/GPP), where ΔC_{soil} is the annual change of soil carbon.

Study	**Rh**	**Ra**	**Rs**	**Re**	**GPP**	**NPP**	**NEP**	**Rh/Re**	**Ra/Re**	**Rs/Re**	**CSE**	**SCSE**
	[g m^{-2} y^{-1}]							**[%]**			**[%]**	
Semi-arid[1]	115	312	295	488	655	282	167	23	64	60	25	8.7
Europe, mean	368	589	657	957	1107	518	150	38	62	69	14	1.8
Europe^{EN}, mean	461	657	381	1117	1475	818	358	41	59	74	24	1.4
Boreal, global	301	561	411	862	982	381	116	35	65	48	12	0.7
Temperate, global	420	730	773	1150	1461	669	306	37	64	67	21	1.4
Tropical, global	877	2184	1412	3061	3351	864	403	29	71	46	12	0.3

[1] This study from November 2015 to October 2016. [EN] Evergreen needleleaf forests. References for all other vegetation types appear in the SI.

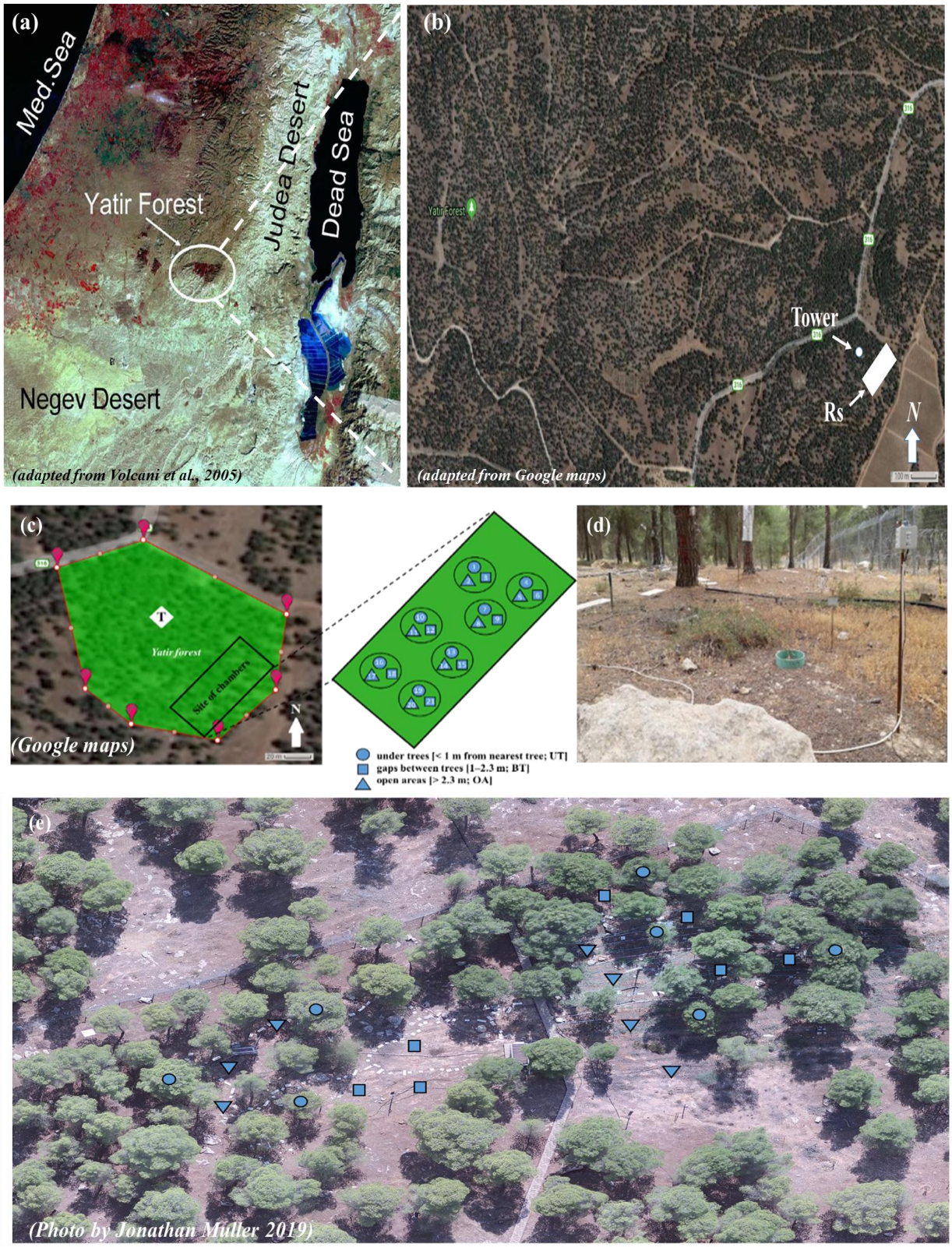

Figure A3.1 | (a) Landsat-TM image of Central Israel, (b) Map of the experimental set-up at the *Pinus halepensis* Yatir forest with white rectangle for soil respiration (Rs) measurements and white dot is the eddy covariance tower (NEE), c, d, and e) Photographs showing conditions of locations, site, and the schematic diagrams describing experiment design.

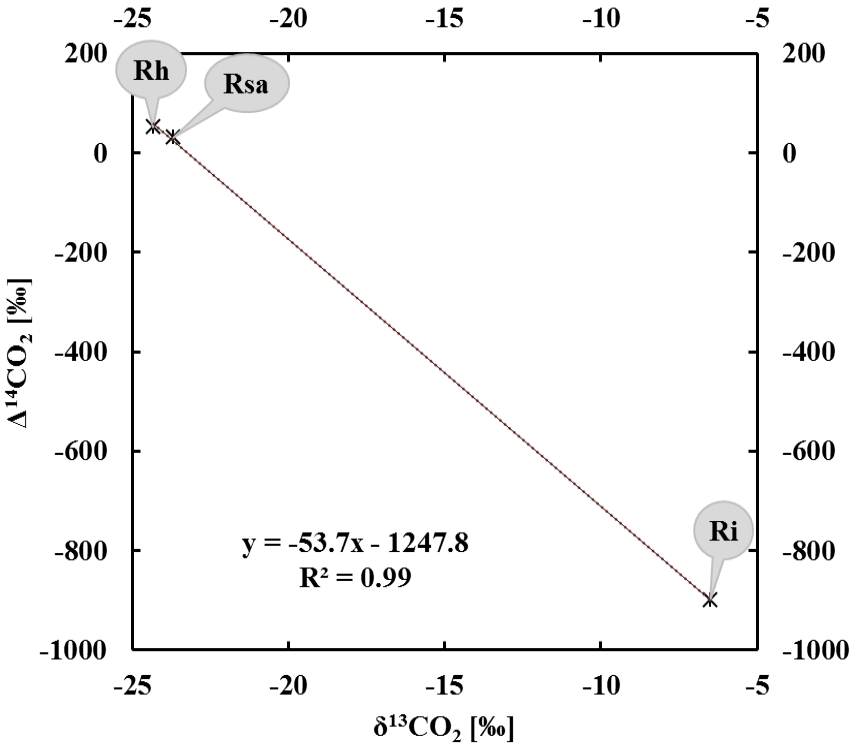

Figure A3.2 | The linear regression line used to estimate the $\Delta^{14}C$ of Rs. The line (dotted) was produced by the correlation between the average of the measured $\delta^{13}C$ values of Rsa, Rsh, and the $\delta^{13}C$ Ri (all from incubation measurements), and the $\Delta^{14}C$ values estimated based on measured $\Delta^{14}C$ at our site (Carmi et al. 2013) adjusted to the present study period and the mean accepted ages of autotrophic and heterotrophic soil organic material (Graven et al., 2012; Levin et al., 2010; Taylor et al., 2015).

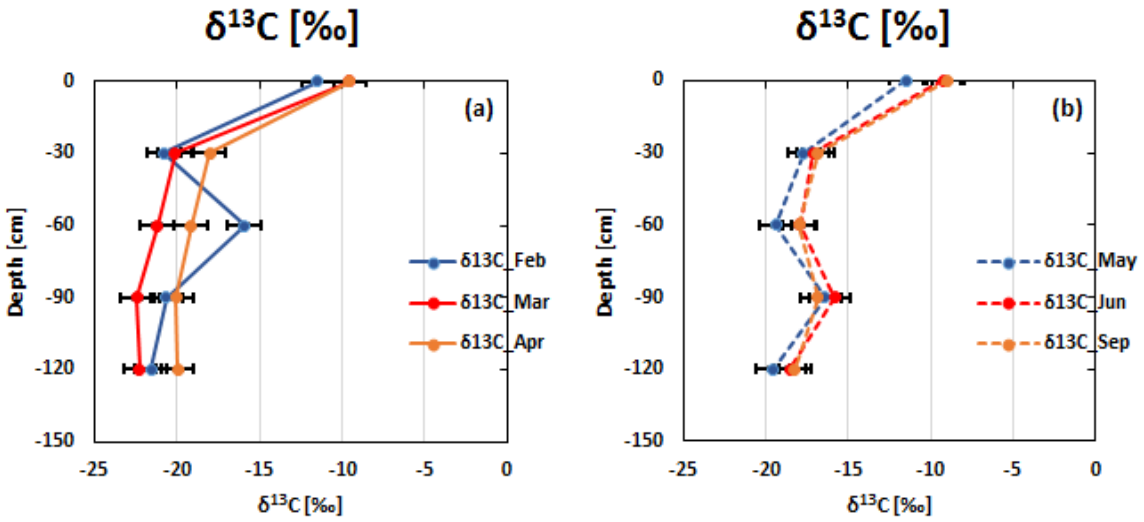

Figure A3.3 | Monthly averages of $\delta^{13}C$ (‰) from the soil CO_2 profile (at 0, 30, 60, 90, and 120 cm soil depth) during some campaigns in 2016 to determine the seasonal variations in the relative contribution of soil autotrophic (Rsa), heterotrophic (Rh), and abiotic (Ri) components to Rs.

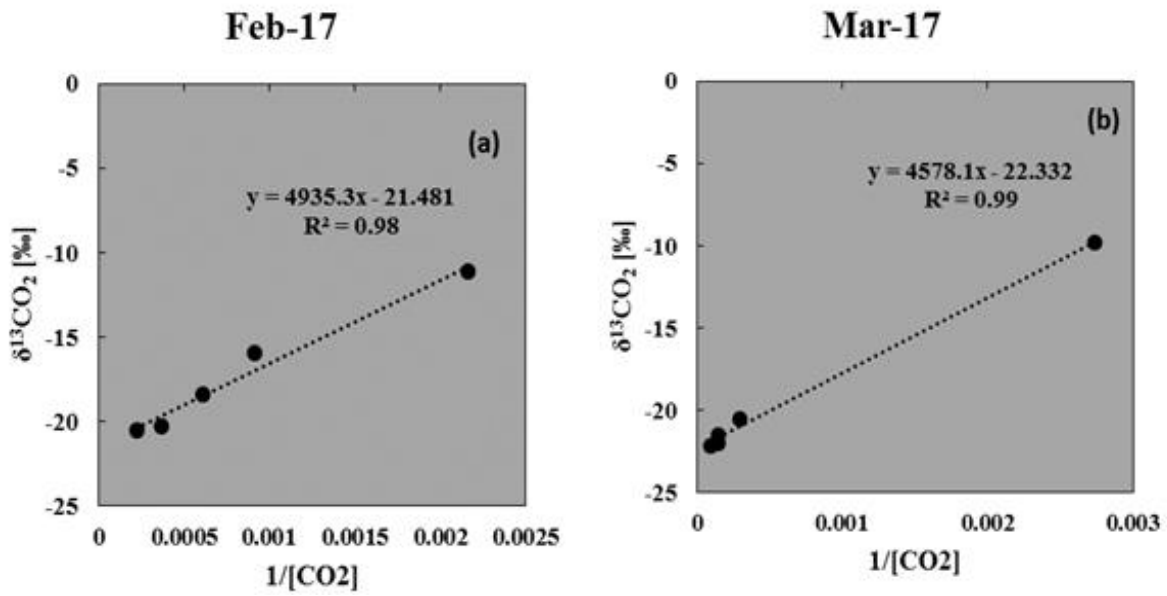

Figure A3.4 | Keeling plot for soil CO_2 profile (at 0, 30, 60, 90, and 120 cm soil depth) during some campaigns in 2016 to determine the seasonal variations in the relative contribution of soil autotrophic (Rsa), heterotrophic (Rh), and abiotic (Ri) components to Rs.

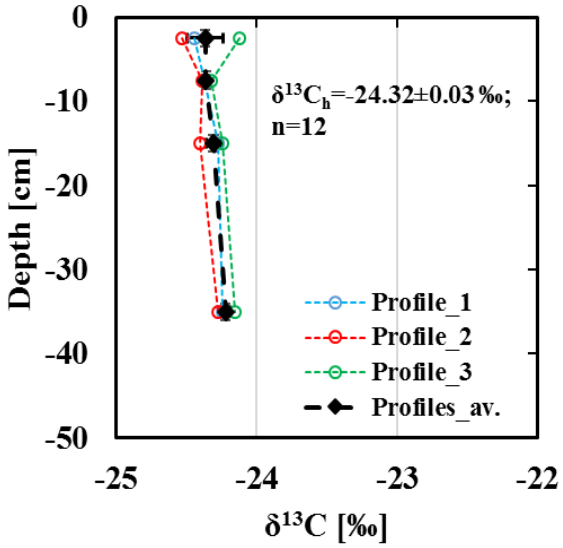

Figure A3.5 | $\delta^{13}C$ of soil organics profile with depth (at 0-5, 5-10, 10-20, and 20-50 cm soil depth) from three sites during some campaigns in 2016 to determine the relative contribution of soil heterotrophic (Rh) to Rs (STDEV of the 12 samples = 0.12‰).

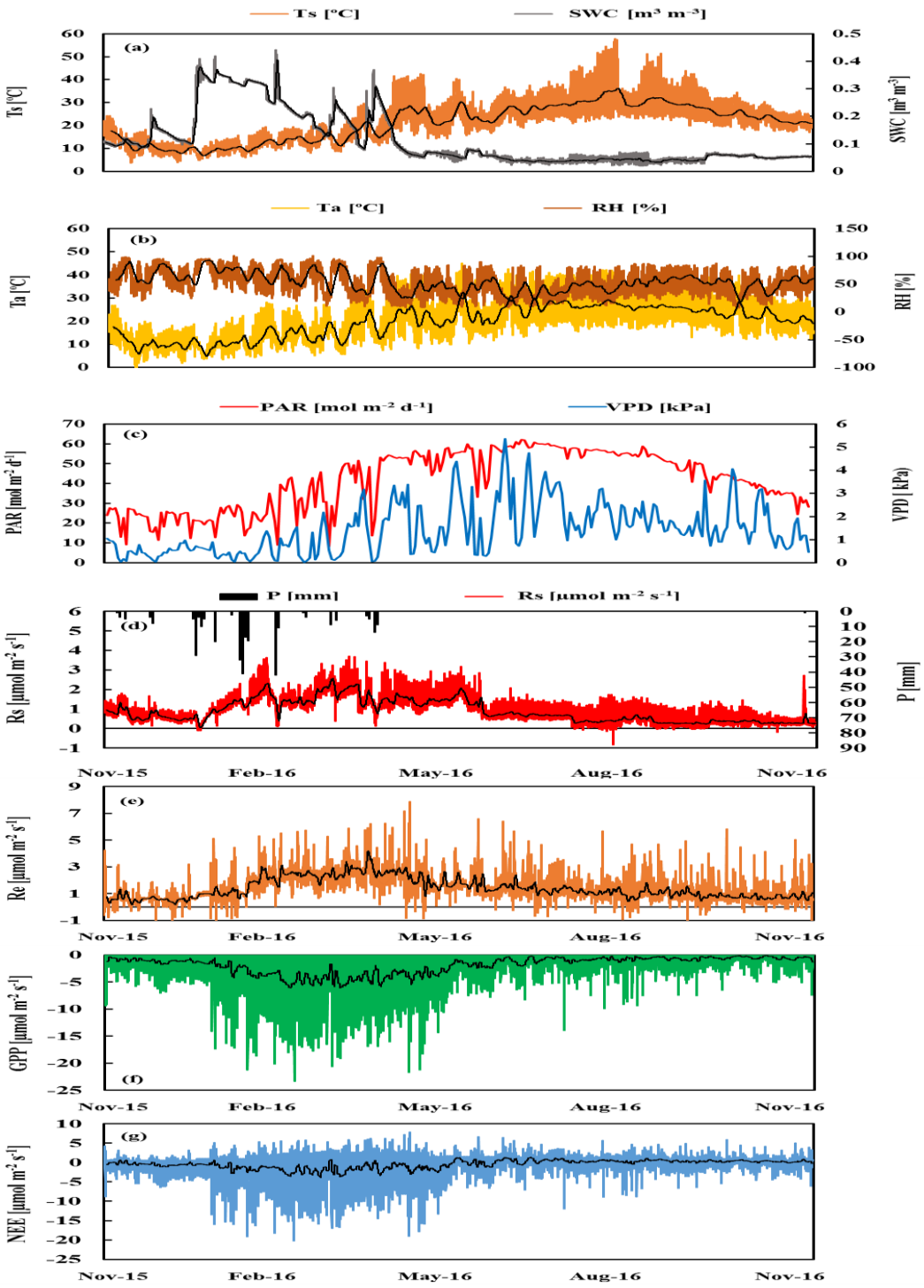

Figure A3.6 | a) half-hour values for soil temperature 5 cm (Ts) and soil water content 10 cm ($SWC_{0\text{-}10cm}$), b) half-hour values for the air temperature at 20 cm (Ta) and relative humidity at 20 cm (RH), c) daily average of incoming photosynthetic activity radiation above canopy (PAR) and vapour pressure deficit (VPD), half-hour values for the following CO_2 fluxes d) up-scaled Rs, e) ecosystem respiration (Re), f) gross primary production (GPP), and g) net ecosystem exchange (NEE). Black lines are a running average for a widows of 2 days.

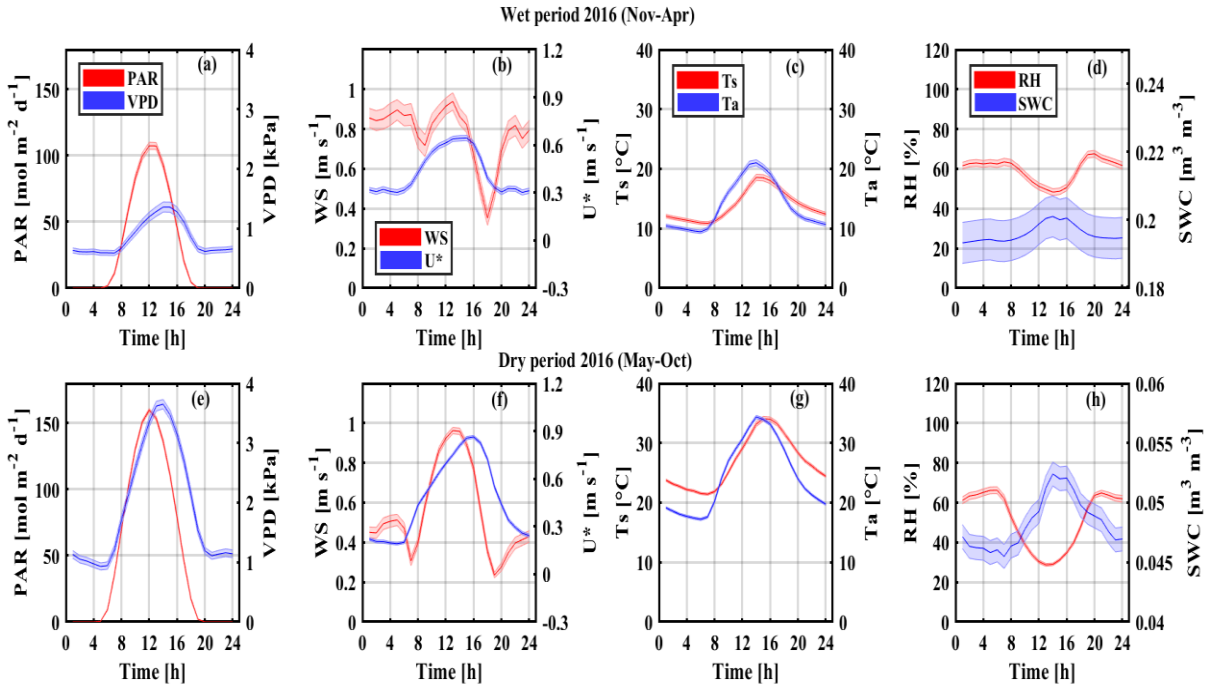

Figure A3.7 | Typical diurnal cycle of the meteorological parameters during the wet period (Nov.-Apr.; upper panels) and for the dry period (May-Oct.; lower panels); each set includes six months of half-hour measurements. a and e) incoming photosynthetic activity radiation above canopy (PAR) and vapour pressure deficit (VPD), b and f) wind speed (WS) and covariation of friction velocity (U*), c and g) soil temperature at 5 cm (Ts) and air temperature at 20 cm (Ta), and d and h) relative humidity (RH) and soil water content at the top 10 cm (SWC0-10cm). Shaded areas indicate ±se.

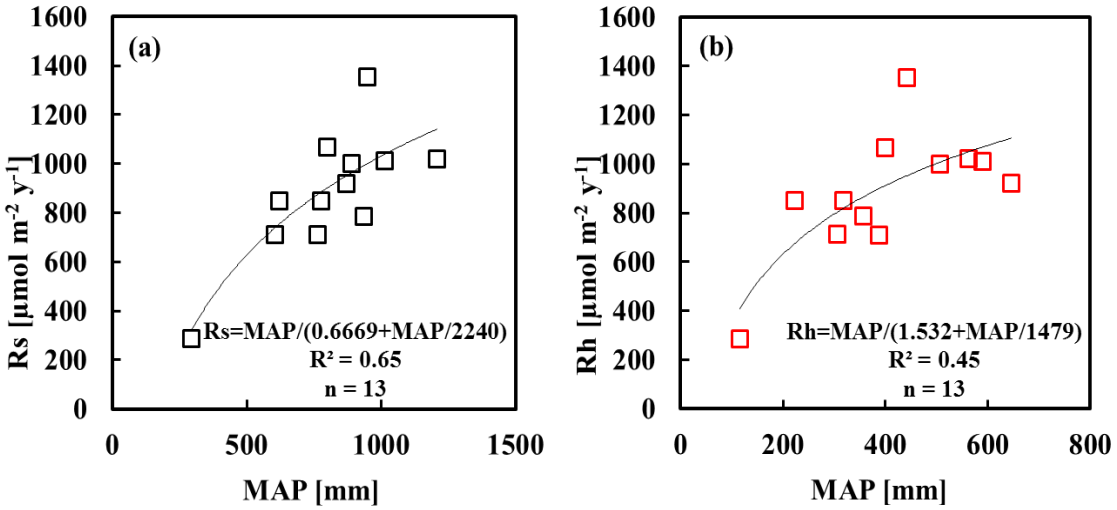

Figure A3.8 | An asymptotic function based on the Michaelis-Menten equation (Kool et al., 2007) was fit to a) Rs or b) Rh vs. MAP from the European Evergreen needleleaf data as follows: Rs = MAP/(0.6669 + MAP/2240), $R^2 = 0.65$, $p < 0.01$, n=13 (Flechard et al., 2019a).

4

ASSESSING CO_2 AND H_2O FLUXES IN A NON-COMMERCIAL URBAN CITRUS ORCHARD

Non-commercial orchards can be useful in enhancing urban ecology and ecosystem services, and in conservation efforts. A few studies have been conducted to assess the water and carbon economy of a Mediterranean non-commercial urban citrus orchards, which remain poorly quantified. Here, we performed a canopy-scale eddy covariance measurements of the net CO_2 exchange (NEE) and evapotranspiration (ET) and partition these fluxes to their components using chamber-based soil fluxes (soil respiration [Rs] and evaporation [Es]). The results provided a basis for comparison with commercial orchards in the same environment. The ratios of soil to ecosystem respiration (Rs/Re) and soil evaporation to ecosystem evapotranspiration (Es/ET) were 0.65 and 0.70 in the wet period and 0.71 and 0.18 in the dry period, respectively. Rs varied systematically among microsites, with mean values (in µmol m^{-2} s^{-1} and SD of ± 0.1 or better) decreasing from 7.0 'under trees' (UT) to 0.7 'between rows' (BR). Es values were highest in the BR microsites during the wet period (associated with precipitation) and in the UT sites during the dry period (associated with drip irrigation). The orchard switched from a carbon sink to a carbon source between the wet and the dry seasons, respectively, with respiration to gross primary productivity, Re/GPP, increasing from 0.8 to 1.1. Carbon stock is estimated at 5,702±524 g C m^{-2} with 67% below ground, with apparent ecosystem carbon turnover time of 5.4±1.0 y. The transpiration ratio (Et/ET) increased from 0.3 to 0.8 from the dry to the wet seasons, with high water use efficiency (WUE) values of 5.5 and 11.7 (NEE/ET or GPP/Et µmol CO_2/mmol H_2O) in the mild winter season when GPP peaks and evaporation diminishes. Compared with published data for a similar nearby commercial orchard with x2 irrigation amount, ET was ~50%, but transpiration efficiency (Et/ET) was similar (~0.7). Our findings highlight the potential of non-commercial citrus orchard with low supplemental drip irrigation to store significant amounts of carbon with high water use efficiency, in addition to providing other ecosystem services not quantified here, such as green cover, community use, and moderating urban surface temperatures. The flux partitioning approach used here can help optimize orchard management based on the contribution of different microsites to canopy-scale fluxes.

This chapter is in review as: Qubaja, R., Tatrinov, F., Yang, F., Amer, M., & Yakir, D. (2019). Assessing CO_2 and H_2O fluxes in a non-commercial urban citrus orchard. Agricultural and Forest Meteorology.

4.1. INTRODUCTION

Approximately half of the world's population currently lives in urban areas, a proportion that is predicted to further increase (ESA-UN, 2014; Singh, 2014), influencing the limited and modified urban green spaces (Lovell and Johnston, 2009; Singh, 2014). Urban green spaces can contribute to a range of ecosystem services, including carbon storage, reducing air pollution, surface cooling and shading, as well as providing aesthetics elements (Millennium Ecosystem Assessment, 2005; McCarthy et al., 2011; Nyelele et al., 2019; Akbari, 2002; Cai et al., 2019). Nunez-Florez et al., (2019) classified 202 species of urban trees in 18 plant functional types (PFTs), indicating that citrus trees shade and carbon sequestration indices were in the highest categories among PFTs. The contribution of urban orchards and other plantations to climate change mitigation, is often neglected because such ecosystem services are not identified or quantified (Nowak et al., 2013). However, it is increasingly recognized that urban plantations are intimately linked to biogeochemical processes that govern carbon, water, and other materials in the environment (Pataki et al., 2011; Pataki et al., 2006).

Citrus orchards represent an important land use type and cover ~22% of the global irrigated agricultural land (Alexandratos and Bruinsma, 2012; Wang et al., 2017), including both commercial (61%) and non-commercial types (39%, Alexandratos and Bruinsma, 2012; Steduto et al., 2012). Partitioning ET in citrus orchards has two interesting aspects. First, their stomatal conductance is lower than in many other crops (~60% in comparison to a range of other crops, Meyer and Green, 1981; Goldhamer and Salinas, 2000) and tends to maximize early in the morning (Steduto et al., 2012), as would be expected in dry environments. Second, orchards represent a row crop in which the evaporation and heat flux measurements are notoriously difficult to make (e.g., Li et al., 2018; Agam et al., 2010; Kordova-Biezuner et al., 2000). Orchards also represent a crop system in which drip or micro irrigation is widely used, modifying soil evaporation (Es), which greatly differ in their rates under trees sites being directly influenced by irrigation and the between rows sites being directly exposed to rainfall and high radiation regimes (Zhao et al., 2018). Partitioning the CO_2 fluxes can also be challenging in orchards (e.g., Paudel et al., 2018).

Understanding the carbon and water economy of any ecosystem requires the partitioning of net fluxes into their components (Rana et al., 2018; Stoy et al., 2019), including semi-arid urban ecosystems, where carbon cycle and water budget are closely linked (Pataki et al., 2011, VPD; McCarthy et al., 2011). The eddy covariance (EC) method is commonly used to measure the net fluxes of energy, water vapor, and carbon dioxide exchange between vegetation and atmosphere, but it requires a further, and often challenging, analysis of the partitioning of these fluxes to their components, such as the evapotranspiration flux (ET) to evaporation and transpiration or the net ecosystem CO_2 exchange (NEE) to photosynthesis and respiration fluxes (Reichstein et al., 2005; Stoy et al., 2006, 2019; Talsma et al., 2018). Partitioning ET, one of the largest components of the ecosystem and the global water cycle (Raz-Yaseef et al., 2010; Stoy et al., 2019; Wang et al., 2014) is important because transpiration, Et, is strongly modified by the physiologically controlled leaf stomata, while soil evaporation, Es, is controlled by physical factors. The different controlling mechanisms of Es and Et are likely to result in differential responses to the changes in environmental and ecological parameters (e.g., Kool et al., 2014a). Methods to assess tree and ecosystem hydrology include lysimeters, whole tree chambers, eddy

covariance measurements of the above- and below-canopy fluxes, up-scaling of sap-flow measurements, and stable isotopes, all of which include some uncertainties and limitations (Cermak and Deml, 1974; Granier, 1987; Kool et al., 2014a; Kalma et al., 2008; Lu et al., 2017). The partitioning of the net ecosystem exchange of CO_2 (NEE) to gross primary productivity (GPP) and ecosystem respiration (Re) is important because of the differential sensitivity of the process underlying the photosynthesis (GPP) and respiration (Re) to environmental changes, such as temperature (e.g., Reichstein et al., 2005). A range of approaches were used to achieve the net CO_2 flux partitioning, including night-time measurements, isotopes, and carbonyl sulfide (COS) as well as meteorological and statistical approaches (e.g., Anderson et al., 2017; Blonquist et al., 2011; Epron et al., 2001; Griffis et al., 2008; Lasslop et al., 2010; Rana et al., 2018; Reichstein et al., 2005; Sulman et al., 2016; Yakir and Wang, 1996; Yang et al., 2018). A relatively new and promising approach is based on the flux-variance similarity (FVS, Rana et al., 2018) but requires leaf-level WUE measurements at a high temporal resolution and, ultimately, relies on challenging leaf temperature estimates. In the present study, direct soil chamber measurements as a basis for the flux partitioning was chosen as the most appropriate for our system of a local Mediterranean urban lemon orchard, and was attractive also because it relies on widely and continuously used measurements at a large number of EC flux sites.

4.2. MATERIALS AND METHODS

4.2.1. SITE DESCRIPTION

This study was conducted in an urban orchard in residential area of the town of Rehovot, Israel (31°54′ N, 34°49′ E, 50 m a.s.l.). The orchard is a lemon tree plantation (*Citrus limonia Osbeck*), whose trees were planted in 1976, with a 5 m distance between rows and 4 m between trees (~500 trees ha^{-1}). The current mean stem diameter is 16.5 cm at base and the mean tree height is 4.2 m. The crown closure is ~59% and the leaf area index (LAI) is 4.6. The mean annual air temperature and precipitation at the site are 19.7 °C and 537 mm, respectively. Most of the precipitation (82%) falls in the winter period, from November to February, with no rain during the June to October dry period. A drip irrigation system was used from May to September with a standard orchard management irrigation plan (total irrigation 230 mm). The soil type is a red sandy soil (*Chromic Luvisols*), with 44% sand, 24% silt, and 32% clay, and has a bulk density of 1.54 g cm^{-3} (Harmonized World Soil Database, 2012; Singer, 2007).

4.2.2. ECOSYSTEM FLUX AND METEOROLOGICAL MEASUREMENTS

A mobile laboratory was employed for the field measurements (Rohatyn et al., 2018; Yang et al., 2018), which included an eddy flux system mounted on top of an adjustable 4–28 m pneumatic mast and an air-conditioned laboratory for analytical instrumentation. Nonradiative flux measurements rely on the EC system to quantify the CO_2, sensible (Hs), and latent heat (LE) fluxes using a 3D sonic anemometer (R3, Gill Instruments, Lymington, UK) and an enclosed-path CO_2/H_2O infrared gas analyzer (IRGA, LI-7200, LI-COR, Lincoln, NE, USA). Radiation measurements included short- and long-wave radiation and photosynthetic radiation sensors (Kipp & Zonen, Delft, Holland). Sensors were placed 6.75 m above the ground at a location that insured the predominance of eddy fluxes within the orchard domain (see Yang et

al., 2018). We assumed a negligible storage flux in this open canopy, low-tree orchard. Data were collected either on a computer or using the Campbell Sci. CR3000 logger (Logan, UT, USA). The mean 30-min nonradiative (CO_2, LE, Hs) fluxes were computed using the Eddypro 5.1.1 software (LiCor, Lincoln, NE, USA). The gross primary production (GPP) was estimated by extrapolating night-time measurements (Reichstein et al., 2005).

The hourly potential evapotranspiration at the site (ET_0) was calculated using solar radiation, wind speed, air temperature, and humidity at 6.75 m above the ground from the EC mast, following the FAO approach, based on the Penman–Monteith model (Kool et al., 2014b).

The air temperature (Ta, °C), relative humidity (RH, %), and soil temperature (Ts, °C) were also measured and calculated, using the soil chambers discussed below (20 cm above the soil surface and 5 cm in depth, respectively), at 21 points and on half hourly time resolution (with up to 3 points measured simultaneously), by LI-8150-203 (LI-COR Lincoln, NE). The volumetric soil water content (SWC_{0-10}) was measured in the upper 10 cm of the soil half hourly by the ThetaProbe model ML2x (Delta-T Devices Ltd., Cambridge, UK) near the chambers (calibrated to the soil composition based on the manufacturer equations).

4.2.3. SOIL CHAMBER-BASED APPROACH

The soil CO_2 flux (Rs) was measured with an automated non-steady-state system, using opaque chambers 20 cm in diameter and a multiplexer to allow for the simultaneous control of several chambers (LI-8150, -8100-101, -8100-104; LI-COR, Lincoln, NE). Soil evaporation (Es) was measured (simultaneously) with the same system used to measure soil CO_2 fluxes. The precision of the chamber air measurements was ± 1.5% within the CO_2 (0–20,000 ppm) and water vapor (0–60 mmol mol^{-1}) ranges. The chamber was closed on preinstalled PVC collars (20 cm diameter, inserted 5 cm into the soil, and 6 cm above the surface), for a short measurement duration (2 min—for both CO_2 and water vapor), and was positioned away from the collar the rest of the time. The air from the chambers was circulated at 2.5 l min^{-1} through the infra-red gas analyzer (IRGA) and the CO_2 and H_2O concentrations were logged in the system logger (1 s^{-1}) half hourly.

The rates of soil respiration and soil evaporation were calculated from the chamber data using a linear fit of change in the water-corrected CO_2 mole and fraction air humidity, respectively (Raz-Yaseef et al., 2010; LiCor Mannual, 2015). Extensive calibration and validation of the evaporation measurements based on the soil chamber system were carried out under both field and greenhouse conditions using high-precision balance (Sartorius TE1502S, Goettingen) and bench top lysimeters (Tedea-Huntleigh Model 1042, VPG Transducers, Malvern) with the precision of 0.01 g (Qubaja et al. unpublished results). Prior to testing, the LI-8100 was also calibrated using a dew point generator (LI-610, LiCor, Nebraska).

The upscaling of the collar measurements to the plot scale was carried out according to the fraction of the relevant ecosystem component on a surface-area basis by first grouping the collars based on their location—under trees (UT, 0.3 m from nearest tree), within rows (WR, 2 m), and between rows (BR, 2.5 m)—and then by estimating the fractional areas (Ø) of the three locations based on the mapping of the sites according to the distances noted above, as has previously been done (Yang et al., 2019):

$$Xs = Xs_{BR} * \emptyset_{BR} + Xs_{WR} * \emptyset_{WR} + Xs_{UT} * \emptyset_{UT} \quad (4.1)$$

$$1 = \emptyset_{BR} + \emptyset_{WR} + \emptyset_{UT} \quad (4.2)$$

where the X values are the Es or Rs components.

The combined EC and chamber-based measurements were used to partition the ecosystem CO_2 and H_2O net fluxes. We used the Rs to partition the night-time ecosystem respiration (Re) in order to estimate the vegetation (foliage and stem) respiration (Rf) and to extrapolate the respirations components from night-time measurements to daytime values. The simultaneous temperature measurement of air and soil (20 cm above the soil surface and 5 cm in depth, respectively) allowed for estimating the temperature sensitivity factors (Q_{10}).

The total ecosystem evapotranspiration flux includes the major components of soil evaporation, Es, and tree transpiration, Et, and the minor component of canopy intercepted precipitations, which could be ignored in our study because no precipitation occurred during our measurement campaigns, simplifying the ET partitioning to:

$$ET = Et + Es \quad (4.3)$$

where the ET and Es were measured by the EC and chamber methodologies.

4.2.4. ECOSYSTEM CARBON STOCK

Standing biomass (C_{tree}): The above-ground biomass, including trees and below-ground roots, was estimated from diameter measurements at breast height (DBH, 0.3 m, 50 trees in 0.1 ha) using a metric steel diameter tape and by applying the citrus orchard allometric equations (Eq. A4.1 to 2; Schrothet al., 2002; Segura et al., 2006). The results from the two equations were then averaged to improve reliability. Dry matter and C contents of individual tree parts were determined on samples dried at 80 °C. The roots (< 2 mm and < 5 mm diameter) were sampled from three points, at 0.3, 2.0, 2.5 m from the trees (2 samples/distance), were washed of soil through a series of sieves before analysis, and the root carbon was included in the C stocks of the tree biomass. The carbon content results were used to convert the dry mass values from the allometric equation to the C stock per surface area (as in Grünzweig et al., 2007). The understory herbaceous biomass was analyzed in the same manner as above and was included in the soil C stocks.

Litter and soil (C_{soil}): The shallow litter layer was sampled in 2016, within a grid of 30×30 cm, from three points at 0.3, 2.0, 2.5 m from the trees (2 samples/distance). The litter C stock was presented as part of the soil carbon fraction. The soil was sampled using a 5 cm diameter core under each of the litter measurement points (Multi-Stage Soil Core Sampler; AMS Inc., Idaho). The coring of the mineral soil was carried out at different depths (0–5, 5–10, 10–20, and 20–50 cm), according to the procedure described in Schulze et al. (2000).

In the lab, the soil samples were air-dried, sieved (2 mm), and mixed. For the C analyses, the subsamples were treated separately (6 cores x 4 layers). The sieved soil was ground to pass a 250 µm sieve and the total C concentrations were determined in an elemental analyzer (EA 1108, Carlo-Erba, Milan, Italy). The soil organic carbon, SOC, was measured following the removal of inorganic carbon by treating the ground soil samples with acid (1N HCl) and by shaking the samples in 180 revolutions min^{-1}

for 24 h, according to the procedure of Midwood and Boutton (1998). The coarse organic matter (more than 2 mm) and the fine fraction were combined in estimating the SOC concentration and stocks. The C stock was corrected for differences in bulk density by the equivalent soil mass method (Grünzweig et al., 2004). Further soil subsamples were dried at 105 °C to determine the moisture content.

4.2.5. CARBON TURNOVER

The mean orchard carbon turnover time (τ) was estimated according to.

$$\tau = C_{stock}/F \quad (4.4)$$

The flux (F) used in Eq. 4.4 was based on first on GPP, assuming a near steady state, and was used for comparison with published values. Recognizing that our ecosystem may not be at a steady state, we subsequently estimated τ also based on Re and used the total ecosystem, tree, and soil stocks (C_{soil}, C_{tree}, where $C_{eco}=C_{soil} + C_{tree}$) to estimate τ_{eco} or τ_{tree} and τ_{soil}, respectively. To obtain separate estimates of the C turnover time for the soil and the standing biomass, we subtracted the live-root C from the total soil C stock and added it to the standing biomass. The live-root C was estimated to be 6 ± 2% (mean ± s.e., n = 6) of the total orchard SOC, according to our measurements at the site (see section 2.4 for root density sampling).

4.2.6. STATISTICAL ANALYSES

A paired t-test was used to detect significant differences in C concentrations, soil stocks at all depths, and tree stock between the open field and the orchard. Calculations of the C stocks and fluxes were normalized using soil cover, plant density, and soil properties (i.e., soil bulk density and gravel content from the present study). The paired t-test was used to detect significant differences in the Rs, Es, and metrological parameters between microsites (BR, WR, and UT) with the significance level set at 0.05. To quantify the spatiotemporal variability of soil fluxes, the coefficient of variation (CV%) was calculated as:

$$CV = \frac{\text{Standard deviation}}{\text{mean}} \times 100\% \quad (4.5)$$

Heterogeneity was considered weak if CV% ≤ 10%, moderate if 10% < CV% ≤ 100%, and strong if CV% > 100%. All the analyses were performed using the Matlab software, Version R2017b (MathWorks Inc.).

4.3. RESULTS

4.3.1. SPATIOTEMPORAL VARIATIONS IN SOIL FLUXES

***Soil CO_2 flux (Rs)*:** On the diurnal time-scale, the Rs values generally peaked between 10:00–11:00 and between 12:00–13:00 during the dry and wet periods, respectively (Figures 4.1 and 2). On the seasonal time-scale, the Rs at the UT microsites showed the highest rates during the dry period (July), with diurnal mean rates of nearly 10.6 µmol m^{-2} s^{-1}, and more moderate ones, ~3.4 µmol m^{-2} s^{-1}, during the wet period

(January, Figure 4.2). At the WR sites, the Rs values were 2.3 µmol m^{-2} s^{-1} during the dry season and 1.6 during the wet period. At the exposed BR sites, a minor emission (less than 1 µmol m^{-2} s^{-1}) was observed in both seasons. The seasonal microsite Rs decreases from dry to wet season were associated with increases in the respiration of the seasonal microsite Q_{10} values by 17, 69, and 78% at the UT, WR, and BR sites, respectively. Noticeably, the microsite Q_{10} values were higher during the wet season than the dry season (Table 4.1).

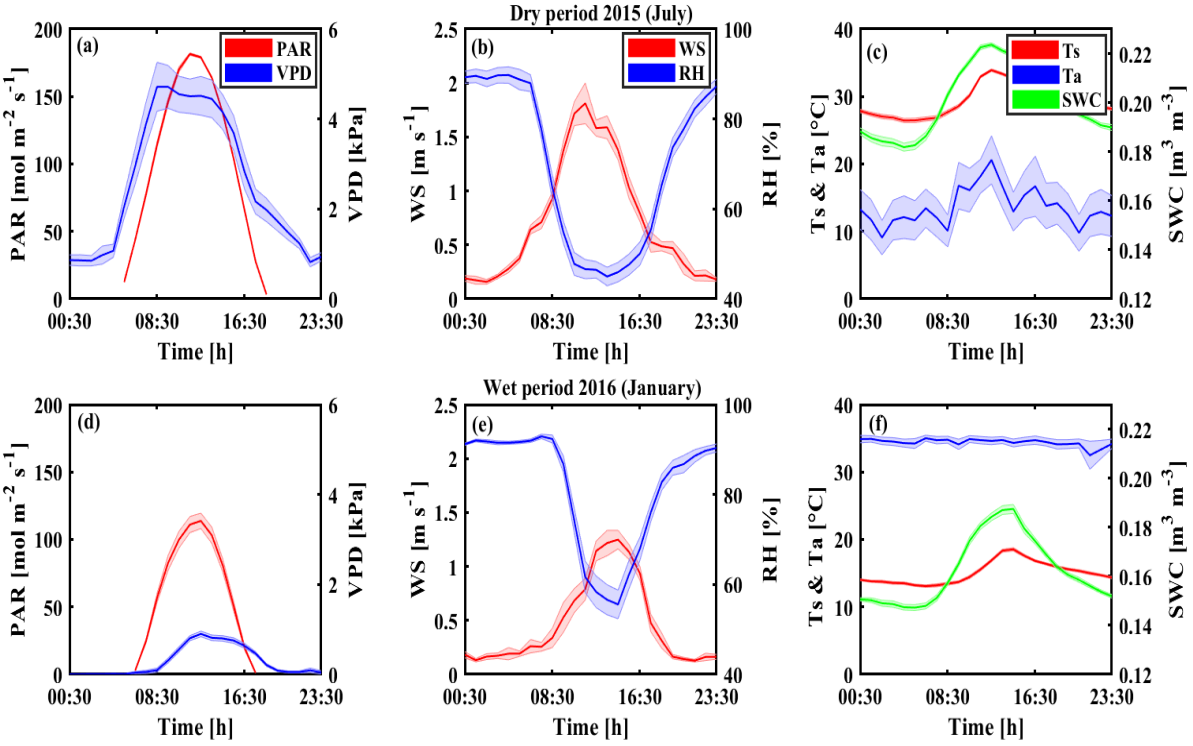

Figure 4.1 | Typical diurnal cycle of the meteorological parameters during the dry period (July 2015; upper panels) and for the wet period (January 2016; lower panels); each set includes a campaign of half-hour measurements. a and d) incoming photosynthetic activity radiation above canopy (PAR) and vapour pressure deficit (VPD); b and e) wind speed (WS) and relative humidity (RH); and c and f) air temperature at 20 cm (Ta), and soil temperature at 5 cm (Ts) and soil water content at the top 10 cm (SWC0-10cm). Shaded areas indicate ±se. PAR measurements from meteorological station Beit Dagan. Based on half-hour values averaged across each campaign.

Soil was always a source of CO_2 due to respiration (combined autotrophic and heterotrophic respiration). Soil fluxes showed significant heterogeneity at both the spatial (microsites) and temporal (diurnal and seasonal, Figure 4.2, Table 4.1) levels. Overall, the hourly soil respiration (Rs) varied from 0.3 to 12.5 µmol m^{-2} s^{-1}, with a mean value of 2.12 ± 0.03 µmol m^{-2} s^{-1}. On the spatial scale, the Rs showed systematic differences among the microsites, with the highest flux under trees (UT), moderate emissions between trees (WR), and lowest emissions in the exposed area between rows (BR), with diurnally mean values across seasons of 7.0, 1.9, and 0.7 µmol m^{-2} s^{-1}, (SD ± 0.1 µmol m^{-2} s^{-1} or better) for the three microsites, respectively. The ecosystem soil Q_{10} value across seasons and microsites was 1.6, with an increase from 1.0 to 1.5 during the dry and wet seasons, respectively.

The spatial variability of Rs for all microsites showed high variations (CV 105%). The Pearson correlation analysis results showed negative correlations of Rs vs. Dt, Ts, and Ta (r = 0.97 and 0.4, 0.4, respectively; significant at $p < 0.01$ only for Dt) and a positive correlation with $SWC_{0\text{-}10}$ and RH (r = 0.8 and 0.4, respectively).

Table 4.1 | Seasonal mean of half-hour values across sites (BR, between-rows; WR, within-rows; UT, under-trees) and study period, of soil respiration (Rs), soil evaporation (Es) and adsorption averaged for event days (Ea; represent fluxes from the atmosphere to the surface), together with the soil water content at 10 cm depth (SWC), soil temperature at 5 cm depth (Ts), air temperature (Ta), relative humidity (RH) at the soil surface, and Q_{10} as derived seasonally and annually for the microsites; Note: all of the water components multiplied by 100 for convenience; numbers in parenthesis indicate ±se.

Season	Sites	Rs	Es	Ea	SWC	Ts	Ta	RH	Q_{10}
		[µmol m^{-2} s^{-1}]	[x100 mmol m^{-2} s^{-1}]		[x100 m^3 m^{-3}]	[ºC]	[ºC]	[%]	S
Dry	UT	10.6 (0.05)	43.8 (1.4)	-10.1 (0.3)	23.0 (0.2)	28.2	29.4	69.5	1.1
	WR	2.3 (0.01)	16.1 (1.1)	-13.8 (0.4)	19.3 (0.1)	28.0	29.2	70.3	0.7
	BR	1.0 (0.01)	6.7 (0.9)	-11.7 (0.3)	8.0 (0.1)	31.5	29.4	69.8	1.5
	Stand	**2.9 (0.01)**	**22.2 (1.0)**	**-11.9 (0.3)**	**15.8 (0.2)**	**29.4**	**29.3**	**70.0**	**1.0**
Wet	UT	3.4 (0.02)	16.2 (1.3)	-3.3 (0.2)	21.4 (0.1)	15.6	15.2	82.2	1.3
	WR	1.6 (0.01)	4.6 (0.9)	-13.7 (0.0)	21.9 (0.0)	14.6	15.2	82.4	1.1
	BR	0.5 (0.01)	60.5 (5.7)	-2.2 (0.0)	19.4 (0.0)	15.5	15.7	79.8	2.6
	Stand	**1.4 (0.01)**	**27.1 (2.3)**	**-2.2 (0.2)**	**21.5 (0.0)**	**15.1**	**15.4**	**81.3**	**1.5**

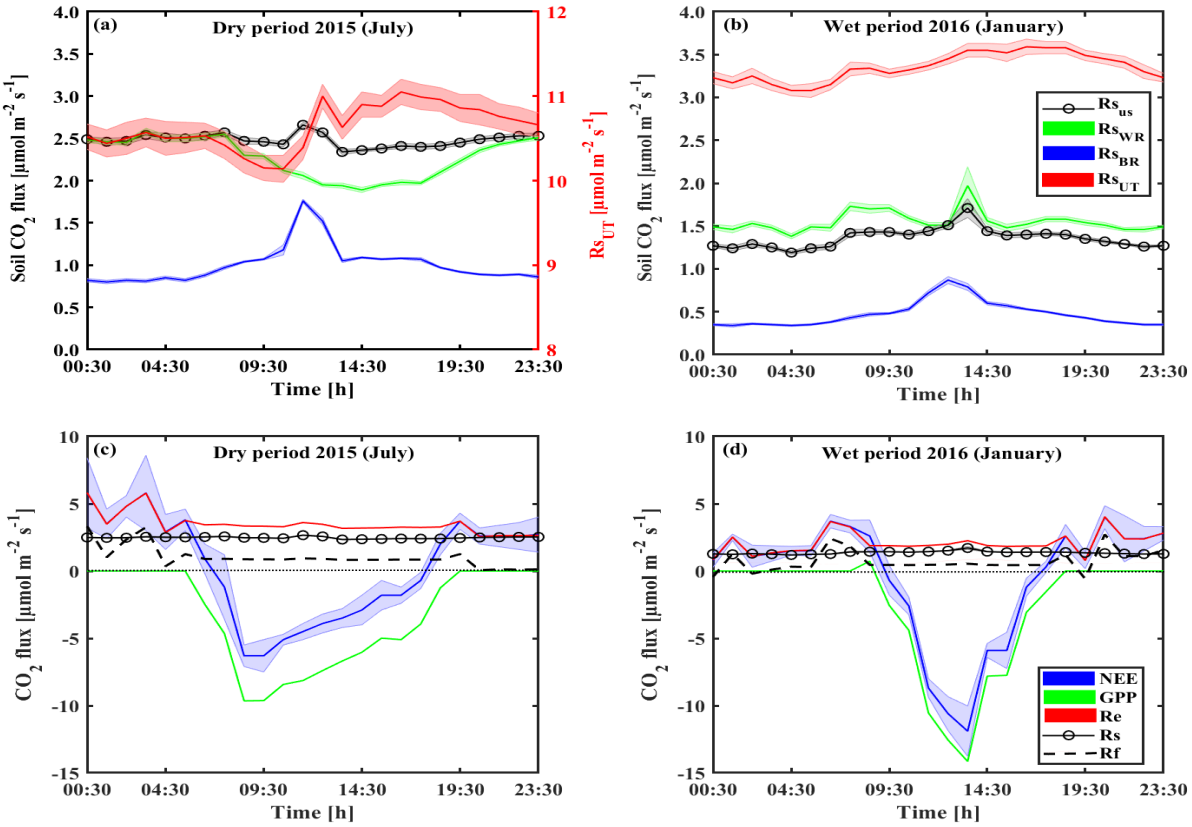

Figure 4.2 | Representative diurnal cycles of soil respiration (Rs; using soil chambers across microsites: between-rows, BR; within-row, WR; under-trees, UT) in panels a and b, and of net ecosystem exchange (NEE; canopy scale eddy covariance) and gross primary production (GPP), and ecosystem respiration (Re) and its partitioning to soil respiration (Rs) and aboveground tree respiration (Rf) in panels c and d, during the dry (July) and wet (January) periods. Based on half-hour values averaged across each campaign; shaded areas indicate ±se; Rf was estimated as the residual as Rf=Re-Rs and was presented as black-dashed line.

The temporal variations in the half-hour values of Rs (CV 31%) reflected the

changes in the soil moisture at 0–10 cm depth, Ts and Ta. The Pearson correlation analysis showed positive correlations of Rs vs. Ts and vs. Ta (r = 0.94 and 0.8, respectively, $p < 0.01$, for both independent variables), whereas there was a negative correlation with SWC (r = 0.7).

A multiple linear regression, combining the Ts and $SWC_{0–10}$ (0–10 cm soil depth for both independent variables), provided a reasonable description of the temporal variability of Rs (μmol m^{-2} s^{-1}; R^2=0.9, p<0.0001):

$$Rs = 1.855 * \exp(0.03649 * Ts - 6.657 * SWC + 14.73 * SWC^2) \qquad (4.6)$$

***Soil evaporation (Es)*:** The soil evaporation (Es) rates varied both spatially and temporally in similar patterns to those of the Rs rates and with an overall range of -0.8 to 6.1 mmol m^{-2} s^{-1}, with a mean value of 0.25 ± 0.01 mmol m^{-2} s^{-1}. The highest Es values were observed at the BR sites during the wet period (January, Table 4.1) and at the UT sites during the dry period (July, Table 4.1), with intermediate (0.16–0.44 mmol m^{-2} s^{-1}) and low values (less than 0.17 mmol m^{-2} s^{-1}) at the UT and WR sites, respectively. On the diurnal time-scale, the Es values were generally peaking in the same trend as the Rs values during the dry and wet periods, declining at night and early morning (Figures 4.2 and 3).

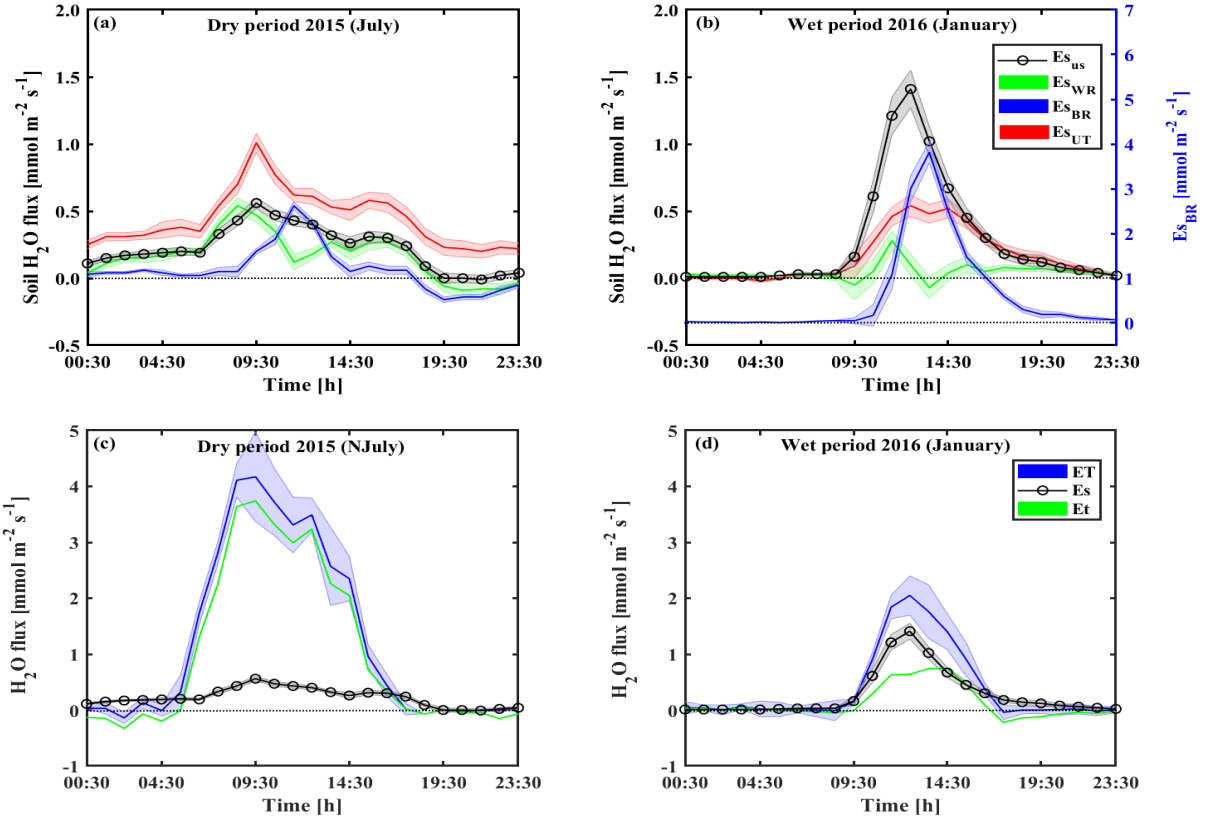

Figure 4.3 | Representative diurnal cycles of soil evaporation (Es; using soil chambers across microsites: between-rows, BR; within-row, WR; under-trees, UT) in panels a and b, and of evapotranspiration (ET; canopy scale eddy covariance), and its partitioning to soil evaporation flux (Es) and tree transpiration (Et) in panels c and d, during the dry (July) and wet (January) periods. Based on half-hour values averaged across each campaign; shaded areas indicate ±se; negative values represent fluxes from the atmosphere to the surface; Et was estimated as the residual as Et=ET-Es).

Soil moisture adsorption events were identified as consistent negative evaporation fluxes (see Methods). The average soil adsorption fluxes were -0.07, -0.14, and -0.07 mmol m^{-2} s^{-1} for the three microsites (UT, WR, and BR), respectively, and had variations around the mean that were smaller than the precision of the measurement Overall, the hourly soil adsorption (Ea) varied from -0.76 to -0.01 mmol m^{-2} s^{-1}, which was negligible when considered on an annual scale.

The soil evaporation for all microsites showed moderate variations (CV 51%). The Pearson correlation analysis, r value) results showed insignificant negative correlations of Es vs. relative humidity (RH), soil moisture (SWC, 0–10 cm soil depth), and distance from trees (Dt), with r = 0.8, 0.5, and 0.2, respectively, and insignificant positive correlations with soil temperature (Ts) and air temperature (Ta) at r = 0.8, without significant differences between the two temperature records.

The temporal variations in the half-hour values of the Es reflected the changes in the Hs and RH at soil surface (not shown, for more meteorological parameters see Fig 4.1). The Pearson correlation analysis showed significant negative correlations of Es vs. Hs and vs. RH (r = -0.7 and 0.6, $p < 0.01$, for both independent variables), whereas there were minor positive correlations with vapor pressure difference, VPD, and SWC (r = 0.3 and 0.1, $p < 0.01$), respectively. The variations in the half-hour values for the up-scaled Es showed a CV of 166%, with the temporal heterogeneity dominated by Hs with high CV > 100% and moderate RH with CV ~34%.

A multiple linear regression, combining the Hs (W m^{-2}), RH (%, 10 cm above the soil surface), and VPD (kPa), provided a reasonable description of the temporal variability of Es (mmol m^{-2} s^{-1}; R^2=0.80, p<0.0001):

$$Es = 1.775 - (0.003 * Hs) - (0.19 * VPD) - (0.017 * RH) \quad (4.7)$$

4.3.2. ECOSYSTEM-SCALE FLUXES PARTITIONING

Table 4.2 | Seasonal and annual values of ecosystem respiration (Re), its components and associated ratios, net ecosystem exchange (NEE; from eddy covariance), gross primary productivity (GPP), carbon turnover times, (τ, years) in the present study (2015-2016). Rs and Rf denote soil, and foliage and wood CO_2 flux. Annual values are based on the diurnal mean (daytime only for GPP) half-hour values of the two seasons and converted to monthly or annual scale arithmetically, to obtain a first approximation of the apparent carbon turnover time in the system (τ=C stock/Re).

		Flux measurements						
		Rs	**Rf**	**Re**	**NEE**	**GPP**	**Rs/Re**	**Rf/Re**
Dry	**[µmole CO_2 m^{-2} s^{-1}]**	2.48	1.02	3.50	0.23	-6.03	0.71	0.29
	[g C m^{-2} $month^{-1}$]	78	32	110	7	-103		
Wet	**[µmole CO_2 m^{-2} s^{-1}]**	1.36	0.72	2.08	-0.57	-6.37	0.65	0.35
	[g C m^{-2} $month^{-1}$]	43	23	66	-18	-84		
Annual	**[g C m^{-2} y^{-1}]**	726±106	329±28	1055±134	-65±76	-1120±58	0.69	0.31
	x/GPP	0.65	0.29	0.94	0.06			

	Carbon stock			Turnover times (based on Re)		
	C_{soil}	**C_{tree}**	**C_{eco}**	**τ_{soil}**	**τ_{tree}**	**τ_{eco}**
	[g m^{-2}]			**[y]**		
Total	3803	1899	5702	4	2	5.4

***Net ecosystem exchange and respiration partitioning*:** The EC-based cumulative

net ecosystem CO_2 uptake (NEE) during the two-campaigns showed a changed from a 'source' of 7 g C m^{-2} $month^{-1}$ during the dry period to a 'sink' of -18 g C m^{-2} $month^{-1}$ during the wet period (Table 4.2). Postprocessing of NEE (see Methods) permitted the estimation of seasonal-scale GPP, indicating a decrease of GPP from 103 to 84 g C m^{-2} $month^{-1}$ over the summer and winter seasons, respectively. In turn, the values of seasonal ecosystem respiration, Re, were estimated at 110 and 66 g C m^{-2} $month^{-1}$ in the summer and winter seasons, respectively.

The seasonal partitioning of ecosystem respiration, Re, into the soil, Rs, as well as foliage and wood, Rf, components was assessed for the orchard system using the integrated ecosystem scale Rs estimate from the three microsites (Figure 4.2). The Rs/Re values were 71% and 65% for the dry and wet seasons, respectively (Table 4.2). Subtracting the Rs from the Re was used to estimate the Rf. The Rf rates ranged between 1.02 and 0.72 µmol m^{-2} s^{-1} in the summer and winter, respectively (Table 4.2). The summer Rf/Re was 29 ± 3% and the winter ratio was 35 ± 7% (Table 4.2).

***Evapotranspiration partitioning*:** The integration of the soil chamber measurements were used to estimate the total soil evaporation (Es) flux and partitioning of the EC-measured ET flux, where both were used to estimate the tree transpiration flux (Et, where Et = ET – Es), using the observed seasonal values of the Es/ET ratios of 0.18 and 0.70 during the dry and wet periods, respectively. The estimated transpiration (Et) rates changed between 1.02 and 0.12 mmol m^{-2} s^{-1} and the Et/ET ratio changed between ~0.82 and 0.30 in the summer and winter seasons, respectively (Table 4.3).

Table 4.3 | Components of the water balance of the ecosystem, its components and associated ratios. ET is evapotranspiration is from eddy-covariance measurements (ET), P, I, Es and Et denote precipitation, irrigation, soil evaporation, tree transpiration. For comparison, values from a similar commercial orchard in the same area are quoted (see text for detail). Annual flux values are based on the measured half-hour values of the two seasons averaged across all days of the same campaign and assuming, for a first approximation that each campaign represent the half year mean (as supported by the reasonable ET/(P+I) ratio.

Study			P [mm y^{-1}]	I [mm y^{-1}]	Es [mmol m^{-2} s^{-1}]	Et [mmol m^{-2} s^{-1}]	ET [mmol m^{-2} s^{-1}]
Present study (2015-2016)	**Dry**	**[mmol m^{-2} s^{-1}]**			0.22	1.02	1.25
		x/ET			0.18	0.82	
	Wet	**[mmol m^{-2} s^{-1}]**			0.28	0.12	0.40
		x/ET			0.70	0.30	
	Average of x/ET				0.44	0.56	
Kalma and Stanhill (1969)	**Dry**	**[mmol m^{-2} s^{-1}]**			0.46	1.34	1.80
		x/ET			0.26	0.74	
	Wet	**[mmol m^{-2} s^{-1}]**			0.31	1.36	1.67
		x/ET			0.19	0.81	
	Average of x/ET				0.25	0.75	
Present study (2015-2016)	**Annual**	**[mm y^{-1}]**	484	230	142±7	325±128	467±121
		x/ET			0.30	0.70	
		x/ET_0			0.12	0.27	0.39
		ET/(P+I)					0.65
Kalma and Stanhill (1969)	**Annual**	**[mm y^{-1}]**	673	483	217	633	850
		x/ET			0.26	0.74	
		x/ET_0			0.14	0.40	0.54
		ET/(P+I)					0.74

***Water use efficiency*:** The seasonal-scale water use efficiency values, based on the linear relationships between the daytime eddy covariance estimates of carbon and water fluxes during the dry (July 2015) and wet (January 2016) periods, showed an

increase from -1.6 in July 2015 to -6.1 µmol CO_2 mol^{-1} H_2O in January of the following year in the ecosystem-scale values (WUEs=NEE/ET, Figure 4.4) and from -1.7 to -11.7 in the canopy-scale values (WUEp=GPP/Et).

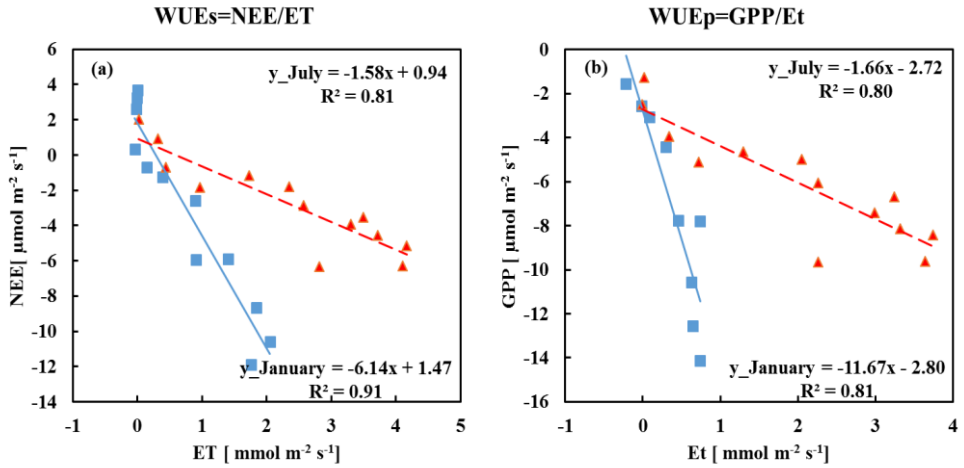

Figure 4.4 | Seasonal changes in water use efficiency (WUE; slope of linear fite line) during the dry (July 2015 campaign) and wet (January 2016 campaign) periods. a) WUE is based on the daytime eddy covarieance measurements of NEE vs. ET; and b) WUE based on daytime GPP vs. Et. Data shown are based on mean daily cycle obtain from hourly data (average of two half hour measurements points) for the same hour averaged across all days of the same campaign.

4.3.3. CARBON ACCUMULATION RATES AND CARBON STOCKS

The current mean C stock was estimated at 5,702 g C m^{-2}, divided between the biomass and the soil organics (1,899 and 3,803 g m^{-2}, respectively, Table 4.2). The carbon in the orchard was stored mainly in the soil (67%, Table 4.2), with 82% of it stored in the upper layers (0–20 cm, Table A4.1). The carbon storage in the above- and below-ground standing biomass was ~27% and 6% of the total C stock, respectively (Table A4.1). The spatial distribution of soil carbon indicated higher C content in the UT and WR microsites in comparison to the BR microsites (by 129% and 111%, respectively). The fine root C stocks for the BR, WR, and UT microsites were 45 ± 27, 98 ± 61, and 1184 ± 296 g m-2 and were scaled to 223 g m^{-2} (6 ± 2% of the total SOC).

Assuming, for a first approximation, that the mean flux values for the wet and dry seasons can be reasonably used to estimate the annual-scale fluxes (the Re, in this case), together with our estimates of the system carbon stock, provides an opportunity to obtain a first estimate of the ecosystem apparent C turnover time ($\tau_{eco\text{-}Re}$, years, Equation 4.4, Table 4.2) and its two main components—the standing biomass, (τ_{tree_Re}) and soil (τ_{soil_Re}). As expected, the results show that the carbon turnover time in the standing biomass was 1.8 years and in the soil 3.6 years, resulting in an overall ecosystem carbon turnover time of 5.4 years (Table 4.2).

4.4. DISCUSSION

4.4.1. CARBON FLUXES AND STOCK

Citrus orchards are a significant global crop with a favorable C sequestration potential

but little information about the carbon balance of citrus orchards to quantitatively support these assessments. Comparing the CO_2 fluxes in this study with the fluxes reported at other sites showed that our mean NEE (-0.17 µmol m^{-2} s^{-1}, range -14.1 to +5.8) was within the NEE range found across other citrus orhards sites (-33 to +17 µmol m^{-2} s^{-1}, Maestre-Valero et al., 2017). It also showed similar seasonal shifts from source during the dry season to sink during the wet season. In comparison to recently reported GPP values for the same site by Yang et al. (2018), the GPP values were 91% (3.3 vs. 3.6 µmol m^{-2} s^{-1}) and 104% (2.7 vs. 2.6 µmol m^{-2} s^{-1}) for the summer and winter seasons, respectively, providing confidence in our measurements, which are within the range reported for other sites (see also Consoli et al., 2014; Peddinti et al., 2019). Our estimates of the soil CO_2 efflux of 2.1 µmol m^{-2} s^{-1} (1.4 during the wet and 2.9 during the dry season) are also consistent with the values obtained across other citrus orchard sites (0.3 to 4.1 µmol m^{-2} s^{-1}, Paudel et al., 2018; Sheng et al., 2010; Liguori et al., 2009; Liu et al., 2008; González-Real et al., 2018).

The Rs vs. soil temperature, Ts, relationships were used to estimate the apparent Q_{10} values and indicated an increase from Q_{10} = 1.0 in the dry season to Q_{10} = 1.5 in the wet season. This represents a similar trend in Q_{10} when compared with the results of Grünzweig et al. (2009) for pine stands in the same region and is consistent with published values that range from Q_{10} of 1.15 to 2.0 among citrus orchards (González-Real et al., 2018; Sheng et al., 2010; Paudel et al., 2018). The low temperature sensitivity in the dry season may be related to reduced microbial activity but may also involve down regulation of the plant activity (Maseyk et al., 2008) and root dormancy (Schiller, 2000). Note that the variations in the Q_{10} of the total soil Rs likely reflect a differential Q_{10} response of the soil heterotrophic and autotrophic respiration, Rh and Rsa (Yu et al., 2017; Matteucci et al., 2015; Kuzyakov, 2006; Rey et al., 2002). Ultimately, low Q_{10} values, should enhance carbon storage.

The type of land-use is an important factor that controls soil organic carbon (SOC) because it affects the processes involved in stabilizing the SOC, such as the amount and quality of litter input, and decomposition rates (Abera and Belachew, 2011). The carbon storage of orchards is considered to be lower than that of forests but higher than that of grasslands, herbaceous crops, and agricultural lands (Janssens et al., 2003; Wang et al., 2014). Soil C accounted for ~67% of the ecosystem C stock in the present study (3,803 gC m^{-2}). This is a similar value to that reported by Song, Li et al. (2005) for agricultural soil (3,840 g m^{-2}). Wang et al. (2017) estimated that the mean SOC in citrus orchards doubled (to 4,170 g m^{-2}) over 28 years.

However, our estimated τ_{eco}, of 5.4 years (Table 4.2) is relatively short in comparison to the wide range of published estimates (10–255 years, Yan et al., 2017; Wu et al., 2018) and similar to that for the temperate cropland-dominated regions with a short τ_{tree} < 4 yr (Wu et al., 2018). Short residence time indicates, in turn, a relatively high sensitivity of the ecosystem carbon storage to any disturbance, changes in environmental conditions, or any factor that influences the carbon fluxes through the system. Note also that, at present, the orchard that served as the site for our study is near steady state with the input and output fluxes being nearly equal (Re/GPP = 0.94, on average).

4.4.2. WATER COMPONENTS

The ET values observed at our site (1.25 and 0.40 mmol m^{-2} s^{-1} during the dry and wet seasons, Table 4.3) are similar to other reported values in commercial orchards and vineyards (Kerridge et al., 2013; Shapland et al., 2012; Yunusa et al., 2004; Kool et

al., 2016; Maestre-Valero et al., 2017; Kalma and Stanhill, 1969). In the winter season, Kalma and Stanhill (1969) reported higher ET values in a nearby commercial orchard than those in the present study, however, this was also associated with about x2 supplement irrigation and the possible effects of higher precipitation preceding the measurements—84 mm vs. 19 mm in the two studies, respectively. Using our seasonal data to obtain a first approximation of the annual scale ET values, we estimate that its fraction from the total input ET/(P + I) was ~0.65 in comparison to ~0.74 obtained at the similar commercial orchard site used by Kalma and Stanhill (1969), with a higher LAI but also wetter year.

Our estimates of Et/ET (0.82 and 0.30 during the dry and wet seasons, Table 4.3) are also consistent with the published values for row crops such as vineyards (Kool et al., 2014a; Ferreira et al., 2012; Kerridge et al., 2013; Yunusa et al., 2004). It is particularly interesting to compare our results to those of Kalma and Stanhill (1969), which were obtained from a study of a similar irrigated commercial citrus orchard in the same area (Table 4.3). As environmental conditions in the two study years were not identical, we specifically considered the hydrological ratios. For example, their dry season Et/ET of 0.74 was similar to the result in the present study, despite the fact that the commercial orchard received about a two-fold higher irrigation. This likely reflected the strong hydraulics and stomatal conductance control over the Et flux in this crop (Meyer and Green, 1981; Goldhamer and Salinas, 2000). Also note that, although the differences in the Et/ET results between the two studies were relatively small, the complementary changes in the fraction of soil evaporation may be more significant with the Es/ET of 0.18 in the present study vs. 0.26 in the earlier study during the dry season. That is, in spite of the lower canopy cover and LAI, the dryer orchard in the present study showed improved water use, thus further reflecting the interactions between stand density and water availability (Breshears, 2006; Adams et al., 2012). Furthermore, unlike the earlier study, where the Et/ET remained high during the wet period (0.81), a large decrease in this season was found in the present study (to 0.30, Table 4.3), which can be influenced by the higher amount of precipitation during the earlier study (by ~40%) and the higher LAI (by ~35%).

4.4.3. WATER USE EFFICIENCY

Estimating the water use efficiency (WUE) is particularly important today, considering the drying trends in many regions, and the rising atmospheric CO_2 concentrations that may influence this parameter. This is true also in urban systems (Grote et al., 2016; Sun et al., 2013). The flux partitioning, as carried out here, allows for a direct assessment of the plant WUE (WUE_p; Guerrieri et al., 2019; Peddinti et al., 2019), as well as for a comparison between the plant and the stand-scale WUE_s (GPP/Et or NEE/ET). In general, the stand-scale WUEs values estimated at the study site (Fig 4.4) are in the range of published values (e.g., Maestre-Valero et al., 2017; Peddinti et al., 2019). The results, however, showed two clear features: A marked change in plant WUE_p across seasons (but not in WUE_s), and a marked increase in WUE in going from the stand-scale to the plant-scale (Fig 4.4). The seasonal changes from high WUE_p in winter to low values in summer seems to reflect the local Mediterranean conditions (Fig 4.1). The mild winters promote high rates of carbon uptake that, with the help of the supplementary irrigation, remain relatively high throughout the year (Table 4.2), with higher peak values in winter but longer days in summer (Fig 4.2). In contrast, plant transpiration, Et, is strongly suppressed in winter (by nearly 90%, associated with the low values of temperature, radiation, and VPD;

Fig 4.1), resulting in the observed large increase in the plant WUE (GPP/Et). Notably WUE_p remains relatively high in the hot and dry summer conditions. This is likely due to maintaining high photosynthetic activities with the supplementary drip irrigation under the trees, while limiting soil evaporation in the exposed BR microsite. This is clearly reflected in the low Es/ET values in summer (Table 4.3).

The large differences between plant and stand level WUE values seems to reflect not only the highly efficient gas exchange of the plants, but also the more modest decrease in ET and Re from summer to winter. This is expected considering the large increase in soil evaporation from the wet soil in winter (when shifting from drip irrigation under the trees to precipitation), compared to the dry soil in summer, in the BR microsites (Table 4.2). Similarly, Re (the difference between GPP and NEE) decreased proportionally much less than ET (~40% vs. ~70%) moderating any change in WUEs.

Thus, the changes in WUE_s reflect more synchronized changes in ecosystem carbon and water fluxes, while WUE_p reflect the strong seasonal adjustment in leaf transpiration. The overall response seems to reflect a relatively efficient gas exchange economy. Interestingly, the seasonal changes in WUE observed in the present study are consistent with those reported for nearby drought resistance semi-arid pine forests (Grünzweig et al., 2009), and higher than reported for other urban trees (e.g. McCarthy et al., 2011), which may further demonstrate the successful ecophysiological adjustments in the urban citrus orchard that produce highly effective ecosystem water and carbon management in these local climatic conditions.

A4. APPENDIX

The stem diameter (DBH) of the orchard trees were sampled at 30 cm above the ground to avoid the grafted stem and the tree forking at 130 cm. Two allometric equations given by Schroth et al., (2002) and Segura et al. (2006), were used to estimate the aboveground biomass. The results from the two equations were then averaged to improve the accuracy.

The aboveground biomass was determined using allometric equations for *Citrus sinensis* as shown in equations A4.1 and 2:

$$AGB_{tree} = 10^{-0.834+2.223*LOG(DBH)} \quad (A4.1)$$

$$AGB_{tree} = \exp(-1.996 + 2.32 * \ln(DBH)) \quad (A4.2)$$

where AGB_{tree} is the aboveground biomass per tree (kg/tree).

The belowground biomass (BGB_{tree}, kg/tree) was estimated from the ratio of the shoot to root ratio of 4:1 (Hairiah et al., 2001). From this relationship, the BGB_{tree} can be calculated as follows:

$$BGB_{tree} = \frac{AGB_{tree}}{4} \quad (A4.3)$$

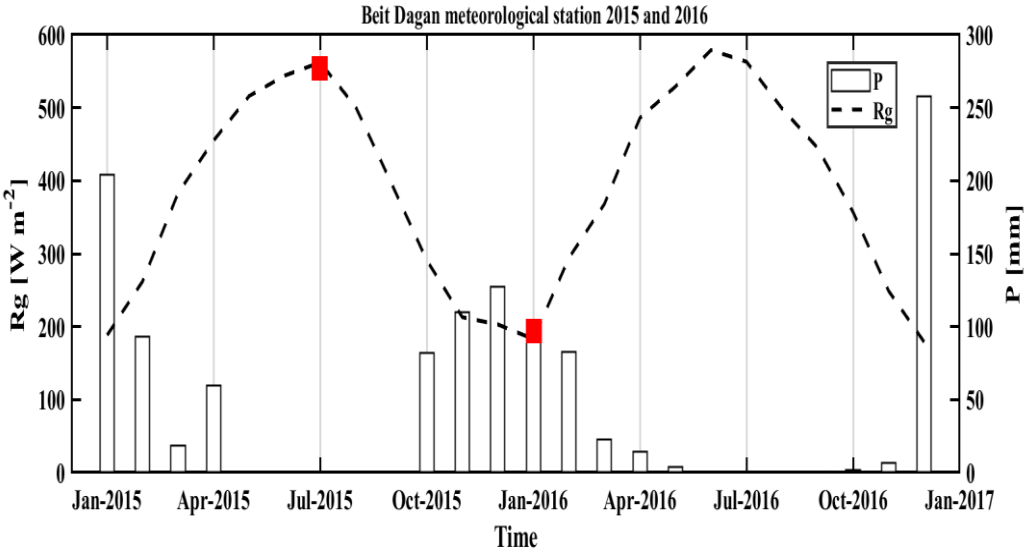

Figure A4.1 | Seasonal trends of monthly mean values of key environmental parameters during two years from nearby meteorological station Beit Dagan, direct radiation (Rg) and precipitation (P), red rectangles are the measurements campaigns in the orchard (July 2015 and January 2016).

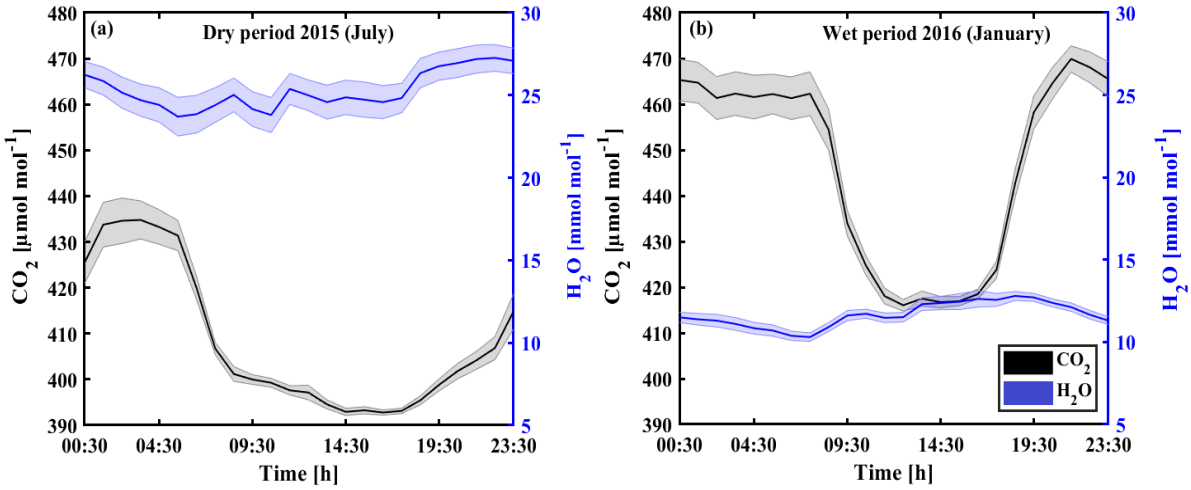

Figure A4.2 | Representative diurnal cycles of the ambient H_2O and CO_2 concentrations above canopy during a) the dry season (July 2015) and b) the wet season (January 2016) periods, each set includes a campaign of half-hour measurements. These concentrations were measured with the EC; shaded areas indicate ±se.

Table A4.1 | Breakdown of the carbon stocks in the orchard as estimated from soil cores samples and using allometric equations of C in 2016; mean±(SE) for plots.

	Carbon stock [g m^{-2}] 2016
1. Standing biomass	
Stem	1545 (142)
Branches	353 (33)
Total standing biomass	**1899 (175)**
2. Soil	
Litter layer	129 (40)
0–5 cm	1461 (52)
5-10 cm	899 (46)
10–20 cm	777 (114)
20–50 cm	538 (200)
Total soil	**3804 (349)**
Total ecosystem (current)	**5702 (524)**

Table A4.2 | Exponential and linear relationships between soil respiration rate (Rs) and abiotic factors July-August, 2015 and January 2016. T: soil temperature; SWC: soil water content; D: distance to the stem. The best-fit model parameters (β_0, β_1, β_2, and β_3) and standard error are reported for each model together with the squared coefficient of regression (R^2), and the root mean squared error (RSME).

a) Individual values (whole half-hour measurements)

Model	β_0	β_1	β_2	β_3	R^2	RMSE
$\beta_0 + \beta_1 T$	1.305	0.087			0.054	2.589
$\beta_0 e^{\beta_1 T}$	2.152	0.018			0.04	2.61
$\beta_0 + \beta_1 \theta$	-1.25	23.56			0.282	2.256
$\beta_0 + \beta_1 F$	0.923	0.226			0.943	0.6342
$\beta_0 + \beta_1 / D$	1.048	0.497			0.783	1.239
$e^{\beta_0+\beta_1\theta+\beta_2\theta^2}$	-2.284	24.38	-35.11		0.307	2.217
$\beta_0 e^{\beta_1 T} e^{\beta_2\theta+\beta_3\theta^2}$	0.017	0.04	32.9	-55.04	0.457	1.9636
$\beta_0 e^{\beta_1 T} e^{\beta_2 D}$	2.339	0.043	-0.747		0.935	0.68

b) Up-scaled values (unscaled time series from the microsites)

Model	β_0	β_1	β_2	β_3	R^2	RMSE
$\beta_0 + \beta_1 \theta$	4.494	-12.38			0.44	0.56
$\beta_0 + \beta_1 T$	-0.045	0.0978			0.88	0.27
$\beta_0 e^{\beta_1 T}$	0.7865	0.0428			0.84	0.31
$e^{\beta_0+\beta_1\theta+\beta_2\theta^2}$	2.542	-14.89	27.25		0.47	0.57
$\beta_0 e^{\beta_1 T} e^{\beta_2\theta+\beta_3\theta^2}$	1.789	0.0383	-6.857	15.1	0.87	0.28
$R_{S(25)} Q_{10}^{(Ts-25)/10}$					0.98	0.33

5

PARTITIONING EVAPOTRANSPIRATION AND ITS LONG-TERM EVOLUTION IN A DRY PINE FOREST USING MEASUREMENT-BASED ESTIMATES OF SOIL EVAPORATION

The future of forests and their productivity in dry environments will depend on both water availability through precipitation and ecosystem and plant water use characteristics. It is increasingly recognized that better understanding water use patterns and their response to change depends on our ability to partition evapotranspiration (ET). Here, we use chamber-based direct measurements of soil evaporation (Es) in a semi-arid Pinus halepensis forest to partition ET to Es and tree transpiration (Et), to assess the daily and seasonal changes and to compare annual-scale values with measurements carried out at the same site ten years earlier. The ecosystem is characterized by a high annual Es/ET ratio of 0.26, and an Et/ET of 0.63. Es diminished in the long dry season, but as much as 74 ± 5% of the residual flux was due to the re-evaporation of nighttime moisture adsorption, which may provide critical protection from soil drying. Over the 10 years observation period concurrent increase in the transpiration ratio (TR=Et/ET; +29%) and in leaf area index (LAI; +44%) were observed, with the ratio of TR/LAI remaining constant at ~0.31, and with persistently closed hydrological balance (ET/P of 0.94–1.07). The observed Et/ET values are similar to the estimated global mean values, but are attained at a much higher aridity index (5.5) than the mean one, demonstrating the potential for expanding forestation into dry regions.

Keywords: *Soil evaporation and adsorption; Semi-arid ecosystem; Pine forest; Evapotranspiration partitioning; Canopy cover; Soil chamber*

This chapter is published as: Qubaja, R., Amer, M., Tatrinov, F., Rotenberg, E., Preisler, Y., Sprintsin, M., & Yakir, D. (2019). Partitioning evapotranspiration and its long-term evolution in a dry pine forest using measurement-based estimates of soil evaporation. Agricultural and Forest Meteorology. doi:10.1016/j.agrformet.2019.107831

5.1. INTRODUCTION

Dryland biomes, with aridity indexes higher than 1.7 (AI=Ep/P; the ratio between annual potential evapotranspiration and annual precipitation), cover ~47% of the global land surface (Bastin et al., 2017; Koutroulis, 2019; Zhang et al., 2019) and could expand by 11 to 23% by the end of the 21st century (Huang et al., 2015). Drought would be most pronounced in warm, semi-arid environments where water is the dominant limitation to vegetation growth. Evapotranspiration (ET) represents the largest flux in water loss from the land ecosystems (with a global mean value of approximately 57% of P; Wei et al., 2017) and is the second largest component in the surface energy balance after net radiation (Jung et al., 2010). In dry ecosystems, however, ET can be 95% of precipitation on average (Raz Yaseef et al., 2010; Stoy et al., 2019; Wang et al., 2014). Evaporation from the soil (Es), evaporation of water intercepted by the canopy (Ei), and leaf transpiration mostly through stomatal pores (Et) are distinct components that comprise the observed ET flux (ET=Es+Ei+Et). Transpiration is strongly modified by plant physiological. Evaporation, in contrast, results from diffusion of water to the soil surface (soil evaporation) or depends on the patterns of the rainfall and the structural characteristics of the vegetation stand (interception) dominated by physical factors. Due to these different controlling mechanisms, Es and Et are likely to have different responses to changes in environmental and ecological parameters (Kool et al., 2014). The ratio of transpiration to evapotranspiration (Et/ET) is often related to aridity (Good et al., 2017) but appears to be sensitive to ecosystem characteristics such as the leaf area index (LAI, Berkelhammer et al., 2016; Fatichi and Pappas, 2017), with higher LAI favoring Et and Ei at the expense of Es. LAI, therefore, could explain some 43% of the variability in annual Et/ET across global ecosystems (Wang et al., 2014). Et/ET ratios were shown to be relatively insensitive to changes in annual precipitation, P (Schlesinger and Jasechko, 2014), and on a global scale, across climates and vegetation types, the terrestrial annual Et/ET ratios have been estimated to range from 0.35 to 0.90 (Coenders-Gerrits et al., 2014; Fatichi and Pappas, 2017; Stoy et al., 2019; Young-Robertson et al., 2018). Similarly, interception from wet canopies can result in the evaporation of 8–30% or more of incident precipitation (Crockford and Richardson, 2000; van Dijk et al., 2015; Zhang et al., 2016).

At least part of the challenge in estimating ET and its partitioning (e.g., by flux measurements, modeling or remote sensing) is the difficulty in reliably measuring the individual ET components at the ecosystem scale (Fisher et al., 2017; McCabe et al., 2017; Stoy et al., 2019; Talsma et al., 2018). In particular, soil evaporation is often considered as a residual because of difficulties in obtaining direct measurements. Additional complications arise from the possible contributions of non-rainfall inputs (NRWI) such as storage across years, ground water, subsurface fluxes, and in particular in dry environments input associated with fog deposition, dew formation, or water vapor adsorption, (Agam et al., 2004; Agam and Berliner, 2006; Kidron et al., 2002; Kosmas et al., 2001; Ramírez et al., 2007; Verhoef et al., 2006). Water vapor from the atmosphere may be directly absorbed by the soil matrix as a result of capillary condensation or physical adsorption (Philip and De Vries, 1957; Rozenstein et al., 2015). Soil adsorption occurs on the soil surface if the surface temperature is higher than dewpoint temperature. Verhoef et al. (2006) indicated that soil moisture adsorption in southern Spain can reach 0.7 mm d^{-1}, while Zhang et al. (2016) reported the adsorption of 0.1 mm d^{-1} in China; Kosmas et al. (2001) indicated that adsorption

in dry conditions could account for as much as ~70% of evaporation in Greece, and Agam and Berliner (2006) measured vapor adsorption in the Negev desert and found the adsorption is ranging between 0.18 and 0.33 mm d^{-1}. All of the above mentioned experiments, regarding adsorption, conducted under semi-arid climate using lysimeters, in soils with clay content ranging from 1% to 35%, included bare soil, rain-fed crops, or shrubby natural vegetation. It has also been suggested that NRWI may contribute to biogeochemical dynamics by promoting microbial activity and nutrient recycling in the upper few centimeters of the soil profile (Baldock et al., 2012; Grover et al., 2012; Smith et al., 2003; Whiteford and Spanu, 2002).

Increasing competition between Es and Et for rainwater associated with climate change in dry regions and the implications for forest adaptation and survival require better understanding of ET partitioning and the underlying processes. In this study, we improved and validated chamber-based direct Es measurements and applied them to quantify the spatiotemporal variations in Es and their contributions to ecosystem ET and assessed the changes in ET partitioning compared with a similar study at our site made one decade ago.

5.2. MATERIALS AND METHODS

5.2.1. SITE DESCRIPTION

The Yatir forest (31°20'49" N; 35°03'07" E) is located in the semi-arid Mediterranean climates (Fig. A5.1), on the edge of the Hebron mountain ridge, with a mean altitude of 650 m. The ecosystem is a semi-arid pine afforestation established in the 1960s and covers approximately 18 km^2. Average air temperature for January and July is 10 and 25.8 ºC, respectively. Mean annual potential ET is 1600 mm, and mean annual precipitation is 285 mm. Only winter precipitation occurs in this region, creates a distinctive wet season (winter, December to March) and an extended dry season (summer, June to October), with short transition periods between them: a wetting season (early winter) and a drying season (spring).

The forest is dominated by Aleppo pine (*Pinus halepensis* Mill.), with smaller proportions of other pine species and cypress and with little understory vegetation (understory aboveground biomass <0.10 kg m^{-2}). Tree density in 2007 was 300 trees ha^{-1}, mean tree height was 10 m and LAI was 1.50 m^2 m^{-2}. The native background vegetation is sparse shrubland with a total vegetation height of 0.30–0.50 m (Grünzweig et al., 2003; 2007).

The soil at the research site is shallow (20–40 cm) aeolian-origin loess with clay-loam texture (31% sand, 41% silt and 28% clay; density: 1.65±0.14 g cm^{-3}) overlying chalk and limestone bedrock. Deeper soils (up to 1.5 m) are sporadically located at topographic hollows. While the natural rocky hill slopes in the region are known to create flash floods, the forested plantation reduces runoff dramatically, to less than 5% of rainfall (Shachnovich et al., 2008). Groundwater is deep (>300 m), reducing the possibility of groundwater recharge due to negative hydraulic conductivity or of water uptake by trees from the groundwater.

5.2.2. FLUX AND METEOROLOGICAL MEASUREMENTS

An instrumented eddy covariance tower was erected in the geographical center of Yatir forest, following Euroflux methodology (Aubinet et al., 2000). The system uses a 3D

sonic anemometer (Omnidirectional R3, Gill Instruments) and a closed path LI-COR 7000 CO_2/H_2O gas analyzer (LI-COR Inc., Nebraska, USA) to measure the evapotranspiration flux (ET) and net CO_2 flux (NEE). The up-scaled evapotranspiration was calculated as the sum of its components (ETup=Et+Es+Ei), while ET was the evapotranspiration flux that was estimated with the tower-based eddy covariance system. Half-hour auxiliary measurements used in this study included photosynthetic activity radiation (PAR mol m^{-2} s^{-1}), vapor pressure deficit (VPD, kPa), wind speed (m s^{-1}), relative humidity (RH, %), and additional measurements are described elsewhere (e.g., Tatarinov et al., 2016). The long-term operation of our EC measurement site (since 2000) provides data for over 80% of the times. Differential gap filling approach is used for missing data, based on the length of the gap in data, as recently described in Tatarinov et al. (2016).

Air temperature (Ta, °C) relative humidity (RH, %), and soil temperature (Ts, °C) were also measured and calculated by the soil chambers discussed below (20 cm above the soil surface and 5 cm depth, respectively). This was done during all soil chamber measurements which are described below by the LI-8150-203 (LI-COR Lincoln, NE). Volumetric soil water content (SWC_{0-10}) was measured in upper 10 cm half hourly by the ThetaProbe model ML2x (Delta-T Devices Ltd., Cambridge, UK) near the chambers (calibrated to the soil composition based on the manufacturer equations).

Precipitation (P) was measured by a standard rain station (Yatir forester station, KKL) in a clearing at a distance of 1.5 km from the tower site, where data have been collected since 1971. Rain data were used to calculate intercepted precipitation (Ei; mm) for individual rain events, based on:

$$Ei = P - Throughfall - Stemflow \quad (5.1)$$

where the Throughfall=0.94P-0.76 (with minimum P threshold of 0.76; R^2=0.996) and Stemflow=1.4% of the Throughfall, based on the detail study at our site by Shachnovich et al. (2008).

5.2.3. TREE SAP Flow

Sap flux (SF) was used to estimate tree transpiration (Et) using the 'Granier system' (Granier, 1987) and the 'Cermak system' (Cermak, 1974). The lab-made Granier system was operated since 2009; the Cermak system (EMS, Brno, Czech Republic) was operated in 2009–11 and then several times for 2–5 months in 2014 and 2016. Measurements were conducted half-hourly (including night hours) in 15–35 trees by the Granier system and in 3–7 trees by Cermak system, representing average forest tree size, age and slope aspect in the flux-tower footprint. A correction factor of 1.72 was applied to the Granier measurements to compensate for measuring to a depth of only 20 mm (Cohen et al., 2008). SF (L h^{-1} $tree^{-1}$) was converted to Et (mm h^{-1}) according to stand density (300 trees ha^{-1}; as in Klein et al., 2016). Alternatively, tree transpiration (Et) was calculated based on the hydrological budget as Et=ET-Es-Ei, where ET was based on EC measurements (see above), and Es was directly estimated as detailed below.

5.2.4. ALLOMETRIC AND LAI ESTIMATE

Leaf area index (LAI) measured with two methods, semi-direct (i.e., by allometry), and indirect (i.e., non-contact optical; TRAC; for more details see Sprintsin et al., 2011). TRAC design and operation are described elsewhere (e.g., Eriksson et al., 2005). It records PAR measured with three Quantum sensors (Licor LI190) at a frequency of 32 Hz. TRAC uses canopy gap fraction to estimate LAIe and also calculates the canopy gap size distribution, which is used to estimate the element clumping index and to convert LAIe into LAI (Leblanc et al., 2005). Sprintsin et al. (2011) used this instrument for long-term LAI measurements record (2001–2013) to produce a long term best fit regression equation.

5.2.5. SOIL EVAPORATION

Soil evaporation (Es) was measured with automated non-steady-state systems originally designed for soil respiration measurements, using 20 cm diameter opaque chambers and a multiplexer to allow the simultaneous control of several chambers (LI-8150, -8100-101, -8100-104; LI-COR, Lincoln, NE). Precision of water vapor in the chamber air is ±1.5% of measurements range (0–60 mmol mol^{-1}). The chamber closes on preinstalled PVC collars (20 cm diameter, inserted 5 cm into the soil, and 6 cm above the surface) for a short measurement time (2 min), and positioned away from the collar for the rest of the time. Data were collected using the original instrument soil respiration system, where air from the chamber is circulated (2.5 l min^{-1}) through infra-red gas analyzer (IRGA) and recording the CO_2 and H_2O concentrations in the system logger (1 s^{-1}). Gap filling of missing Es data due to technical problems (i.e., 27 % of the data across the study period of 2015–2016) was based on the average diurnal cycle of each month.

The rates of soil evaporation, Es was calculated from chamber data using a linear fit of air humidity, using equation 5.2 (Raz-Yaseef et al., 2010; LiCor manual, 2015; see Fig. A5.2):

$$Es = C\frac{dH}{dt} \cdot \frac{v\,P}{s\,T_a R} \qquad (5.2)$$

where Es is water vapor flux (mmol H_2O m^{-2} s^{-1}), C empirical correction factor, dH/dt the initial slope of water vapor (mmol mol^{-1} s^{-1}), v the system volume (m^3), s the soil surface area within the collar (m^2), P the chamber pressure (Pa), Ta the chamber air temperature (K), and R is the gas constant (J mol^{-1} K^{-1}). A measurement period of 10–50 s was used based on preliminary tests with the highest R^2 values, and the linear best fit was used in Eq. 5.2, for positive flux (evaporation flux from soil to atmosphere; Ev) and negative regression (adsorption flux from atmosphere to soil; Ea, where Es=Ev+Ea).

Soil evaporation in the experimental plot was measured between November 2015 and October 2016 with three measurement chambers using 21 collars grouped in 7 sites in the forest stand, with three locations (i.e. three collars) per site, based on different distance from the nearest tree. Data were recorded on half-hour basis (48 daily records). The 3 chambers were rotated between the 7 sites every 1–2 week to cover all sites and assess the spatial and temporal variations.

Upscaling of the collar measurements to the plot scale soil evaporation, Es, was carried out by grouping the collars based on the three locations: Under trees (<1 m from nearest tree; UT), in gaps between trees (1–2.3 m; BT), and in open area (>2.3 m; OA), and estimating the fractional areas (Ø) of the three locations based on

mapping the sites according to the distances noted above as previously done (Raz-Yaseef et al., 2010):

$$Es = Es_{OA} * \emptyset_{OA} + Es_{BT} * \emptyset_{BT} + Es_{UT} * \emptyset_{UT} \quad (5.3)$$

$$1 = \emptyset_{OA} + \emptyset_{BT} + \emptyset_{UT} \quad (5.4)$$

5.2.6. CALIBRATION OF Es MEASURMENTS

Calibration and validation of the evaporation measurements based on the soil chamber system was carried out under both field and greenhouse conditions using high-precision balance (Sartorius TE1502S, Goettingen) installed in the field below the soil collars, and bench top lysimeters (Tedea-Huntleigh Model 1042, VPG Transducers, Malvern) with precision of 0.01 g (Fig. A5.3). The combined results were used to produce the correction factor of chambers-based Es. Estimates based on either the balance (Es_{ba}; mmol m^{-2} s^{-1}) or lysimeter (Es_{ly}; mmol m^{-2} s^{-1}) were based on:

$$Es_{ba} \text{or } Es_{ly} = \frac{dm}{dt} \cdot \frac{1000}{s\, M_{H_2O}} \quad (5.5)$$

where dm/dt is rate of mass change (g s^{-1}), M_{H_2O} is molar mass of water. The greenhouse testing included comparison of transparent and opaque chambers, and long vs short tubing, and the effects of radiation and wind speed. Prior to testing, the LI-8100 was also calibrated with dew point generator (LI-610, LiCor, Nebraska). Soil samples for the calibration tests were taken from the upper part of the soil profile at the Yatir forest, and re-packed into 20 cm collar sealed onto a plastic tray placed on the balance (field) or lysimeter (greenhouse). Tests included soil in its original dry state as collected in the field (SWC~0.05 m^3 m^{-3}) and soil samples re-wetted to different levels.

Field tests were carried out under natural conditions with chamber-based soil evaporation (Es) automatically measured every 30 min by the standard chamber operating system, followed by manually recording of the weight of the soil collar to obtain the Es_{ba}. Empirical correction factors for the LI-8100 was based on the linear regression between the Es and the Es_{ba} values.

In the greenhouse, four lysimeter units were positioned around the LI-8100A. The same Yatir soil was used in the lysimeters and the LI-8100A collar (sealed from the bottom). Calibration was based on linear fit comparing each chamber auto-sampling (every 30 min) with the mean value of the four simultaneous lysimeter units for the wet and dry soil respectably. A temperature correction is required for the greenhouse lysimeter measurements and was obtained using the greenhouse temperature records following Fares et al. (2009). The proper operation of the lysimeters was also tested following Wheeler and Ganji (1996) using bricks of known weight and covered with thick plastic to prevent mass change during the calibration (Allen and Fisher, 1990).

In addition, the greenhouse system discussed above was also used to identify the factors contributing to the relatively constant and robust, but large, correction factor. This included comparing first, the opaque (metal) and the transparent (glass), chambers offered with the LI-8100 system; second, assessing the effect of reducing the tubing length between the chamber and the IRGA; third, assessing the effect of coating the inner surface of the chamber with hydrophobic material (Dow Corning High-Vacuum Grease; USA); and fourth, validating soil water uptake from the

atmosphere, extending the experiments with dry soil (relevant meteorological data at the time of experiment are given in Fig. A5.4). The results of these tests are summarized in Table A5.1 and Figures A5.2, 3, 4).

The results from the field and greenhouse tests were similar and produced the same correction chamber factor (c.f. = 2.5; Fig A5.3a and b). The Ta and RH values inside and outside the chamber showed no significant differences. In the greenhouse, Ta was higher by 9% and RH lower by 8% than the greenhouse air values on average (not significant; Fig. A5.3). Note also that both in the greenhouse and in the field (Figure A5.4d and 5a), the Td values inside the chamber were lower than Ts during the entire measurements period, indicating that the non-rainwater moisture uptake was likely associated with direct adsorption and not with dew formation.

5.2.7. DEW COMPUTATION

Soil evaporation measurements were sometime negative indicating moisture uptake and to check if this was due to dew formation, the dew point temperature (Td, °C) during these periods was calculated (Lawrence, 2005):

$$T_d = \frac{B\left[\ln\left(\frac{e_a}{e_S}\right)+\frac{A\,T_a}{B+T_a}\right]}{A-\ln\left(\frac{e_a}{e_S}\right)-\frac{A\,T_a}{B+T_a}} \quad (5.6)$$

where e_a and e_S are the actual water vapor pressure and the saturated water vapor pressure in the air (mb), respectively and A=17.625 and B=243.04°C were evaluated by Alduchov and Eskridge (1996) and the relevant meteorological measurements for this comparison (Ta, Ts, RH) by LI-8150-203. It was assumed that for dew formation, the surface temperature (Ts) needs to be equal to or lower than the dew point temperature. Saturation vapour pressure (e_S; mb) was calculated using air temperature (Ta; °K), t_{Ra}=1-(373.15/Ta); e_S=101325*exp(13.3185(t_{Ra})-1.9760(t_{Ra})^2-0.6445(t_{Ra})^3-0.1229(t_{Ra})^4); partial vapour pressure (e_a; mb) was calculated using relative humidity (RH; %) information as: e_a=(RH*e_S)/100.

5.2.8. LONG-TERM ET PARTITIONING

Following Scott and Biederman (2017) approach, the relationships of monthly values of GPP as a function of ET are fitted with a linear equation assuming of the form ET=mGPP+E, where E can be obtained from the intercept of the best fit line (and were E=Es+Ei). We used our site long-term records of ET, P and GPP and applied this approach to our study site.

5.2.9. STATISTICAL ANALYSES

The paired t-test was used to detect significant differences in Es and metrological parameters between the chamber and the greenhouse measurements. Furthermore, the effect of location (OA, BT and UT), sites and their interactions were checked with Tow-way ANOVA at a significance level set at 0.001. Pearson correlation analysis (*r*) was used to detect the correlation between the water fluxes and the meteorological parameters. To quantify Spatio-temporal variability in Es, the coefficient of variation (CV%) was calculated as [(STDEV/Mean) x 100%]. All the analyses were performed using Matlab software, Version R2017b (MathWorks, Inc.).

5.3. RESULTS

5.3.1. SPATIAL VARIATIONS

Table 5.1 | Annual mean of half-hour values across sites (OA, open area; BT, between trees; UT, under tree) Annual mean of half-hour values across locations (OA, open area; BT, between trees; UT, under tree) in 7 sites during study period, of soil evaporation flux rates (Es) and adsorption averaged for event days (Ea^1) or for the study period (Ea^2), together with the soil water content at 10 cm depth (SWC; x100 m3 m-3), minimum distances from nearby tree (Dt), soil temperature at 5 cm depth (Ts), and air temperature (Ta) and relative humidity (RH) at the soil surface; (numbers in parenthesis indicate ±se).

Locations	Sites	Es	Ea^1	Ea^2	SWC	Dt	Ts	Ta	RH
		[x100 mm d^{-1}]				[m]	[K]	[K]	[%]
OA	1	66.1	-1.9	-16.4	16.5	2.9	288.7	288.5	59.7
	2	29.5	-4.8	-22.3	14.5	3.6	289.1	288.2	58.4
	3	58.4	-6.9	-30.6	19.3	7.0	293.8	291.3	53.5
	4	46.1	-10.6	-20.0	11.3	3.0	295.7	294.0	58.9
	5	8.4	-10.5	-18.2	5.8	3.0	298.7	297.2	43.1
	6	1.5	-3.2	-20.0	5.7	2.8	303.2	299.3	51.8
	7	3.6	-4.0	-23.6	6.1	3.5	298.6	296.3	44.5
	Average	**31 (1)**	**-6 (3)**	**-22 (0)**	**11 (0)**	**3.7**	**295 (0)**	**294 (0)**	**53 (0)**
	CV [%]	**88%**	**-58%**	**-21%**	**50%**	**41%**	**2%**	**1%**	**13%**
BT	1	21.6	-2.7	-7.8	10.5	1.8	289.3	288.4	60.5
	2	18.1	-1.3	-6.9	12.1	1.5	287.9	287.9	59.5
	3	29.0	-3.9	-13.7	20.4	2.7	293.2	291.5	54.1
	4	26.8	-7.0	-12.4	14.4	2.7	296.4	294.4	58.5
	5	4.0	-7.8	-14.2	3.9	2.0	297.8	297.1	43.2
	6	0.8	-1.7	-10.8	3.3	2.5	302.2	299.1	52.5
	7	7.8	-1.2	-11.3	5.5	1.2	297.1	295.9	45.7
	Average	**15 (1)**	**-4 (2)**	**-11 (0)**	**10 (0)**	**2.0**	**295 (0)**	**293 (0)**	**53 (0)**
	CV [%]	**73%**	**-75%**	**-25%**	**63%**	**29%**	**2%**	**1%**	**13%**
UT	1	25.0	-4.2	-13.3	9.3	0.2	288.9	288.4	60.0
	2	24.7	-1.6	-9.9	14.0	0.3	288.0	287.9	59.4
	3	48.8	-3.2	-15.3	19.8	0.5	292.1	291.2	54.5
	4	34.8	-8.1	-16.4	11.3	0.6	295.1	293.9	59.0
	5	9.8	-7.4	-15.4	4.0	0.4	297.0	296.8	44.1
	6	-2.2	-3.6	-19.6	4.5	0.2	302.6	299.1	52.7
	7	8.7	-1.8	-14.1	5.2	0.2	298.1	296.1	45.5
	Average	**21 (1)**	**-4 (2)**	**-15 (0)**	**10 (0)**	**0.3**	**295 (0)**	**293 (0)**	**54 (0)**
	CV [%]	**81%**	**-60%**	**-20%**	**60%**	**46%**	**2%**	**1%**	**12%**
All	**Average (SE)**	**27 (0)**	**-5 (1)**	**-16 (0)**	**11 (0)**	**2.0 (0.4)**	**294 (0)**	**293 (0)**	**54 (0)**
	Max	**66**	**-1**	**-7**	**20**	**7.0**	**303**	**299**	**60**
	Min	**-2**	**-11**	**-31**	**3**	**0.2**	**288**	**288**	**43**
	CV [%]	**88%**	**-64%**	**-35%**	**55%**	**82%**	**2%**	**1%**	**12%**
Two-way ANOVA (*P* value)	**Site**	**0.000**	**0.000**	**0.000**	**0.000**		**0.000**	**0.000**	**0.000**
	Location	**0.000**	**0.000**	**0.000**	**0.000**		**0.000**	**0.220**	**0.074**
	Site x	**0.000**	**0.000**	**0.000**	**0.000**		**0.000**	**0.645**	**0.961**
Pearson Correlation with Es			**-.15**	**-.26**	**.84****	**.35**	**-.62****	**-.65****	**.59****
Pearson Correlation with		**-.26**			**-.14**	**-.65****	**-.28**	**-.21**	**.21**

**. Correlation is significant at the 0.01 level (2-tailed).

The spatial variations in soil evaporation, Es, and adsorption (Ea) fluxes across collars, locations, and sites, together with other measured variables, are reported in Table 5.1.

The results indicated an overall mean Es value of 0.29±0.10 mm d^{-1} with distinct values in the three locations. Es was greater at the OA than at the BT and UT locations, by 95% and 42% respectively, which is consistent with the higher soil temperatures and radiation at this location. The average soil adsorption fluxes (negative Es) during the days when it occurred were of similar magnitude to the Es flux (-0.16 vs. +0.29 mm d^{-1}, respectively) but were substantially smaller when considered on an annual scale (-0.05±0.01; Table 5.1).

The spatial variability among locations was also apparent in the daily cycle (Fig. 5.1), with clear differences between the wet season (November to April), in which the OA showed consistently higher Es values than the other locations (by a factor of approximately 2), and the dry season, in which Es rates and the differences between locations greatly diminished. Note that the daily peak in Es remains at midday in both the wet and dry seasons. A unique feature of the dry season was the consistent observations of negative fluxes of moisture adsorption in the evening and early night hours (Fig. 5.1b). This was associated with sharp decreases in air temperature, which did not reach the estimated dew point, indicating no dew formation.

Overall, when all the 21 collars were considered together, Es was positively correlations with soil moisture and with RH (r = 0.84 and 0.59; p < 0.01, respectively); similar, but negative correlations with soil and air temperatures (Ts and Ta; r~0.6; p < 0.01). Adsorption showed significant inverse correlations to distance from trees, Dt, (r = -0.65, p < 0.01), but was not correlated with either RH, Dt, Ta or Ts. Two-way ANOVA showed that the locations, sites, and their interaction had significant effects on the Es and Ea (p < 0.001; Table 5.1).

5.3.2. TEMPORAL DYNAMICS

Irrespective of the spatial variations discussed above, temporal changes in the evaporative fluxes at the diurnal time-scale showed typical daily cycles (Fig. 5.1). As expected, on average all evaporative fluxes are higher by a factor of approximately 2, in the wet period than in the dry season. Note, however, that the physically dominated Es values showed peak values around midday in both the wet and dry seasons. At night, continued evaporative fluxes were observed during the wet period, while nighttime adsorption (negative values) were consistently observed in the dry period, reaching, on some nights, rates equivalent to -0.8 mm d^{-1}. ET also showed a shift from mid-day (approximately 11:00–14:00) to early morning (08:00–11:00) in the dry season, reflecting the physiological response associated with leaf transpiration and stomatal closure. This was not clearly observed in the sap-flux-based Et patterns, likely reflecting limitations of the method (compared to the ET-Es approach), especially in the dry period and in the day-night transition to the night when fluxes are low and are often around the detection limit. As indicated above, our ET partitioning showed a decrease in Es/ET and an increase in Et/ET from winter to summer, which is clearly apparent midday values (Fig. 5.1).

The monthly temporal variations in our integrated soil evaporation estimates, together with other estimated fluxes, are reported in Fig 5.2 (see also Fig. A5.3 and 5 for ½ hour data) and exhibit the sharp differences between the wet and long dry seasons. As is typical for this semi-arid site, all evaporative fluxes peak during March-April. In contrast, the adsorption fluxes, though small, clearly peak in summer, during June-August. The contrast of wet vs. dry season also indicates a shift in ET partitioning, with increase in Et/ET from 28% in November to 102% in July and a decline in Es/Et from 35% to 7% on average in the wet and the dry seasons,

respectively. On an annual basis, the ET partitioning reflected the low density (300 trees ha^{-1}) nature of the semi-arid forest, with Es/ET of 26%. Et/ET was 63%, which reflected a seasonal change of Et from the dry season daily mean value of 0.74±0.2 mm d^{-1} to peak values in February/April of up to 3.4 mm d^{-1} (Fig. 5.1 and 2, Table A5.3).

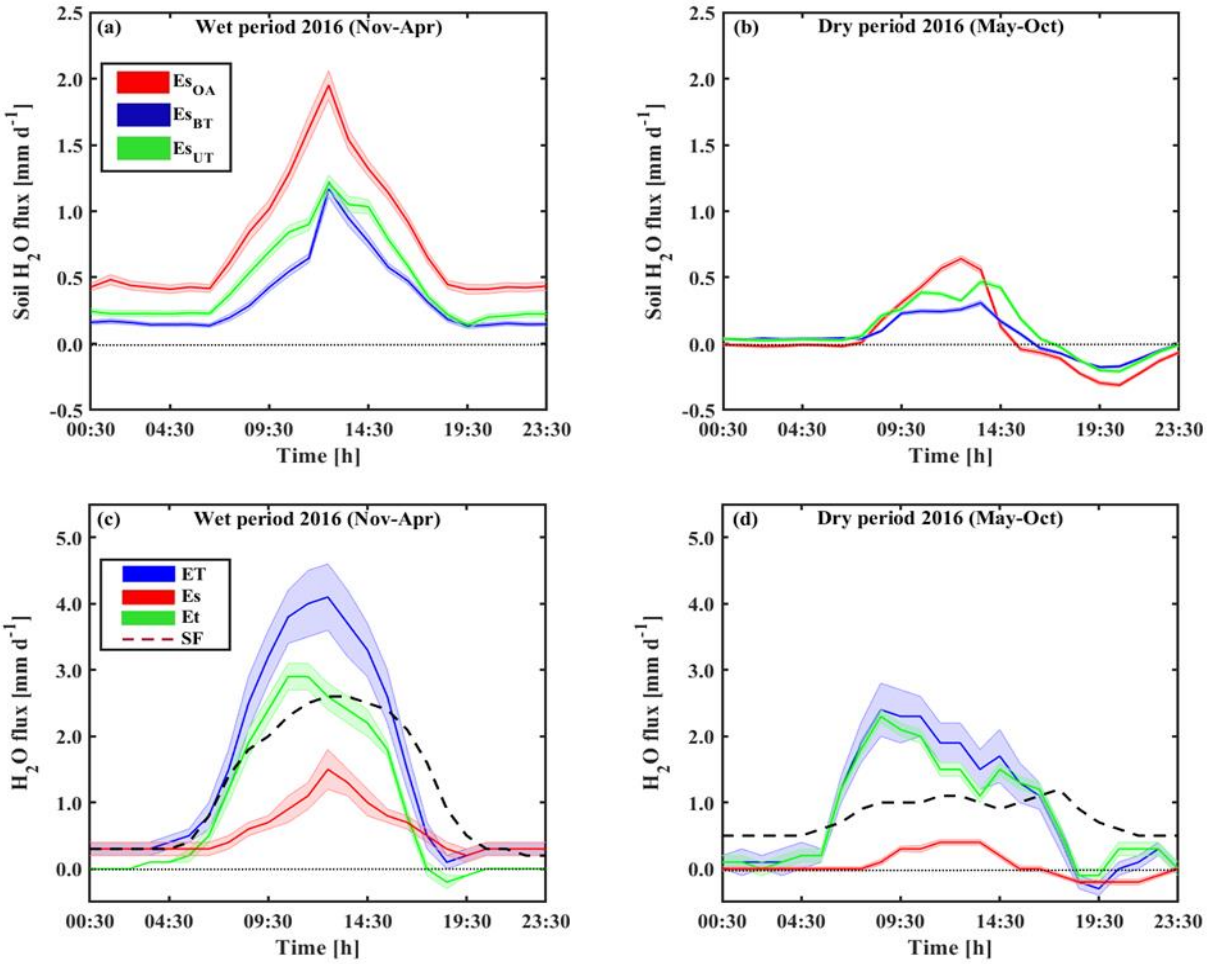

Figure 5.1 | Representative diurnal cycles of soil evaporation (Es; using mean soil chambers data across locations: open-area, OA; between-trees, BT; under-trees, UT) in panels a and b, and of evapotranspiration (ET; canopy scale eddy covariance), and its partitioning to soil evaporation flux (Es) and tree transpiration (Et) in panels c and d, during the wet (Nov-Apr) and dry (May-Oct) periods. Based on half-hour values over the diurnal cycle; shaded areas indicate ±se; negative values represent fluxes from the atmosphere to the surface; Et was estimated as the residual as Et=ET-Es-Ei); interception, Ei, was considered during the wet period assuming uniform distribution during the day; and alternatively, as sap flux (SF; black-dashed line).

The high-resolution data (Table A5.2) showed that in winter (February), peak Es rates were associated with clear days, high Ta and low RH and were not clearly expressed in the ET flux. Note that following rainy days, the daily Es values could reach up to 7.5 mm d^{-1} (not shown), but otherwise, Es was, on average, 0.52±0.08 mm d^{-1} during the wet period and diminished by ~90% in the dry season to a mean daily value of 0.05±0.02 mm day^{-1}. The partitioning of the Es fluxes, shown in Fig. 5.2b, clearly show that the adsorption phenomenon was limited to the summer months. It is also evident that the magnitude of adsorption, Ea, was similar to that of the evaporation flux (Ev in Fig. 5.2; remembering that Es=Ev+Ea) and that the ratio of Ea/Ev could reach ~1.15, reflecting the potential significance of this phenomenon. Due to the balance between Ev and Ea values, monthly average Es values were near zero and

were rarely negative.

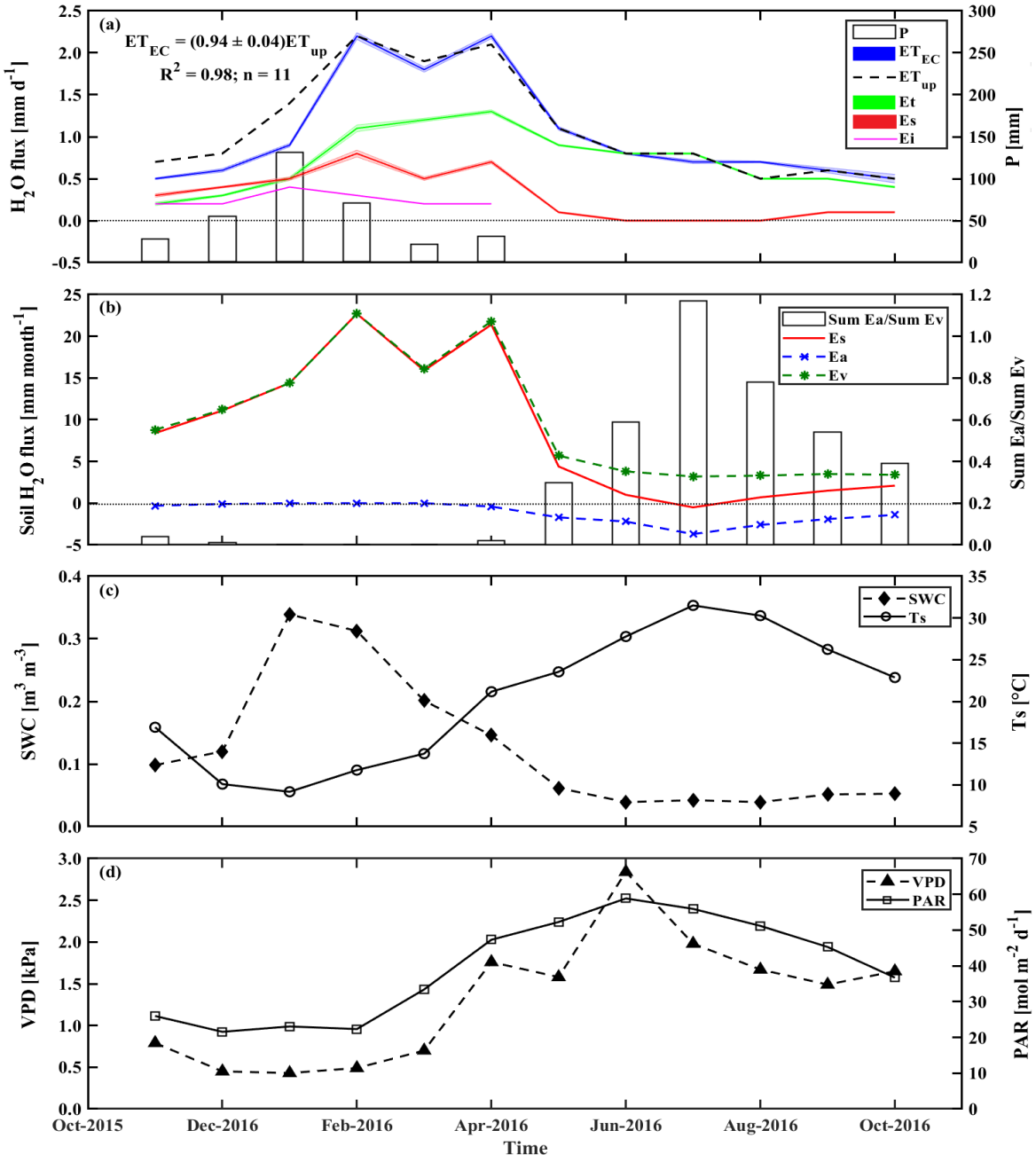

Figure 5.2 | Seasonal trends of monthly mean values during the research period of a) the fluxes of soil evaporation (Es), tree transpiration (Et), and intercepted precipitation (Ei), b) monthly sum of soil H_2O flux (Es) and its components evaporation (Ev; the positive flux from soil to atmosphere) and adsorption (Ea; the negative flux from atmosphere to soil); and monthly mean of key environmental parameters, c) soil water content at the top 10 cm ($SWC_{0\text{-}10}$) and soil temperature at 5 cm (Ts), and d) vapor pressure deficit (VPD) and photosynthetic activity radiation (PAR). ETup is obtained from the sum of Et+Es+Ei; ET_{EC} is obtained from eddy covariance measurements, with correlation between the two estimates indicated in panel a (n=number of months included in analysis).

In spring (April) all evaporative fluxes seemed to peak at a crossover in the trends of decreasing soil moisture and increasing temperature and radiation. The temporal variations in the half-hour values of Es reflected changes in PAR and soil moisture at 0–5 cm depth (r=0.4, p<0.01, for both variables) and showed a negative correlation

with RH and with Ts (r=-0.3 and -0.2; p<0.01, respectively).

A reasonable forecast of the temporal variations in Es (R^2=0.70, p<0.0001) was obtained based on a multiple linear regression based on $SWC_{0\text{-}10}$ and vapor pressure difference values, calculated based on the Ta and RH records:

$$Es\ (mm\ d^{-1}) = -1.86 * 10^{-4}\ (e_S - e_a)\ (1 - (25.93\ x\ SWC_{0-10}) \qquad (5.8)$$

where e_a and e_S are the ambient and saturation water vapor pressures of the air with (mb).

The variations in Ea values (CV=87%) seemed to reflect those in the environmental parameters (Ts, Ta, SWC, and RH) and showed negative correlations between Ea and Ts and between Ea and Ta (r=0.4 and 0.3, respectively; p<0.01), and positive correlations with SWC and RH (r=0.3 and 0.1, respectively; p<0.01).

During the wet season, the daily ET was characterized by relatively high fluxes with a mean value of 1.4±0.3 mm d^{-1}, and a range of -3.6–12.6 mm d^{-1}, peaking with mean values of ~2.2 mm d^{-1} in February-April (Fig. 5.2; Table A5.2). ET fluxes rapidly decreased after rain cessation and reached the lowest fall values in October with mean dry period values of 0.7±0.1 mm d^{-1} (Fig. 5.2, Table A5.2).

Estimated values of daily interception, Ei, were in the range of 0.0–0.44 mm d^{-1}, with a mean value of 0.24±0.04 mm d^{-1} during the wet period (Fig. 5.2, Table A5.2), peaking in January. On individual days, Ei could reach up to 2.7 mm d^{-1}, such as after the main storm events in 25 Jan and 21 Feb.

Figure 5.3 summarizes the seasonal variations in ET partitioning. Note that both the lowest and highest Et fractions (~0.28 and nearly 1) along the seasonal cycle are associated with low total ET fluxes, both in fall before tree transpiration peak up in spring and in summer when physiological controls limit water loss. During the peak season in March-April, the Et fraction is ~0.6 as is the annual mean value. Interception can reach significant proportions but in absolute terms are significant only during the peak rain period and are irrelevant during the long dry period (see Table A5.2).

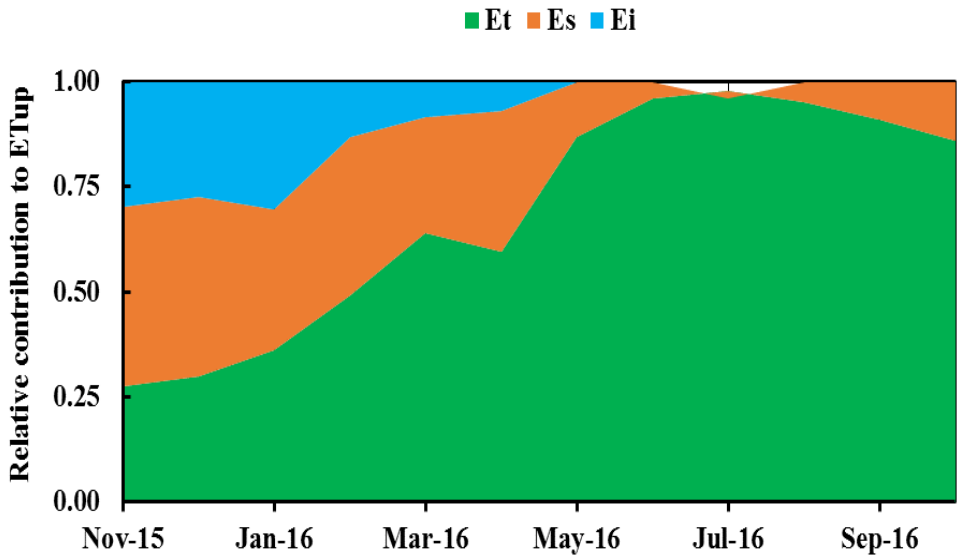

Figure 5.3 | Seasonal variations in the relative contribution to total ETup of tree transpiration (Et; SF-based), soil evaporation (Es), and intercepted precipitation (Ei), means for the study period. Total ETup is the sum of its components (the effect of adsorption is noticeable in summer). Note that Et/ET can be both low (0.28) and high (0.91) during times of low total ET flux (~0.6 mm d^{-1}).

5.3.3. ANNUAL-SCALE AND LONG-TERM TRENDS

On an annual scale during the study period, P was 352 mm, and the estimated ET based on EC measurements was 376 mm, with an ET/P ratio of 1.07. This is likely within the measurement precision but may also reflect utilization of soil water storage across years, as was previously observed at this site. Our estimates of the evaporative flux components resulted in annual values of Es, Ei, and Et of 103, 44, and 253 mm y^{-1} (with Ea, the adsorption component within the Es flux, of -14 mm y^{-1}; see Table A5.2). As a result, the component-based hydrological budget was consistent with the EC-based one: (Es+Et+Ei)/P=1.07, indicating an essentially closed hydrological budget, and within the range observed earlier by Raz-Yaseef et al. (2012).

On average, across the measurement period, tree transpiration was the main water flux, making up 63% of ET, but soil evaporation was also a significant component, accounting for 26% of ET, including annual values of soil water adsorption and re-evaporation equivalent to ~4% of the precipitation inputs, while evaporation of intercepted precipitation accounts for ~11% of ET (Fig. 5.2; Table A5.2).

Using the site records of nearly 20 years and a comparison of our results with a previous ecohydrological study 10 years earlier (Raz-Yaseef et al., 2010 and 2012), we assessed the long-term trends in ET and its partitioning. Notably, P and ET showed no clear long-term trend in time across the 20 years observation period (not shown), with a mean value of precipitation of 287±70 mm y^{-1} and a long-term ratio of ET/P of 0.93±0.22 (with independent evidence for negligible runoff and infiltration to depth; Shachnovich et al., 2008) but note that the two periods we compared had different annual P, which can partly explain the increase in Et and TR.

Table 5.2 | Mean annual values of ecosystem evapotranspiration (ET), its components and associated ratios, and the canopy leaf area index (LAI) in the present study (2015–2016) and in comparison, to results obtained previously (2003–2007) in the semi-arid pine forest site. ET_{up} and ET_{EC} indicate upscaling from individual components or from eddy-covariance measurements. Ei, Es, Et and P denote intercepted precipitation, soil evaporation, and tree transpiration and precipitation, Δ indicates difference across the 10 years observation period (2005 to 2015; using mean values for the two study periods).

Study	Ei	Es	Et	ET_{up}	ET_{EC}	P	LAI
	[mm y^{-1}]						[m^2 m^{-2}]
2003–2007	31	103	129	263	267	285	1.4
2015–2016	44	103	253	400	376	352	2.1

Study	Ei/ ET	ER= Es/ET	TR= Et/ET	ET_{EC}/ ET_{up}	ET_{EC}/ P	ER/ LAI	TR/ LAI	ΔER/ ΔLAI	ΔTR/ ΔLAI
2003–2007	0.12	0.39	0.49	1.02	0.94	0.27	0.34	-0.21	0.23
2015–2016	0.11	0.26	0.63	0.94	1.07	0.13	0.31		

Et/ET (transpiration ratio; TR) has increased from 0.49 to 0.63 (+29%), and Es/ET has decreased correspondingly from 0.39 to 0.26 (-34%) over the 10-year observation period (summarized in Table 5.2). During the same period, LAI at the site increased from 1.4 to 2.1 (+44%; see Fig. A5.7 and Table 5.2).

Applying the Scott and Biederman (2017) approach to the long-term record at our site (https://fluxnet.fluxdata.org/), we obtained an E estimate of 6.8–9.0 mm $month^{-1}$ (Fig. 5.4). This is equivalent to 82–108 mm y^{-1}, which is similar to our annual Es

estimate of 104 mm (but lower than the estimated total E value during the current study year of 148 mm). As noted above, Ei is a small hydrological component at our site and is relevant only during the few rainy months (mainly December-March; see Fig. 5.2 and Table 5.2). Using the long-term mean P value (287 mm) indicated E/P ratios of 0.28–0.38.

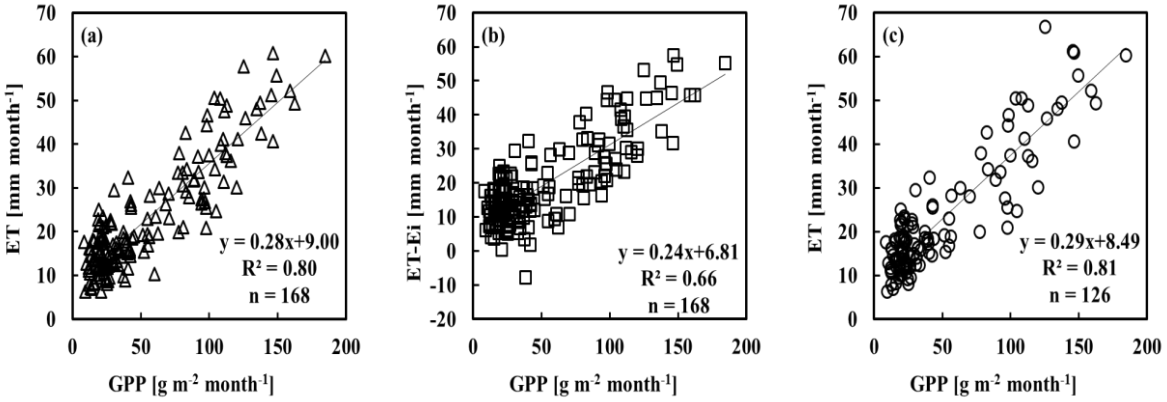

Figure 5.4 | Monthly mean values of evapotranspiration (ET) and gross primary production (GPP) from eddy covariance measurements at the Yatir Forest site for 2002–2016 and the linear best fit line used to estimate total evaporation. For comparison with measured Es values, regressions included the entire dataset of ET and GPP values (a); after subtracting canopy interception (Ei) from the ET values (b), or eliminating the three high-precipitation months (Dec-Feb, 72% of P) when canopy interception was most pronounced (c). n indicates the number of months included in generating the regression equation.

5.4. DISCUSSION

The future of forests and their productivity in dry environments will depend on both water availability through precipitation and ecosystem and plant water use characteristics. To better understand water use patterns and their response to change, we employed a modified chamber-based method to directly estimate soil evaporation and took advantage of our site characteristics with no runoff and with unreachable ground water, resulting in simple and essentially closed energy and hydrological budgets (Raz-Yaseef et al., 20010; Rotenberg and Yakir, 2011). Large efforts were invested in extensively testing and validating the unconventional use of automated soil chambers, both in controlled greenhouse conditions and in the field. Although originally designed for soil respiration studies, the empirical results indicated robust and sensitive results in estimating soil evaporation, consistent with other similar attempts (Cohen et al., 2015).

The sensitivity of the method was useful to show the low but persistent water loss to Es during the long summer drought (Table 5.1; Fig. 5.1, and SI-A), when the soil moisture near the surface approaches that of oven dried soil samples. However, the results also indicated that this could involve the significant re-evaporation of adsorbed atmospheric moisture. The persistently observed negative Es values indicating soil adsorption were also supported by periodic observations of negative ET fluxes at the canopy scale in summer (Fig. A5.8), as well as with the large diurnal changes in canopy temperature and humidity in the same period (see also Uclés et al., 2015) and the expected hygroscopic soil characteristics due to its clay content (Klein et al., 2014; Kosmas et al., 1998). Our estimated Ea values are generally consistent with the few published values in the range of 0.10–1.44 mm d^{-1}, mostly for bare soil (Jacobs et al.,

2000; Kosmas et al., 2001; Ninari and Berliner, 2002; Verhoef et al., 2006). The results also indicated that the non-rainwater uptake was associated with direct adsorption and most likely not with dew formation, since the near surface temperatures did not drop to the estimated dew point temperatures.

Notably, although the adsorption fluxes, Ea, are small, they could account for 74% of the daily residual summer Es flux. On an annual scale, the estimated Ea was equivalent only to ~4% to precipitation, but it may provide critical protection from drying in the long dry season, such as by slowing the upward movement and loss of soil water remaining in the root-zone levels. The spatial variations in Ea values, with values in the OA greater by 65% and 40% than in the BT and UT locations, further enhance the possible protection effect by this bias to the most vulnerable locations in the forest floor and could be additive with other effects that help explain the forest survival and high productivity in the harsh conditions (Preisler et al., 2019).

Further adjustments to the stressful environment were reflected in the seasonal shifts in the diurnal patterns in the physically or the physiologically dominated Es and Et fluxes, respectively. This reflected the differential controls over these fluxes, with Es remaining synchronized with environmental parameters (e.g., PAR, Ta), which was not the case for the Et that dominates ET (Fig. 5.1). The early-morning maximum in Et and ET values is consistent with earlier studies at this site (e.g., Raz-Yaseef et al., 2012) and the with the isohydric nature of the Aleppo pine trees (Klein et al., 2013).

Et and Ei are often assumed to be strongly influenced by canopy cover (Lawrence et al., 2007; Simonin et al., 2007; Wei et al., 2017) and increases in these fluxes were expected to follow the observed increases in LAI, by about 44% over our 10 years observation period. Ei was shown in an extensive study at our site to be a relatively minor component of the hydrological budget (Shachnovich et al., 2008) and only a minor increase was expected due to changes in LAI, to the current estimate of 12% of annual P. However, note that at the onset of the wet period, when leaf activity was still low, Ei value could be significant and reached ~25% of ET, and then remained at zero during the long seasonal drought (Figs. 5.2, 3).

Our direct estimates of Es yielded mean Es/ET ratios of 0.26 and, consequently, mean transpiration ratio, Et/ET (TR), of ~0.63 (Table 5.2). These results are within the global range of Et/ET of 0.35–0.90 and near the estimated global optimum, but are distinct from temperate pine forests with values of 0.7–0.75 (Good et al. 2017; Stoy et al., 2019). Relatively low Et/ET and high Es/ET on annual scale are consistent with the aridity effects (Good et al., 2017) and highlight the importance of soil evaporation fluxes in low-density semi-arid forests. This was also apparent in the spatial distribution of Es, showing nearly twofold differences in the Es values between the exposed and shaded locations (Table 5.1, Fig. 5.1).

Notably, the current study provided an opportunity to compare our chamber-based ET partitioning and estimating Et to the more conventional approach based on sap flux (SF; Fig. 5.1). The results clearly reflected the difficulties in SF measurements in the dry conditions (Fig. 5.1d), and the likely complicating effects of understory in this low-density stand (estimated at ~18% of Et) in other periods (Klein et al., 2014. This is in addition to other limitations of the SF approach, such as the limited stem cross section measured (65% in our study site) and the difficulties in calibrations (Cohen et al. 2008).

Based on our "long-term" results in Table 5.2, we estimated an increase of 25% in the transpiration fraction (TR) per unit change in LAI ($\Delta TR/\Delta LAI$ of 0.14/0.6=+0.23; and correspondingly, and $\Delta ER/\Delta LAI$ of -0.21). Note, however, that at the same time the TR/LAI values remain nearly constant (0.49/1.4=0.34 and 0.63/2.1=0.31 across

the 10-year observation period). Such trends may be typical to low density semi-arid forests (relatively low LAI) but may change with higher LAI and associated feedbacks of increasing canopy cover on Et (Villegas et al., 2015; see also Adams et al., 2012; Breshears, 2006; Wei et al., 2017).

The changes in LAI over the 10 years preceding the present study and our long flux records at the site (Qubaja et al., 2019) indicate that this 54-year-old forest is still growing. However, it is possible that the observed changes in ET partitioning are also part of the global-scale trends of increasing ET and the shift from Es to Et (e.g., Zhang et al., 2016). The increasing trends in LAI have been attributed to factors such as the CO_2 fertilization effect (Donohue, et al., 2013), global warming (Jiang, et al., 2013), or afforestation and forest protection (Piao et al., 2009; Siry et al., 2005). The increase in atmospheric CO_2 concentrations, in turn, is often assumed to increase ecosystem water use efficiency, which was indeed observed at our site based on tree ring analyses (Maseyk et al., 2011).

Addressing the need for ET partitioning and the difficulties in estimating Es, Scott and Biederman (2017) recently proposed a simple approach to assess the long-term mean ecosystem evaporation based on eddy covariance measurements, suggesting that these systems would be particularly suitable to dry environments. The approach is based on the argument that the relationships of monthly values of GPP as a function of ET can be described by a linear equation of the form ET=mGPP+E, where E can be obtained from the intercept of the best fit line (and were E=Es+Ei). As shown in Fig. 5.4, applying this approach showed good agreement with the more direct estimates obtained in the present study. These results seem, therefore, to provide support for the application of the simple Scott & Biederman approach. Note however, that E estimate using this approach provides a single value (possibly time averaged one) while the results here indicate significant dynamics in this parameter.

Finally, we note the Good et al. (2017) recent proposal of a global pattern of ecosystem water use in relation to available precipitation and the aridity index (the ratio of potential evaporation to precipitation, Ep/P). Their analysis shows that biological water use by vegetation maximizes under mesic conditions with a mean aridity index of 1.9 and a water use fraction, Et/P, of ~0.6. Our results show that the semi-arid forest plantation at the dry timberline (mean P of 287 mm) reached this optimal water use fraction of 0.6 but at an aridity index of 5.5, which was markedly higher than the Good et al. estimated optimum. These results may have several implications. They demonstrate that forest plantations, such as the 54 years Yatir forest, could extend into semi-arid regions beyond the range of natural forestation usually observed. This, in turn, may reflect potential adjustments of dry ecosystems to global change, such as increases in water use efficiency (Maseyk et al., 2011), resilience to stress (Tatarinov et al., 2016) and seasonal adjustments (Maseyk et al., 2008; Rotenberg and Yakir, 2010), promoting survival even when increasing mortality is identified in some climatic regions and biomes.

A5. APPENDIX

Table A5.1 | The correction factors between opaque or transparent chambers vs. lysimeters for the soil evaporation (Es) were conducted in greenhouse. Opaque chamber (Op), Transparent chamber (Tr), long tube (Lt; 15m), short tube (St; 1m), chamber painted with hydrophobic material (Hi). Note: the ±se of the main correction factor that used in the Es Eq. 5.2, is presented in parenthesis.

Opaque chamber		Transparent chamber	
Treatment	**Correction factor**	**Treatment**	**Correction factor**
Op+St	1.5	Tr+St	1.8
Op+Lt+Hi	2.2	Tr+Lt+Hi	1.6
Op+St+Hi	1.3	Tr+St+Hi	1.0
Op+Lt	2.5(0.1)	Tr+Lt	2.9

Table A5.2 | Monthly mean values of total evapotranspiration (ET), transpiration (Et), soil flux (Es), soil adsorption (Ea) and intercepted precipitation (Ei) during study period. Adsorption averaged for all days (Ea^1) or only for days when it occurred (Ea^2). Note: all of the water components multiplied with 100 for more convenient; the numbers in parenthesis is the ±se.

Season	Month	ET_{EC}	ET_{up}	E_t	E_i	E_s	E_a^1	E_a^2
		[x100 mm d^{-1}]						
Wet season (Nov-Apr)	Nov	53 (4)	66	18 (0)	20	28 (2)	-1.1 (1.4)	-10 (1)
	Dec	57 (2)	85	25 (0)	24	36 (1)	-0.2 (1.0)	-5 (1)
	Jan	90 (7)	140	50 (0)	44	46 (2)	-0.1 (0.5)	-2 (0)
	Feb	216 (12)	214	106 (0)	26	81 (4)	0.0 (0.8)	-2 (1)
	Mar	181 (8)	187	120 (0)	16	51 (2)	-0.1 (0.3)	-2 (0)
	Apr	219 (7)	214	128 (0)	15	71 (2)	-1.4 (1.1)	-13 (1)
	Average [mm d^{-1}]	**136 (32)**	**151 (26)**	**74 (20)**	**24 (4)**	**52 (8)**	**-1 (0)**	**-6 (2)**
	Season sum [mm]	**244 (9)**	**271 (8)**	**134 (6)**	**44 (1)**	**94 (2)**	**-1 (0)**	**-1 (0)**
	x/ETup [%]	**90**		**49**	**16**	**35**	**>1**	**>1**
Dry season (May-Oct)	May	109 (4)	108.1	94 (2)		14 (1)	-5.4 (0.5)	-14 (1)
	Jun	76 (4)	79.0	76 (1)		3 (1)	-7.4 (0.6)	-18 (1)
	Jul	72 (5)	79.5	81 (2)		-2 (1)	-12.0 (0.6)	-21 (1)
	Aug	70 (6)	47.9	46 (1)		2 (1)	-8.2 (0.5)	-16 (1)
	Sep	56 (3)	55.9	51 (3)		5 (1)	-6.2 (0.5)	-14 (1)
	Oct	46 (2)	48.4	42 (5)		7 (1)	-4.4 (0.6)	-14 (1)
	Average [mm d^{-1}]	**72 (9)**	**70 (10)**	**65 (9)**	**-**	**5 (2)**	**-7 (1)**	**-16 (1)**
	Season sum [mm]	**132 (3)**	**128 (3)**	**119 (3)**	**-**	**9 (1)**	**-13 (0)**	**-13 (0)**
	x/ETup [%]	**103**		**93**	**-**	**7**	**-10**	**-11**
Annual	**Average (SE)**	**104 (19)**	**110 (18)**	**70 (11)**	**24 (4)**	**29 (8)**	**-4 (1)**	**-11 (2)**
	Annual sum (SE)	**376 (6)**	**400 (5)**	**253 (3)**	**44 (1)**	**103 (2)**	**-14 (0)**	**-14 (0)**
	x/ETup [%]	**94**		**63**	**11**	**26**	**-4**	**-4**
	CV [%]	**62%**	**57%**	**52%**	**43%**	**99%**	**-103%**	**-62%**

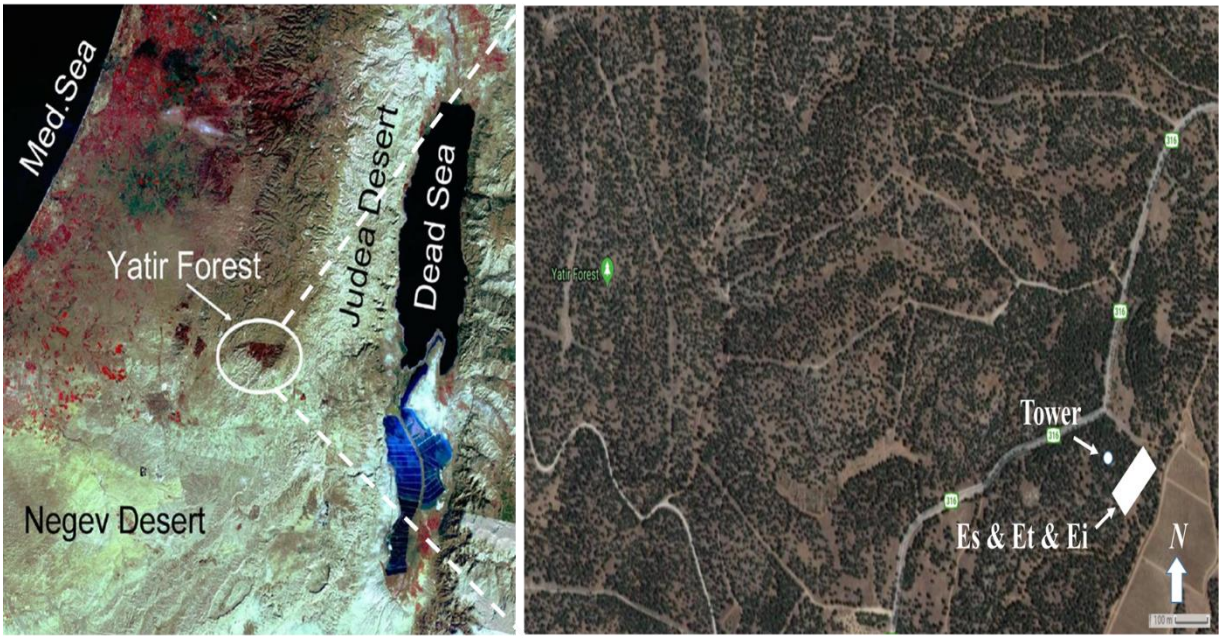

Figure A5.1 | (a) Landsat-TM image of Central Israel. (b) Map of the experimental set-up at the *Pinus halepensis* Yatir forest with white rectangle site of soil flux, transpiration, and interception (Es, Et, and Ei) measurements and white dot is the location of the eddy covariance tower (ET).

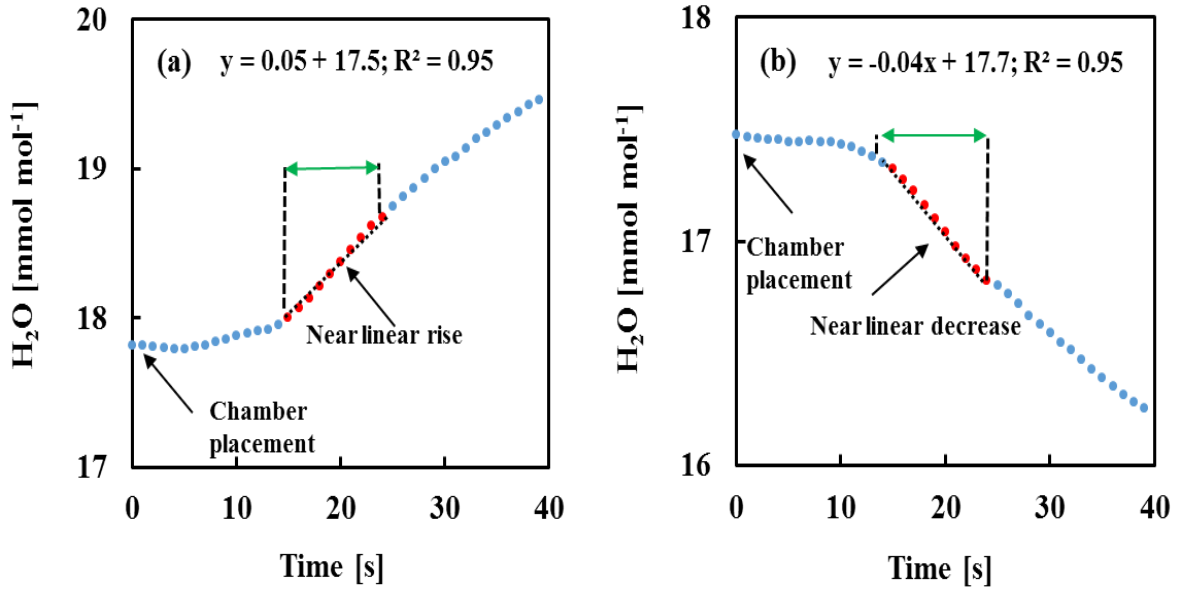

Figure A5.2 | Representative soil evaporation (Es) output from a LI-8100 measurements; for a) evaporation (Ev) with positive slope (efflux of water from soil to atmosphere) and b) adsorption (Ad) with negative slope (influx of water from atmosphere to soil), respectively. Note: Red points are included in the linear regression, whose slope is used to calculate flux.

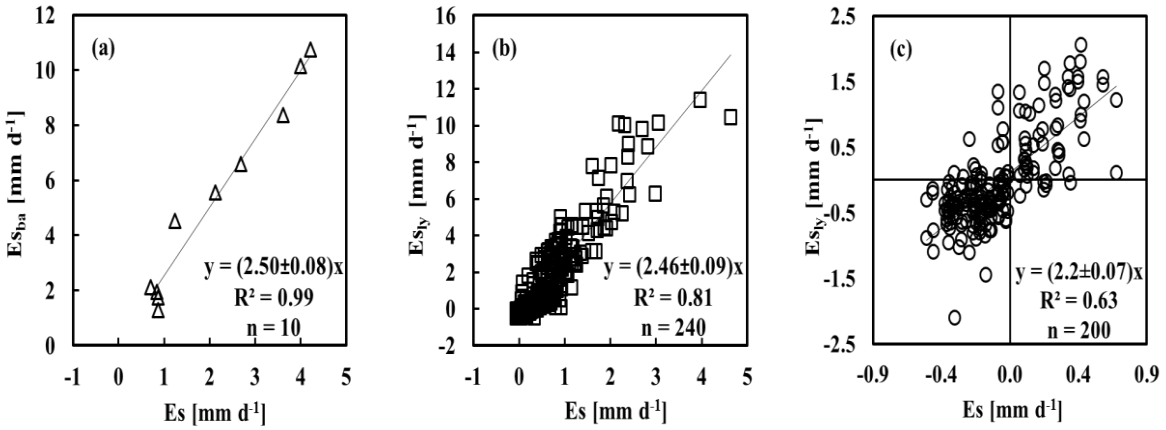

igure A5.3 | a) Calibration of soil evaporation (Es) measurements by LI-8100 (a) using simple balance system (ba) to estimate Es compared with estimates based on the commercial LI-8100 chamber system, under in-situ field conditions; b) using high precision commercial bench-top lysimeters (ly) to estimate of Es compared with LI-8100 chamber system for wet soil dry up and c) using high precision commercial bench-top lysimeters (ly) to estimate of Es compared with LI-8100 chamber system for dry soil to show the capability to measure the adsorption in the greenhouse during the summer period with conditions similar to field (4 days of half-hour measurements), the meteorological parameters presented in Figures A5.1-3. An opaque chamber was used in the LI-8100 system. Linear best fit lines and regression coefficients, and the number of comparisons are indicated.

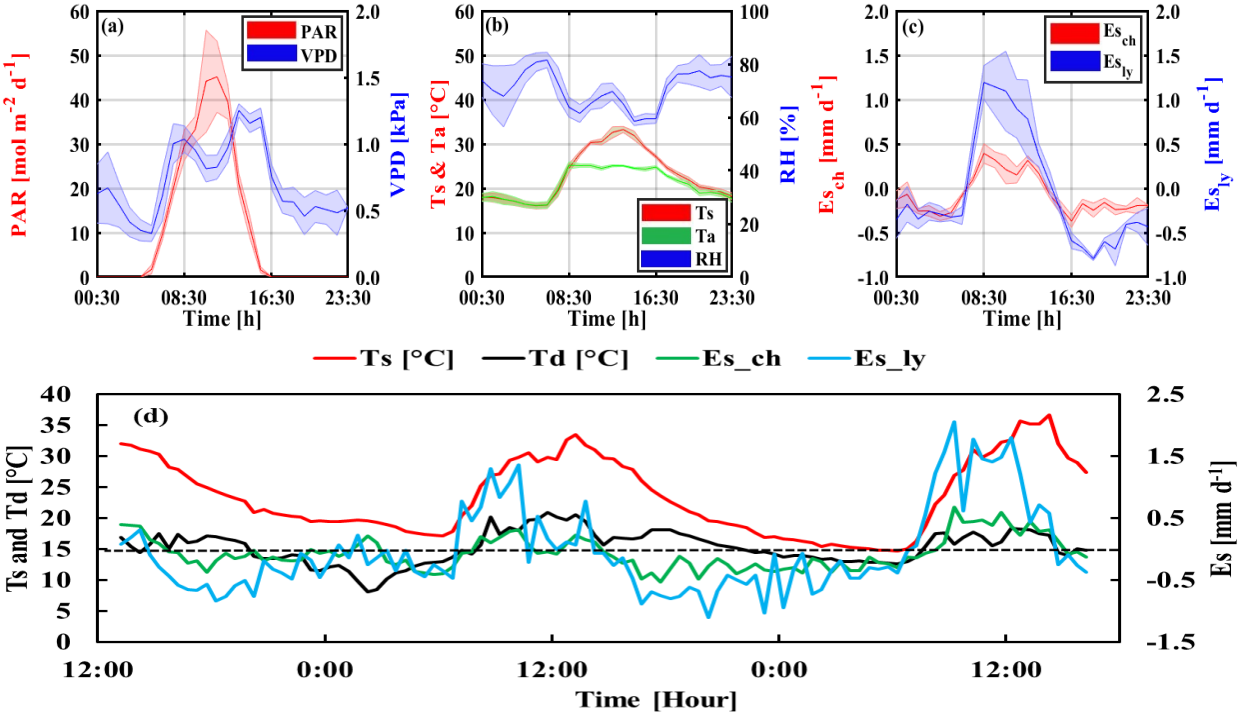

Figure A5.4 | Typical diurnal cycle of the meteorological parameters during comparing the lysimeter and chambers in the greenhouse for the dry Yatir soil for 4 days of half-hour measurements in the greenhouse to support the occurrence of the adsorption (following Figure A5.2-3c). a) Photosynthetic activity radiation (PAR) and vapour pressure deficit (VPD), b) soil temperature 5 cm (Ts) with air temperature at 20 cm (Ta) and relative humidity (RH), c) the soil evaporation Es for both approaches (half-hour measurements averaged for diurnal cycle) and d) 2 days of diurnal cycle of soil temperature 5 cm (Ts) and dew temperature 5 cm (Td). Note: 1- Td was calculate following Eq. 5.6 to check the capability of adsorption or dew formation; 2- the shaded areas are ±se.

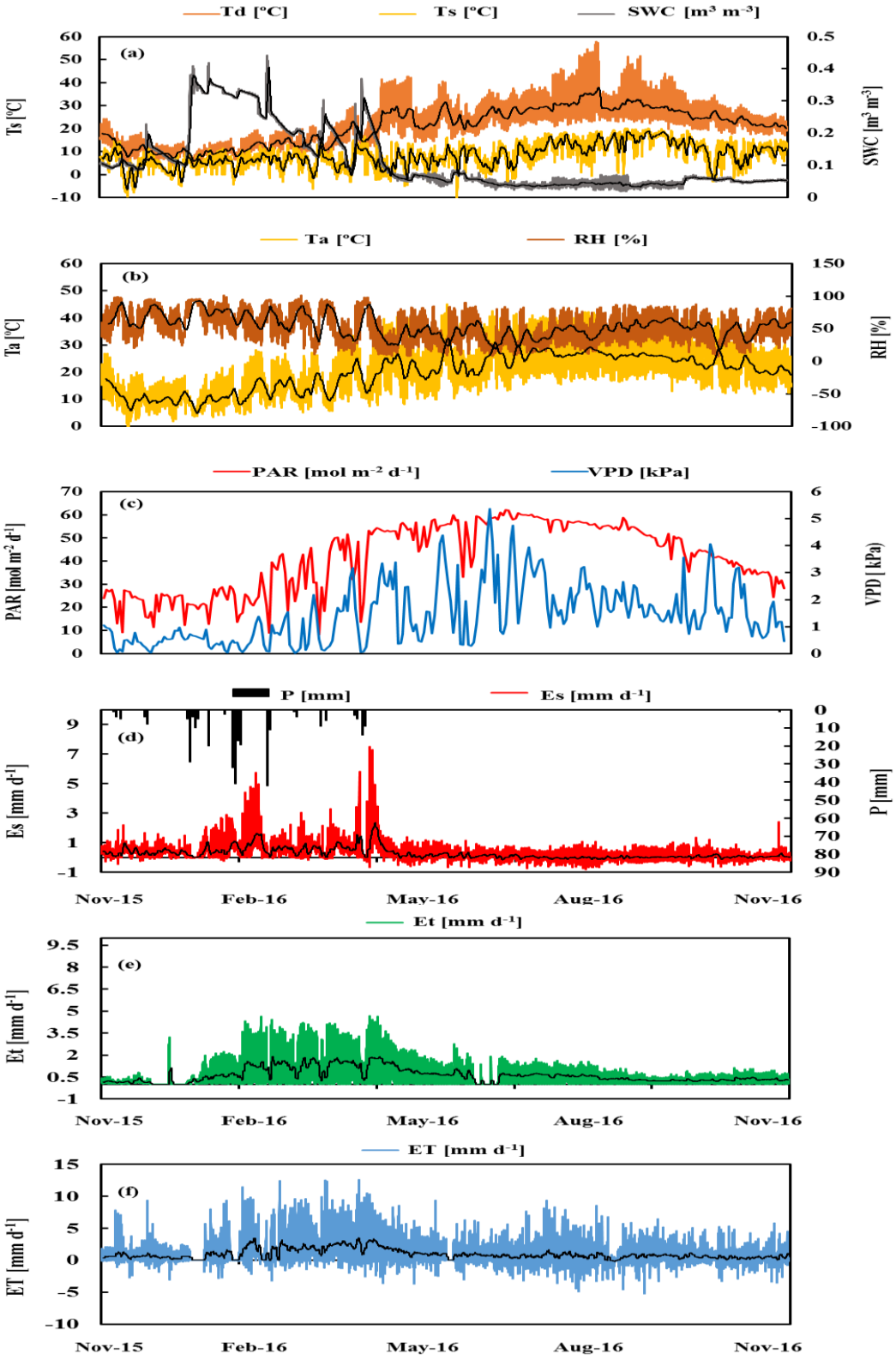

Figure A5.5 | a) half-hour values for soil temperature 5 cm (Ts), dew temperature 5 cm (Td), and soil water content 10 cm ($SWC_{0\text{-}10cm}$), b) half-hour values for the air temperature at 20 cm (Ta) and relative humidity at 20 cm (RH), c) daily average of incoming photosynthetic activity radiation above canopy (PAR) and vapour pressure deficit (VPD), d) half-hour values up-scaled Es and the precipitation (P), e) half-hour values transpiration (Et), and f) half-hour values evapotranspiration (ET). Black lines are a running average for a window of two days.

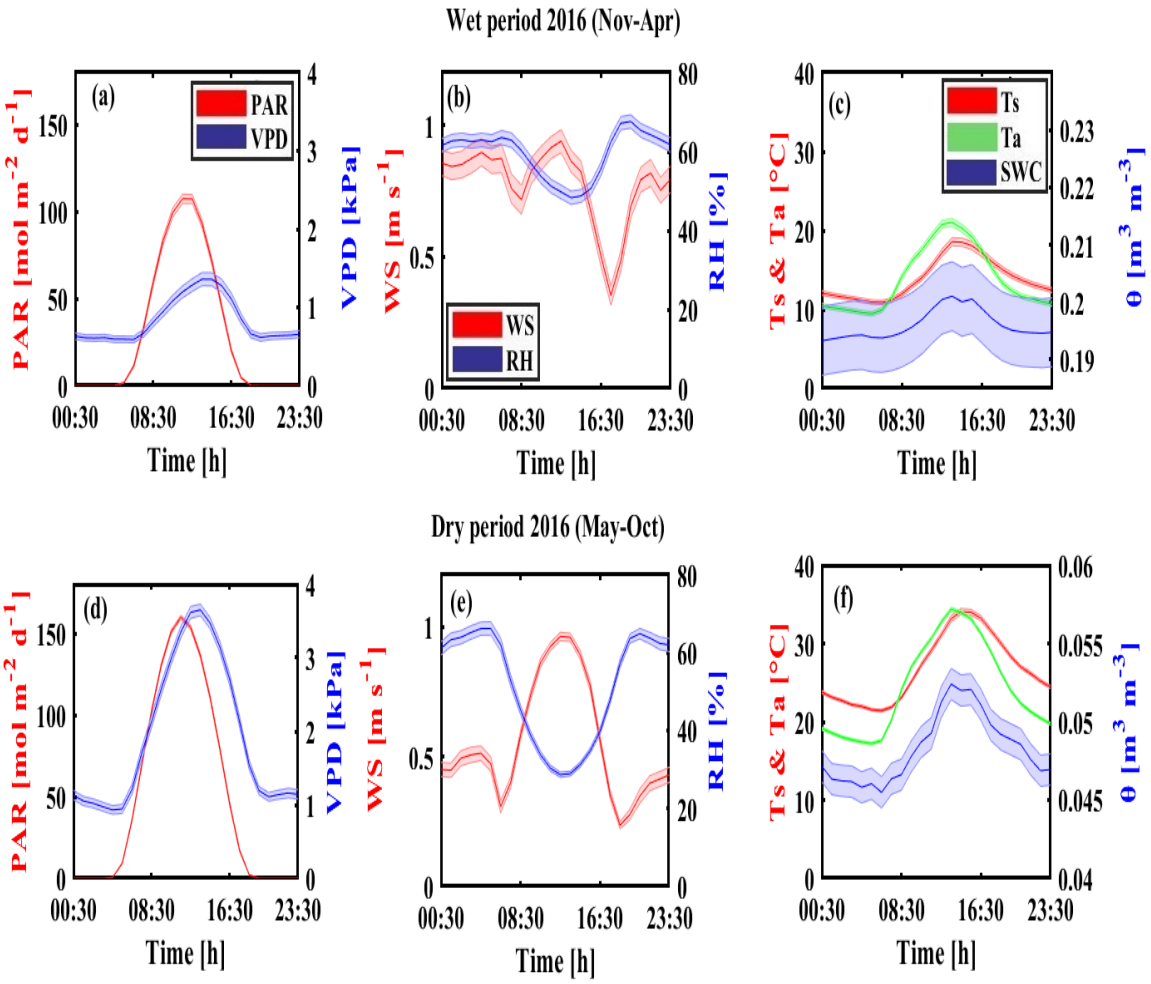

Figure A5.6 | Typical diurnal cycle of the meteorological parameters during the wet period (Nov.-Apr.; upper panels) and for the dry period (May-Oct.; lower panels); each set includes six months of half-hour measurements. Soil temperature at 5 cm (Ts), air temperature at 20 cm (Ta) and soil water content 10 cm ($SWC_{0\text{-}10cm}$). Shaded areas indicate ±se.

5

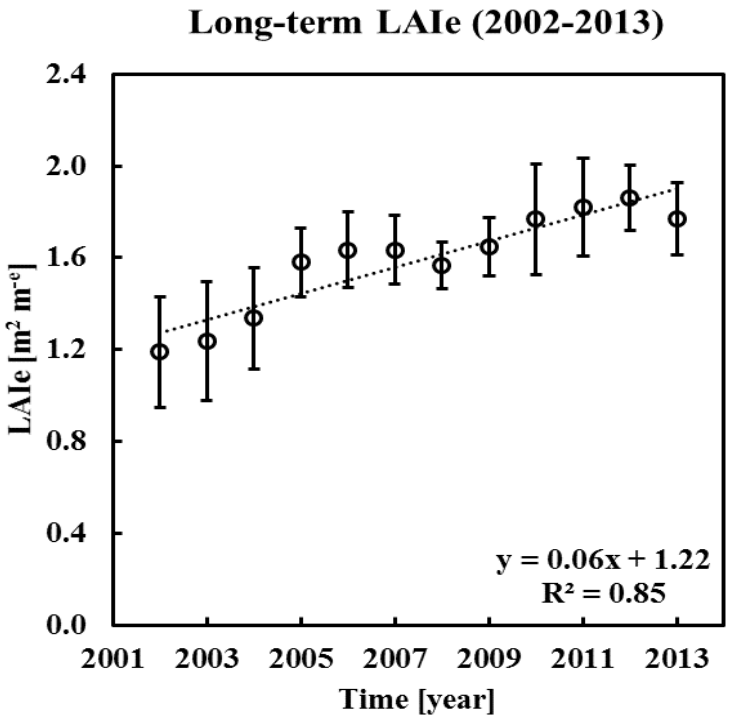

Figure A5.7 | Temporal changes in ecosystem leaf area index, LAIe, for the 2002 to 2013 period (subsequent measurements were more sporadic). Vertical bars represent ± one standard error of the measurements. The dotted line is the best fit regression line used to estimate LAI for the present study.

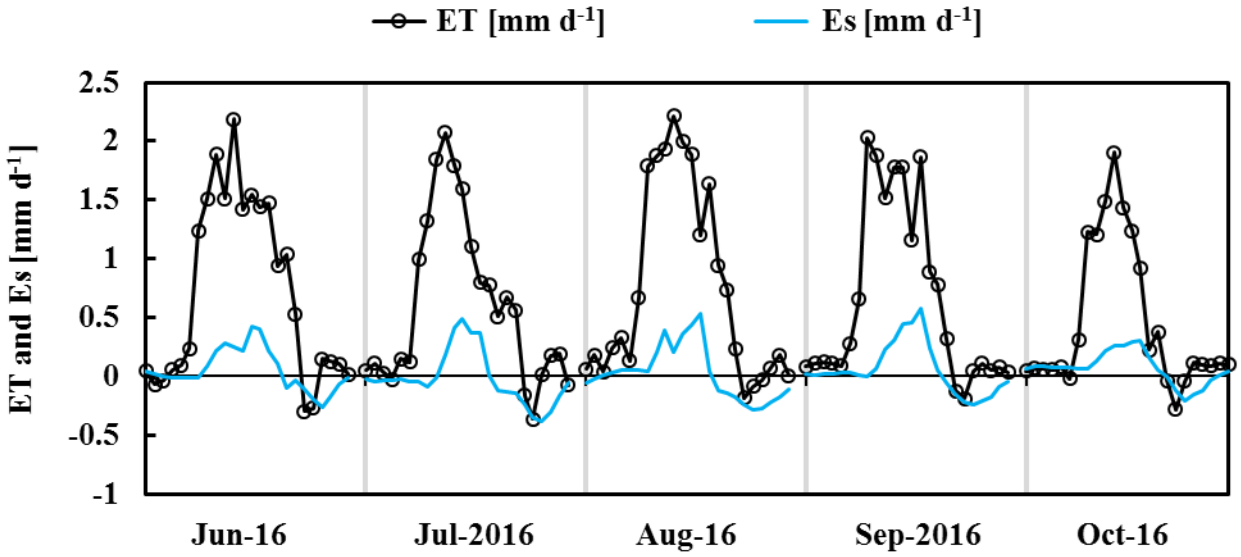

Figure A5.8 | Monthly-typical diurnal cycles of evapotranspiration (ET) and soil evaporation (Es) during the dry period (Jun-Oct), 2016. Half-hour measurements averaged for diurnal cycle and the negative values represent downward fluxes from the atmosphere to the forest or soil.

BIBLIOGRAPHY

Abera, Y., & Belachew, T. (2011). Effect of land use on soil organic carbon and nitrogen in the soils of Bale, Southeastern Ethiopia. Trop. Subtrop. Agro Ecosyst., 14: 229-235.

Adachi, M., Ito, A., Yonemura, S., & Takeuchi, W. (2017). Estimation of global soil respiration by accounting for land-use changes derived from remote sensing data. Journal of Environmental Management, 200, 97-104.

Adams, H. D., Luce, C. H., Breshears, D. D., Allen, C. D., Weiler, M., Hale, V. C., . . . Huxman, T. E. (2012). Ecohydrological consequences of drought- and infestation- triggered tree die-off: insights and hypotheses. Ecohydrology, 5(2), 145-159. doi:10.1002/eco.233

Afik, T., (2009). Quantitative estimation of CO2 fluxes in a semi-arid forest and their dependence on climatic factors. Thesis submitted to R.H. Smith Faculty of Agriculture, Food and Environment of Hebrew University, Rehovot, Israel (in Hebrew).

Agam, N., & Berliner, P. R. (2006). Dew formation and water vapor adsorption in semi-arid environments - A review. Journal of Arid Environments, 65(4), 572-590.

Agam, N., Berliner, P. R., Zangvil, A., & Ben-Dor, E. (2004). Soil water evaporation during the dry season in an arid zone. Journal of Geophysical Research-Atmospheres, 109(D16).

Agam, N., Kustas, W. P., Anderson, M. C., Norman, J. M., Colaizzi, P. D., Howell, T. A., . . . Wilson, T. B. (2010). Application of the Priestley-Taylor Approach in a Two-Source Surface Energy Balance Model. Journal of Hydrometeorology, 11(1), 185-198. doi:10.1175/2009jhm1124.1

Ahlström, A., Raupach, M. R., Schurgers, G., Smith, B., Arneth, A., Jung, M., . . . Zeng, N. (2015). The dominant role of semi-arid ecosystems in the trend and variability of the land CO2 sink. Science, 348(6237), 895-899. doi:10.1126/science.aaa1668

Akbari, H. (2002). Shade trees reduce building energy use and CO2 emissions from power plants. Environmental Pollution, 116, S119-S126. doi:10.1016/s0269-7491(01)00264-0

Alduchov, O. A., & Eskridge, R. E. (1996). Improved magnus form approximation of saturation vapor pressure. Journal of Applied Meteorology, 35(4), 601-609.

Alexandratos, N., & Bruinsma, J. (2012). World agriculture towards 2030/2050: the 2012 re-vision ESA Working paper No. 12–03. http://www.fao.org/docrep/016/ap106e/ap106e.pdf (Accessed May 15 2015).

Allen, R. G., & Fisher, D. K. (1990). LOW-COST ELECTRONIC WEIGHING LYSIMETERS. Transactions of the Asae, 33(6), 1823-1833.

Amundson R & Biardeau L (2018) Soil carbon sequestration is an elusive climate mitigation tool. PNAS, 115, 11652-11656

Anderson, R. G., Alfieri, J. G., Tirado-Corbala, R., Gartung, J., McKee, L. G., Prueger, J. H., . . . Kustas, W. P. (2017). Assessing FAO-56 dual crop coefficients using eddy covariance flux partitioning. Agricultural Water Management, 179, 92-102. doi:10.1016/j.agwat.2016.07.027

Angert, A., Yakir, D., Rodeghiero, M., Preisler, Y., Davidson, E. A., & Weiner, T. (2015). Using O-2 to study the relationships between soil CO2 efflux and soil respiration. Biogeosciences, 12(7), 2089-2099.

Asaf, D., Rotenberg, E., Tatarinov, F., Dicken, U., Montzka, S. A., & Yakir, D. (2013). Ecosystem photosynthesis inferred from measurements of carbonyl sulphide flux. Nature Geoscience, 6(3), 186-190. doi:10.1038/ngeo1730

Aubinet, M., (2008). Eddy covariance CO2 flux measurements in nocturnal conditions: an analysis of the problem. Ecol. Appl. 18, 1368–1378

Aubinet, M., Grelle, A., Ibrom, A., Rannik, U., Moncrieff, J., Foken, T., . . . Vesala, T. (2000). Estimates of the annual net carbon and water exchange of forests: The EUROFLUX methodology. Advances in Ecological Research, Vol 30, 30, 113-175.

Aubinet, M., Vesala, T., & Papale, D. (2012). Eddy Covariance: A Practical Guide to Measurement and Data Analysis (Springer).

Avitabile, V., & Camia, A. (2018). An assessment of forest biomass maps in Europe using harmonized national statistics and inventory plots. Forest Ecology and Management, 409, 489-498.

Bahn, M., Janssens, I. A., Reichstein, M., Smith, P., & Trumbore, S. E. (2010). Soil respiration across scales: towards an integration of patterns and processes. New Phytologist, 186(2), 292-296.

Baldocchi, D., Falge, E., Gu, L. H., Olson, R., Hollinger, D., Running, S., . . . Wofsy, S. (2001). FLUXNET: A new tool to study the temporal and spatial variability of ecosystem-scale carbon dioxide, water vapor, and energy flux densities. Bulletin of the American Meteorological Society, 82(11), 2415-2434. doi:10.1175/1520-0477(2001)082<2415:fantts>2.3.co;2

Baldock, J. A., Wheeler, I., McKenzie, N., & McBrateny, A. (2012). Soils and climate change: potential impacts on carbon stocks and greenhouse gas emissions, and future research for Australian agriculture. Crop & Pasture Science, 63(3), 269-283.

Balogh, J., Pinter, K., Foti, S., Cserhalmi, D., Papp, M., & Nagy, Z. (2011). Dependence of soil respiration on soil moisture, clay content, soil organic matter, and CO2 uptake in dry grasslands. Soil Biology & Biochemistry, 43(5), 1006-1013.

Bar Massada, A., Carmel, Y., Tzur, G. E., Grünzweig, J. M., & Yakir, D. (2006). Assessment of temporal changes in aboveground forest tree biomass using aerial photographs and allometric equations. Canadian Journal of Forest Research-Revue Canadienne De Recherche Forestiere, 36(10), 2585-2594. doi:10.1139/x06-152

Barford, C. C., Wofsy, S. C., Goulden, M. L., Munger, J. W., Pyle, E. H., Urbanski, S. P., et al. (2001). Factors controlling long- and short-term sequestration of atmospheric CO2 in a mid-latitude forest. Science, 294(5547), 1688-1691.

Bastin, J. F., Berrahmouni, N., Grainger, A., Maniatis, D., Mollicone, D., Moore, R., et al. (2017). The extent of forest in dryland biomes. Science, 356(6338), 635-+.

Bellamy, P. H., Loveland, P. J., Bradley, R. I., Lark, R. M., & Kirk, G. J. D. (2005). Carbon losses from all soils across England and Wales 1978-2003. Nature, 437(7056), 245-248. doi:10.1038/nature04038

Berkelhammer, M., Noone, D. C., Wong, T. E., Burns, S. P., Knowles, J. F., Kaushik, A., et al. (2016). Convergent approaches to determine an ecosystem's transpiration fraction. Global Biogeochemical Cycles, 30(6), 933-951.

Betts, R. A. (2000). Offset of the potential carbon sink from boreal forestation by decreases in surface albedo. Nature, 408(6809), 187-190. doi:10.1038/35041545

Biederman, J. A., Scott, R. L., Bell, T. W., Bowling, D. R., Dore, S., Garatuza-Payan, J., . . . Goulden, M. L. (2017). CO2 exchange and evapotranspiration across dryland ecosystems of southwestern North America. Global Change Biology, 23(10), 4204-4221. doi:10.1111/gcb.13686

Binkley, D., Stape, J. L., Takahashi, E. N., & Ryan, M. G. (2006). Tree-girdling to separate root and heterotrophic respiration in two Eucalyptus stands in Brazil. Oecologia, 148(3), 447-454.

Black, K., Bolger, T., Davis, P., Nieuwenhuis, M., Reidy, B., Saiz, G., et al. (2007). Inventory and eddy covariance-based estimates of annual carbon sequestration in a Sitka spruce (Picea sitchensis (Bong.) Carr.) forest ecosystem. European Journal of Forest Research, 126(2), 167-178.

Blonquist, J. M., Montzka, S. A., Munger, J. W., Yakir, D., Desai, A. R., Dragoni, D., . . . Bowling, D. R. (2011). The potential of carbonyl sulfide as a proxy for gross primary production at flux tower sites. Journal of Geophysical Research-Biogeosciences, 116. doi:10.1029/2011jg001723

Bonan, G. B. (2008). Ecological climatology : concepts and applications (2nd ed.. ed.). Cambridge: Cambridge : Cambridge University Press.

Bond-Lamberty, B., & Thomson, A. (2010). Temperature-associated increases in the global soil respiration record. Nature, 464(7288), 579-U132.

Breshears, D. D. (2006). The grassland-forest continuum: trends in ecosystem properties for woody plant mosaics? Frontiers in Ecology and the Environment, 4(2), 96-104. doi:10.1890/1540-9295(2006)004[0096:tgctie]2.0.co;2

Buchmann, N. (2000). Biotic and abiotic factors controlling soil respiration rates in Picea abies stands. Soil Biology & Biochemistry, 32(11-12), 1625-1635.

Cai, Y. B., Chen, Y. H., & Tong, C. (2019). Spatiotemporal evolution of urban green space and its impact on the urban thermal environment based on remote sensing data: A case study of Fuzhou City, China. Urban Forestry & Urban Greening, 41, 333-343. doi:10.1016/j.ufug.2019.04.012

Campioli, M., Malhi, Y., Vicca, S., Luyssaert, S., Papale, D., Penuelas, J., . . . Janssens, I. A. (2016). Evaluating the convergence between eddy-covariance and biometric methods for assessing carbon budgets of forests. Nature Communications, 7. doi:10.1038/ncomms13717

Carbone, M. S., Winston, G. C., & Trumbore, S. E. (2008). Soil respiration in perennial grass and shrub ecosystems: Linking environmental controls with plant and microbial sources on seasonal and diel timescales. Journal of Geophysical Research-Biogeosciences, 113(G2).

Carmi, I., Yakir, D., Yechieli, Y., Kronfeld, J., & Stiller, M. (2013). VARIATIONS IN SOIL CO2 CONCENTRATIONS AND ISOTOPIC VALUES IN A SEMI-ARID REGION DUE TO BIOTIC AND ABIOTIC PROCESSES IN THE UNSATURATED ZONE. Radiocarbon, 55(2-3), 932-942.

Carvalhais, N., Forkel, M., Khomik, M., Bellarby, J., Jung, M., Migliavacca, M., . . . Reichstein, M. (2014). Global covariation of carbon turnover times with climate in terrestrial ecosystems. Nature, 514(7521), 213-+. doi:10.1038/nature13731

Casals, P., Lopez-Sangil, L., Carrara, A., Gimeno, C., & Nogues, S. (2011). Autotrophic and heterotrophic contributions to short-term soil CO2 efflux following simulated summer precipitation pulses in a Mediterranean dehesa. Global Biogeochemical Cycles, 25. doi:10.1029/2010gb003973

Cermak, J., & Deml, M. (1974). Method of water transport measurements in woody species, especially in adult trees (in Czech). Patent (Certification of authorship) CSFR, No. 155622 (P.V. 5997- 1972). Bureau for Inventions and Discoveries, PragueCoenders-Gerrits, A. M. J., van der Ent, R. J., Bogaard, T. A., Wang-Erlandsson, L., Hrachowitz, M., & Savenije, H. H. G. (2014). Uncertainties in transpiration estimates. Nature, 506(7487), E1-E2.

Chapin, F. S., Woodwell, G. M., Randerson, J. T., Rastetter, E. B., Lovett, G. M., Baldocchi, D. D., . . . Schulze, E. D. (2006). Reconciling carbon-cycle concepts, terminology, and methods. Ecosystems, 9(7), 1041-1050. doi:10.1007/s10021-005-0105-7

Chen, D., Zhang, Y., Lin, Y., Zhu, W., & Fu, S. (2010). Changes in belowground carbon in Acacia crassicarpa and Eucalyptus urophylla plantations after tree girdling. Plant and Soil, 326(1-2), 123-135.

Chen, S. T., Zou, J. W., Hu, Z. H., Chen, H. S., & Lu, Y. Y. (2014). Global annual soil respiration in relation to climate, soil properties and vegetation characteristics: Summary of available data. Agricultural and Forest Meteorology, 198, 335-346.

Coenders-Gerrits, A. M. J., van der Ent, R. J., Bogaard, T. A., Wang-Erlandsson, L., Hrachowitz, M., & Savenije, H. H. G. (2014). Uncertainties in transpiration estimates. Nature, 506(7487), E1-E2.

Cohen, L. R., Raz-Yaseef, N., Curtis, J. B., Young, J. M., Rahn, T. A., Wilson, C. J., et al. (2015). Measuring diurnal cycles of evapotranspiration in the Arctic with an automated chamber system. Ecohydrology, 8(4), 652-659.

Cohen, Y., Cohen, S., Cantuarias-Aviles, T., & Schiller, G. (2008). Variations in the radial gradient of sap velocity in trunks of forest and fruit trees. Plant and Soil, 305(1-2), 49-59.

Conant, R. T., Klopatek, J. M., Malin, R. C., & Klopatek, C. C. (1998). Carbon pools and fluxes along an environmental gradient in northern Arizona. Biogeochemistry, 43(1), 43-61.

Conen, F., Zerva, A., Arrouays, D., Jolivet, C., Jarvis, P. G., Grace, J., & Mencuccini, M. (2005). The carbon balance of forest soils: detectability of changes in soil carbon stocks in temperate and Boreal forests, SEB Exp. Biol. Ser., 235–249.

Consoli, S., Facini, O., Nardino, M., & Rossi, F. (2014). Carbon balance and energy fluxes of a Mediterranean crop. Italian Journal of Agrometeorology-Rivista Italiana Di Agrometeorologia, 19(3), 15-24.

Correia, A. C., Minunno, F., Caldeira, M. C., Banza, J., Mateus, J., Carneiro, M., . . . Pereira, J. S. (2012). Soil water availability strongly modulates soil CO2 efflux in different Mediterranean ecosystems: Model calibration using the Bayesian approach. Agriculture Ecosystems & Environment, 161, 88-100. doi:10.1016/j.agee.2012.07.025

Crockford, R. H., & Richardson, D. P. (2000). Partitioning of rainfall into throughfall, stemflow and interception: effect of forest type, ground cover and climate. Hydrological Processes, 14(16-17), 2903-2920.

Curtis, P. S., Hanson, P. J., Bolstad, P., Barford, C., Randolph, J. C., Schmid, H. P., & Wilson, K. B. (2002). Biometric and eddy-covariance based estimates of annual carbon storage in five eastern North American deciduous forests. Agricultural and Forest Meteorology, 113(1-4), 3-19. doi:10.1016/s0168-1923(02)00099-0

Davidson, E. A., & Janssens, I. A. (2006). Temperature sensitivity of soil carbon decomposition and feedbacks to climate change. Nature, 440(7081), 165-173.

De Vos, B., Cools, N., Ilvesniemi, H., Vesterdal, L., Vanguelova, E., & Camicelli, S. (2015). Benchmark values for forest soil carbon stocks in Europe: Results from a large scale forest soil survey. Geoderma, 251, 33-46.

Delgado-Baquerizo, M., Maestre, F. T., Gallardol, A., Bowker, M. A., Wallenstein, M. D., Quero, J. L., . . . Zaady, E. (2013). Decoupling of soil nutrient cycles as a function of aridity in global drylands. Nature, 502(7473), 672-+. doi:10.1038/nature12670

DeLucia, E. H., Drake, J. E., Thomas, R. B., & Gonzalez-Meler, M. (2007). Forest carbon use efficiency: is respiration a constant fraction of gross primary production? Global Change Biology, 13(6), 1157-1167.

Deng, Q., Hui, D., Zhang, D., Zhou, G., Liu, J., Liu, S., et al. (2012). Effects of Precipitation Increase on Soil Respiration: A Three-Year Field Experiment in Subtropical Forests in China. Plos One, 7(7).

Ding, J. Z., Chen, L. Y., Ji, C. J., Hugelius, G., Li, Y. N., Liu, L., . . . Yang, Y. H. (2017). Decadal soil carbon accumulation across Tibetan permafrost regions. Nature Geoscience, 10(6), 420-+. doi:10.1038/ngeo2945

Donohue, R. J., Roderick, M. L., McVicar, T. R., & Farquhar, G. D. (2013). Impact of CO2 fertilization on maximum foliage cover across the globe's warm, arid environments. Geophysical Research Letters, 40(12), 3031-3035.

Epron, D., Le Dantec, V., Dufrene, E., & Granier, A. (2001). Seasonal dynamics of soil carbon dioxide efflux and simulated rhizosphere respiration in a beech forest. Tree Physiology, 21(2-3), 145-152. doi:10.1093/treephys/21.2-3.145

Eriksson, H., Eklundh, L., Hall, K., & Lindroth, A. (2005). Estimating LAI in deciduous forest stands. Agricultural and Forest Meteorology, 129(1-2), 27-37.

ESA-UN, 2014. World Urbanization Prospects. Accessed from esa.un.org on 07 October, 2014.

Etzold, S., Ruehr, N. K., Zweifel, R., Dobbertin, M., Zingg, A., Pluess, P., et al. (2011). The Carbon Balance of Two Contrasting Mountain Forest Ecosystems in Switzerland: Similar Annual Trends, but Seasonal Differences. Ecosystems, 14(8), 1289-1309.

Etzold, S., Zweifel, R., Ruehr, N. K., Eugster, W., & Buchmann, N. (2013). Long-term stem CO2 concentration measurements in Norway spruce in relation to biotic and abiotic factors. New Phytologist, 197(4), 1173-1184. doi:10.1111/nph.12115

Falge, E., Baldocchi, D., Tenhunen, J., Aubinet, M., Bakwin, P., Berbigier, P., et al. (2002). Seasonality of ecosystem respiration and gross primary production as derived from FLUXNET measurements. Agricultural and Forest Meteorology, 113(1-4), 53-74.

Fares, A., Safeeq, M., & Jenkins, D. M. (2009). Adjusting Temperature and Salinity Effects on Single Capacitance Sensors. Pedosphere, 19(5), 588-596.

Fatichi, S., & Pappas, C. (2017). Constrained variability of modeled T:ET ratio across biomes. Geophysical Research Letters, 44(13), 6795-6803.

Feng, Q., Endo, K. N., & Cheng, G. D. (2002). Soil carbon in desertified land in relation to site characteristics. Geoderma, 106(1-2), 21-43. doi:10.1016/s0016-7061(01)00099-4

Ferreira, M. I., Silvestre, J., Conceicao, N., & Malheiro, A. C. (2012). Crop and stress coefficients in rainfed and deficit irrigation vineyards using sap flow techniques. Irrigation Science, 30(5), 433-447. doi:10.1007/s00271-012-0352-2

Finnigan, J. J., & Belcher, S. E. (2004). Flow over a hill covered with a plant canopy. Quarterly Journal of the Royal Meteorological Society, 130(596), 1-29. doi:10.1256/qj.02.177

Fisher, J. B., Melton, F., Middleton, E., Hain, C., Anderson, M., Allen, R., et al. (2017). The future of evapotranspiration: Global requirements for ecosystem functioning, carbon and climate feedbacks, agricultural management, and water resources. Water Resources Research, 53(4), 2618-2626.

Flechard, C. R., Ibrom, A., Skiba, U. M., de Vries, W., van Oijen, M., Cameron, D. R., et al. (2019). Carbon / nitrogen interactions in European forests and semi-natural vegetation. Part I: Fluxes and budgets of carbon, nitrogen and greenhouse gases from ecosystem monitoring and modelling, Biogeosciences Discuss., https://doi.org/10.5194/bg-2019-333, in review, 2019.

Flechard, C. R., van Oijen, M., Cameron, D. R., de Vries, W., Ibrom, A., Buchmann, N., Dise, N. B., et al. (2019). Carbon / nitrogen interactions in European forests and semi-natural vegetation. Part II: Untangling climatic, edaphic, management and nitrogen deposition effects on carbon sequestration potentials, Biogeosciences Discuss., https://doi.org/10.5194/bg-2019-335, in review, 2019.

Frank, A. B., Liebig, M. A., & Hanson, J. D. (2002). Soil carbon dioxide fluxes in northern semiarid grasslands. Soil Biology & Biochemistry, 34(9), 1235-1241.

Frey, B., Hagedorn, F., & Giudici, F. (2006). Effect of girdling on soil respiration and root composition in a sweet chestnut forest. Forest Ecology and Management, 225(1-3), 271-277.

Garcia-Pausas, J., Casals, P., Camarero, L., Huguet, C., Thompson, R., Sebastia, M. T., & Romanya, J. (2008). Factors regulating carbon mineralization in the surface and subsurface soils of Pyrenean mountain grasslands. Soil Biology & Biochemistry, 40(11), 2803-2810. doi:10.1016/j.soilbio.2008.08.001

Gebauer, R. L. E., & Ehleringer, J. R. (2000). Water and nitrogen uptake patterns following moisture pulses in a cold desert community. Ecology, 81(5), 1415-1424. doi:10.1890/0012-9658(2000)081[1415:wanupf]2.0.co;2

Gelfand, I., Grünzweig, J. M., & Yakir, D. (2012). Slowing of nitrogen cycling and increasing nitrogen use efficiency following afforestation of semi-arid shrubland. Oecologia, 168(2), 563-575. doi:10.1007/s00442-011-2111-0

Giardina, C. P., & Ryan, M. G. (2002). Total belowground carbon allocation in a fast-growing Eucalyptus plantation estimated using a carbon balance approach. Ecosystems, 5(5), 487-499.

Gielen, B., De Vos, B., Campioli, M., Neirynck, J., Papale, D., Verstraeten, A., . . . Janssens, I. A. (2013). Biometric and eddy covariance-based assessment of decadal carbon sequestration of a temperate Scots pine forest. Agricultural and Forest Meteorology, 174, 135-143. doi:10.1016/j.agrformet.2013.02.008

Gielen, B., De Vos, B., Campioli, M., Neirynck, J., Papale, D., Verstraeten, A., et al. (2013). Biometric and eddy covariance-based assessment of decadal carbon sequestration of a temperate Scots pine forest. Agricultural and Forest Meteorology, 174, 135-143.

Gile, L. H., & Grossman, R. B. (1979). The desert project soil monograph. USDA-SCS, Washington, D.C.

Gillabel, J., Cebrian-Lopez, B., Six, J., & Merckx, R. (2010). Experimental evidence for the attenuating effect of SOM protection on temperature sensitivity of SOM decomposition. Global Change Biology, 16(10), 2789-2798. doi:10.1111/j.1365-2486.2009.02132.x

Gockede, M., Foken, T., Aubinet, M., Aurela, M., Banza, J., Bernhofer, C., . . . Yakir, D. (2008). Quality control of CarboEurope flux data - Part 1: Coupling footprint analyses with flux data quality assessment to evaluate sites in forest ecosystems. Biogeosciences, 5(2), 433-450.

Goldhamer, D., & Salinas, m. (2000). Evaluation of regulated defcit irrigation on mature orange trees grown under high evaporative demand. In: Proceedings of the International Society of Citriculture IX Congress. Orlando, FL. December 3-7, 2000: 227-231.

Gonzalez-Real, M. M., Martin-Gorriz, B., Egea, G., Nortes, P. A., & Baille, A. (2018). Characterization and modelling of soil CO2 efflux in old and young irrigated citrus orchards. Catena, 162, 376-385. doi:10.1016/j.catena.2017.10.025

Good, S. P., Moore, G. W., & Miralles, D. G. (2017). A mesic maximum in biological water use demarcates biome sensitivity to aridity shifts. Nature Ecology & Evolution, 1(12), 1883-+.

Granier, A. (1987). Evaluation of transpiration in a douglas-fir stand by means of sap flow measurements. Tree Physiology, 3(4), 309-319.

Granier, A., Breda, N., Longdoz, B., Gross, P., & Ngao, J. (2008). Ten years of fluxes and stand growth in a young beech forest at Hesse, North-eastern France. Annals of Forest Science, 65(7). doi:10.1051/forest:2008052

Graven, H. D., Guilderson, T. P., & Keeling, R. F. (2012). Observations of radiocarbon in CO2 at La Jolla, California, USA 1992-2007: Analysis of the long-term trend. Journal of Geophysical Research-Atmospheres, 117.

Griffis, T. J., Sargent, S. D., Baker, J. M., Lee, X., Tanner, B. D., Greene, J., . . . Billmark, K. (2008). Direct measurement of biosphere-atmosphere isotopic CO2 exchange using the eddy covariance technique. Journal of Geophysical Research-Atmospheres, 113(D8). doi:10.1029/2007jd009297

Grote, R., Samson, R., Alonso, R., Amorim, J. H., Carinanos, P., Churkina, G., . . . Calfapietra, C. (2016). Functional traits of urban trees: air pollution mitigation potential. Frontiers in Ecology and the Environment, 14(10), 543-550. doi:10.1002/fee.1426

Grover, S. P. P., Livesley, S. J., Hutley, L. B., Jamali, H., Fest, B., Beringer, J., et al. (2012). Land use change and the impact on greenhouse gas exchange in north Australian savanna soils. Biogeosciences, 9(1), 423-437.

Grüenzweig, J. M., Hemming, D., Maseyk, K., Lin, T., Rotenberg, E., Raz-Yaseef, N., . . . Yakir, D. (2009). Water limitation to soil CO2 efflux in a pine forest at the semiarid "timberline". Journal of Geophysical Research-Biogeosciences, 114. doi:10.1029/2008jg000874

Grünzweig, J. M., Gelfand, I., Fried, Y., & Yakir, D. (2007). Biogeochemical factors contributing to enhanced carbon storage following afforestation of a semi-arid shrubland. Biogeosciences, 4(5), 891-904.

Grünzweig, J. M., Hemming, D., Maseyk, K., Lin, T., Rotenberg, E., Raz-Yaseef, N., et al. (2009). Water limitation to soil CO2 efflux in a pine forest at the semiarid "timberline". Journal of Geophysical Research-Biogeosciences, 114.

Grünzweig, J. M., Lin, T., Rotenberg, E., Schwartz, A., & Yakir, D. (2003). Carbon sequestration in arid-land forest. Global Change Biology, 9(5), 791-799. doi:10.1046/j.1365-2486.2003.00612.x

Grünzweig, J. M., Sparrow, S. D., Yakir, D., & Chapin, F. S. (2004). Impact of agricultural land-use change on carbon storage in boreal Alaska. Global Change Biology, 10(4), 452-472. doi:10.1111/j.1529-8817.2003.00738.x

Hagedorn, F., Joseph, J., Peter, M., Luster, J., Pritsch, K., Geppert, U., . . . Arend, M. (2016). Recovery of trees from drought depends on belowground sink control. Nature Plants, 2(8). doi:10.1038/nplants.2016.111

Hashimoto, S., Carvalhais, N., Ito, A., Migliavacca, M., Nishina, K., & Reichstein, M. (2015). Global spatiotemporal distribution of soil respiration modeled using a global database. Biogeosciences, 12(13), 4121-4132.

Hassink, J. (1997). The capacity of soils to preserve organic C and N by their association with clay and silt particles. Plant and Soil, 191(1), 77-87. doi:10.1023/a:1004213929699

Hassink, J., & Whitmore, A. P. (1997). A model of the physical protection of organic matter in soils. Soil Science Society of America Journal, 61(1), 131-139. doi:10.2136/sssaj1997.03615995006100010020x

Hassink, J., Whitmore, A. P., & Kubat, J. (1997). Size and density fractionation of soil organic matter and the physical capacity of soils to protect organic matter. European Journal of Agronomy, 7(1-3), 189-199. doi:10.1016/s1161-0301(97)00045-2

Hemming, D., Yakir, D., Ambus, P., Aurela, M., Besson, C., Black, K., . . . Vesala, T. (2005). Pan-European delta C-13 values of air and organic matter from forest ecosystems. Global Change Biology, 11(7), 1065-1093. doi:10.1111/j.1365-2486.2005.00971.x

Hogberg, P., Bhupinderpal, S., Lofvenius, M. O., & Nordgren, A. (2009). Partitioning of soil respiration into its autotrophic and heterotrophic components by means of tree-girdling in old boreal spruce forest. Forest Ecology and Management, 257(8), 1764-1767.

Hooker, T. D., & Compton, J. E. (2003). Forest ecosystem carbon and nitrogen accumulation during the first century after agricultural abandonment. Ecological Applications, 13(2), 299-313. doi:10.1890/1051-0761(2003)013[0299:fecana]2.0.co;2

Huang, M. T., Piao, S. L., Sun, Y., Ciais, P., Cheng, L., Mao, J. F., et al. (2015). Change in terrestrial ecosystem water-use efficiency over the last three decades. Global Change Biology, 21(6), 2366-2378.

Hui, D. F., & Luo, Y. Q. (2004). Evaluation of soil CO2 production and transport in Duke Forest using a process-based modeling approach. Global Biogeochemical Cycles, 18(4).

Hursh, A., Ballantyne, A., Cooper, L., Maneta, M., Kimball, J., & Watts, J. (2017). The sensitivity of soil respiration to soil temperature, moisture, and carbon supply at the global scale. Global Change Biology, 23(5), 2090-2103. doi:10.1111/gcb.13489

IPCC, (2014). Climate Change 2014: Mitigation of Climate Change. Contribution of Working Group III to the Fifth Assessment Report of the Intergovernmental Panel on Climate Change [Edenhofer, O., R. et al.]. Cambridge University Press, Cambridge and New York.

Jackson, R. B., Banner, J. L., Jobbagy, E. G., Pockman, W. T., & Wall, D. H. (2002). Ecosystem carbon loss with woody plant invasion of grasslands. Nature, 418(6898), 623-626. doi:10.1038/nature00910

Jacobs, A. F. G., Heusinkveld, B. G., & Berkowicz, S. M. (2000). Dew measurements along a longitudinal sand dune transect, Negev Desert, Israel. International Journal of Biometeorology, 43(4), 184-190.

Janssens, I. A., Freibauer, A., Ciais, P., Smith, P., Nabuurs, G. J., Folberth, G., . . . Dolman, A. J. (2003). Europe's terrestrial biosphere absorbs 7 to 12% of European anthropogenic CO2 emissions. Science, 300(5625), 1538-1542. doi:10.1126/science.1083592

Janssens, I. A., Lankreijer, H., Matteucci, G., Kowalski, A. S., Buchmann, N., Epron, D., . . . Valentini, R. (2001). Productivity overshadows temperature in determining soil and ecosystem respiration across European forests. Global Change Biology, 7(3), 269-278. doi:10.1046/j.1365-2486.2001.00412.x

Jiang, H., Deng, Q., Zhou, G., Hui, D., Zhang, D., Liu, S., et al. (2013). Responses of soil respiration and its temperature/moisture sensitivity to precipitation in three subtropical forests in southern China. Biogeosciences, 10(6), 3963-3982.

Jiang, N., Zhu, W. Q., Zheng, Z. T., Chen, G. S., & Fan, D. Q. (2013). A Comparative Analysis between GIMSS NDVIg and NDVI3g for Monitoring Vegetation Activity Change in the Northern Hemisphere during 1982-2008. Remote Sensing, 5(8), 4031-4044.

Jobbagy, E. G., & Jackson, R. B. (2000). The vertical distribution of soil organic carbon and its relation to climate and vegetation. Ecological Applications, 10(2), 423-436. doi:10.1890/1051-0761(2000)010[0423:tvdoso]2.0.co;2

Johnson, D. W., Todd, D. E., Trettin, C. F., & Sedinger, J. S. (2007). Soil carbon and nitrogen changes in forests of walker branch watershed, 1972 to 2004. Soil Science Society of America Journal, 71(5), 1639-1646. doi:10.2136/sssaj2006.0365

Joseph, J., Kulls, C., Arend, M., Schaub, M., Hagedorn, F., Gessler, A., & Weiler, M. (2019). Application of a laser-based spectrometer for continuous in situ measurements of stable isotopes of soil CO2 in calcareous and acidic soils. Soil, 5(1), 49-62. doi:10.5194/soil-5-49-2019

Jung, M., Reichstein, M., Ciais, P., Seneviratne, S. I., Sheffield, J., Goulden, M. L., et al. (2010). Recent decline in the global land evapotranspiration trend due to limited moisture supply. Nature, 467(7318), 951-954.

Kalma, J. D., McVicar, T. R., & McCabe, M. F. (2008). Estimating Land Surface Evaporation: A Review of Methods Using Remotely Sensed Surface Temperature Data. Surveys in Geophysics, 29(4-5), 421-469. doi:10.1007/s10712-008-9037-z

Kalma, J., & Stanhill, G. (1969). TRANSPIRATION, EVAPORATION AND DEEP DRAINAGE LOSSES FROM AN ORANGE PLANTATION. Publication of The Volcani Institute of Agricultural Research.

Kemanian, A. R., & Stöckle, C. O. (2010). C-Farm: A simple model to evaluate the carbon balance of soil profiles. European Journal of Agronomy, 32(1), 22-29. doi:10.1016/j.eja.2009.08.003

Kerridge, B. L., Hornbuckle, J. W., Christen, E. W., & Faulkner, R. D. (2013). Using soil surface temperature to assess soil evaporation in a drip irrigated vineyard. Agricultural Water Management, 116, 128-141. doi:10.1016/j.agwat.2012.07.001

Kidron, G. J., Herrnstadt, I., & Barzilay, E. (2002). The role of dew as a moisture source for sand microbiotic crusts in the Negev Desert, Israel. Journal of Arid Environments, 52(4), 517-533.

Klein, T., Di Matteo, G., Rotenberg, E., Cohen, S., & Yakir, D. (2013). Differential ecophysiological response of a major Mediterranean pine species across a climatic gradient. Tree Physiology, 33(1), 26-36.

Klein, T., Rotenberg, E., Cohen-Hilaleh, E., Raz-Yaseef, N., Tatarinov, F., Preisler, Y., . . . Yakir, D. (2014). Quantifying transpirable soil water and its relations to tree water use dynamics in a water- limited pine forest. Ecohydrology, 7(2), 409-419. doi:10.1002/eco.1360

Klein, T., Rotenberg, E., Tatarinov, F., & Yakir, D. (2016). Association between sap flow-derived and eddy covariance-derived measurements of forest canopy CO2 uptake. New Phytologist, 209(1), 436-446.

Kominami, Y., Jomura, M., Dannoura, M., Goto, Y., Tamai, K., Miyama, T., et al. (2008). Biometric and eddy-covariance-based estimates of carbon balance for a warm-temperate mixed forest in Japan. Agricultural and Forest Meteorology, 148(5), 723-737.

Kool, D. M., Chung, H. G., Tate, K. R., Ross, D. J., Newton, P. C. D., & Six, J. (2007). Hierarchical saturation of soil carbon pools near a natural CO2 spring. Global Change Biology, 13(6), 1282-1293. doi:10.1111/j.1365-2486.2007.01362.x

Kool, D., Agam, N., Lazarovitch, N., Heitman, J. L., Sauer, T. J., & Ben-Gal, A. (2014a). A review of approaches for evapotranspiration partitioning. Agricultural and Forest Meteorology, 184, 56-70. doi:10.1016/j.agrformet.2013.09.003

Kool, D., Ben-Gal, A., Agam, N., Simunek, J., Heitman, J. L., Sauer, T. J., & Lazarovitch, N. (2014b). Spatial and diurnal below canopy evaporation in a desert vineyard: Measurements and modeling. Water Resources Research, 50(8), 7035-7049. doi:10.1002/2014wr015409

Kool, D., Kustas, W. P., Ben-Gal, A., Lazarovitch, N., Heitman, J. L., Sauer, T. J., & Agam, N. (2016). Energy and evapotranspiration partitioning in a desert vineyard. Agricultural and Forest Meteorology, 218, 277-287. doi:10.1016/j.agrformet.2016.01.002

Kordova-Biezuner, L., Mahrer, I., & Schwartz, C. (2000). Estimation of actual evapotranspiration from vineyard by utilizing eddy correlation method. Proceedings of the Third International Symposium on Irrigation of Horticultural Crops, Vols 1 and 2(537), 167-175. doi:10.17660/ActaHortic.2000.537.17

Körner, C. (2017). A matter of tree longevity. Science, 355(6321), 130-131.doi:10.1126/science.aal2449

Kosmas, C., Danalatos, N. G., Poesen, J., & van Wesemael, B. (1998). The effect of water vapour adsorption on soil moisture content under Mediterranean climatic conditions. Agricultural Water Management, 36(2), 157-168.

Kosmas, C., Marathianou, M., Gerontidis, S., Detsis, V., Tsara, M., & Poesen, J. (2001). Parameters affecting water vapor adsorption by the soil under semi-arid climatic conditions. Agricultural Water Management, 48(1), 61-78.

Koutroulis, A. G. (2019). Dryland changes under different levels of global warming. Science of the Total Environment, 655, 482-511. doi:10.1016/j.scitotenv.2018.11.215

Kowalski, A. S., Serrano-Ortiz, P., Janssens, I. A., Sanchez-Moral, S., Cuezva, S., Domingo, F., et al. (2008). Can flux tower research neglect geochemical CO2 exchange? Agricultural and Forest Meteorology, 148(6-7), 1045-1054.

Kuzyakov, Y. (2006). Sources of CO2 efflux from soil and review of partitioning methods. Soil Biology & Biochemistry, 38(3), 425-448. doi:10.1016/j.soilbio.2005.08.020

Lal, R. (2004). Carbon sequestration in dryland ecosystems. Environmental Management, 33(4), 528-544. doi:10.1007/s00267-003-9110-9

Lal, R. (2018). Digging deeper: A holistic perspective of factors affecting soil organic carbon sequestration in agroecosystems. Global Change Biology, 24(8), 3285-3301. doi:10.1111/gcb.14054

Lasslop, G., Reichstein, M., Papale, D., Richardson, A. D., Arneth, A., Barr, A., . . . Wohlfahrt, G. (2010). Separation of net ecosystem exchange into assimilation and respiration using a light response curve approach: critical issues and global evaluation. Global Change Biology, 16(1), 187-208. doi:10.1111/j.1365-2486.2009.02041.x

Law, B. E., Thornton, P. E., Irvine, J., Anthoni, P. M., & Van Tuyl, S. (2001). Carbon storage and fluxes in ponderosa pine forests at different developmental stages. Global Change Biology, 7(7), 755-777. doi:10.1046/j.1354-1013.2001.00439.x

Lawrence, D. M., Thornton, P. E., Oleson, K. W., & Bonan, G. B. (2007). The partitioning of evapotranspiration into transpiration, soil evaporation, and canopy evaporation in a GCM: Impacts on land-atmosphere interaction. Journal of Hydrometeorology, 8(4), 862-880.

Lawrence, M. G. (2005). The relationship between relative humidity and the dewpoint temperature in moist air - A simple conversion and applications. Bulletin of the American Meteorological Society, 86(2), 225-+.

Le Houérou, H. N. (1997). Climate, flora and fauna changes in the Sahara over the past 500 million years. Journal of Arid Environments, 37(4), 619-647. doi:10.1006/jare.1997.0315

Le Quéré, C., Andrew, R. M., Friedlingstein, P., Sitch, S., Hauck, J., Pongratz, J., . . . Zheng, B. (2018a). Global Carbon Budget 2018. Earth System Science Data, 10(4), 2141-2194. doi:10.5194/essd-10-2141-2018

Le Quéré, C., Andrew, R. M., Friedlingstein, P., Sitch, S., Pongratz, J., Manning, A. C., . . . Zhu, D. (2018b). Global Carbon Budget 2017. Earth System Science Data, 10(1), 405-448. doi:10.5194/essd-10-405-2018

Leblanc, S. G., Chen, J. M., Fernandes, R., Deering, D. W., & Conley, A. (2005). Methodology comparison for canopy structure parameters extraction from digital hemispherical photography in boreal forests. Agricultural and Forest Meteorology, 129(3-4), 187-207.

Lelieveld, J., Hadjinicolaou, P., Kostopoulou, E., Chenoweth, J., El Maayar, M., Giannakopoulos, C., . . . Xoplaki, E. (2012). Climate change and impacts in the Eastern Mediterranean and the Middle East. Climatic Change, 114(3-4), 667-687. doi:10.1007/s10584-012-0418-4

Lellei-Kovacs, E., Kovacs-Lang, E., Botta-Dukat, Z., Kalapos, T., Emmett, B., & Beier, C. (2011). Thresholds and interactive effects of soil moisture on the temperature response of soil respiration. European Journal of Soil Biology, 47(4), 247-255.

Levin, I., Naegler, T., Kromer, B., Diehl, M., Francey, R. J., Gomez-Pelaez, A. J., et al. (2010). Observations and modelling of the global distribution and long-term trend of atmospheric (CO2)-C-14 (vol 62, pg 26, 2010). Tellus Series B-Chemical and Physical Meteorology, 62(3), 207-207.

Li, Y., Kustas, W. P., Huang, C. L., Kool, D., & Haghighi, E. (2018). Evaluation of soil resistance formulations for estimates of sensible heat flux in a desert vineyard. Agricultural and Forest Meteorology, 260, 255-261. doi:10.1016/j.agrformet.2018.06.019

Liguori, G., Gugliuzza, G., & Inglese, P. (2009). Evaluating carbon fluxes in orange orchards in relation to planting density. Journal of Agricultural Science, 147, 637-645. doi:10.1017/s002185960900882x

Lin, G. H., Ehleringer, J. R., Rygiewicz, P. T., Johnson, M. G., & Tingey, D. T. (1999). Elevated CO2 and temperature impacts on different components of soil CO2 efflux in Douglas-fir terracosms. Global Change Biology, 5(2), 157-168.

Litton, C. M., Raich, J. W., & Ryan, M. G. (2007). Carbon allocation in forest ecosystems. Global Change Biology, 13(10), 2089-2109.

Liu, H., Zhao, P., Lu, P., Wang, Y. S., Lin, Y. B., & Rao, X. Q. (2008). Greenhouse gas fluxes from soils of different land-use types in a hilly area of South China. Agriculture Ecosystems & Environment, 124(1-2), 125-135. doi:10.1016/j.agee.2007.09.002

Loescher, H. W., Law, B. E., Mahrt, L., Hollinger, D. Y., Campbell, J., & Wofsy, S. C. (2006). Uncertainties in, and interpretation of, carbon flux estimates using the eddy covariance technique. Journal of Geophysical Research-Atmospheres, 111(D21). doi:10.1029/2005jd006932

Lopez-Ballesteros, A., Serrano-Ortiz, P., Kowalski, A. S., Sanchez-Canete, E. P., Scott, R. L., & Domingo, F. (2017). Subterranean ventilation of allochthonous CO2 governs net CO2 exchange in a semiarid

Mediterranean grassland. Agricultural and Forest Meteorology, 234, 115-126. doi:10.1016/j.agrformet.2016.12.021

Lovell, S. T., & Johnston, D. M. (2009). Creating multifunctional landscapes: how can the field of ecology inform the design of the landscape? Frontiers in Ecology and the Environment, 7(4), 212-220. doi:10.1890/070178

Lu, X. F., Liang, L. Y. L., Wang, L. X., Jenerette, G. D., McCabe, M. F., & Grantz, D. A. (2017). Partitioning of evapotranspiration using a stable isotope technique in an arid and high temperature agricultural production system. Agricultural Water Management, 179, 103-109. doi:10.1016/j.agwat.2016.08.012

Luo, Y. Q., & Weng, E. S. (2011). Dynamic disequilibrium of the terrestrial carbon cycle under global change. Trends in Ecology & Evolution, 26(2), 96-104. doi:10.1016/j.tree.2010.11.003

Luyssaert, S., Ciais, P., Piao, S. L., Schulze, E. D., Jung, M., Zaehle, S., . . . Team, C.-I. S. (2010). The European carbon balance. Part 3: forests. Global Change Biology, 16(5), 1429-1450. doi:10.1111/j.1365-2486.2009.02056.x

Luyssaert, S., Inglima, I., Jung, M., Richardson, A. D., Reichstein, M., Papale, D., . . . Janssens, I. A. (2007). CO2 balance of boreal, temperate, and tropical forests derived from a global database. Global Change Biology, 13(12), 2509-2537. doi:10.1111/j.1365-2486.2007.01439.x

Ma, X. L., Huete, A., Cleverly, J., Eamus, D., Chevallier, F., Joiner, J., . . . Ponce-Campos, G. (2016). Drought rapidly diminishes the large net CO2 uptake in 2011 over semi-arid Australia. Scientific Reports, 6. doi:10.1038/srep37747

Maestre-Valero, J. F., Testi, L., Jimenez-Bello, M. A., Castel, J. R., & Intrigliolo, D. S. (2017). Evapotranspiration and carbon exchange in a citrus orchard using eddy covariance. Irrigation Science, 35(5), 397-408. doi:10.1007/s00271-017-0548-6

Maseyk K, Lin T, Cochavi A, Schwartz A and Yakir D (2019) Quantification of leaf-scale light energy allocation and photoprotection processes in a Mediterranean pine forest under extensive seasonal drount. Tree Physiology, doi:10.1093/treephys/tpz079

Maseyk, K., Grunzweig, J. M., Rotenberg, E., & Yakir, D. (2008). Respiration acclimation contributes to high carbon-use efficiency in a seasonally dry pine forest. Global Change Biology, 14(7), 1553-1567. doi:10.1111/j.1365-2486.2008.01604.x

Maseyk, K., Hemming, D., Angert, A., Leavitt, S. W., & Yakir, D. (2011). Increase in water-use efficiency and underlying processes in pine forests across a precipitation gradient in the dry Mediterranean region over the past 30 years. Oecologia, 167(2), 573-585.

Mathieu, J. A., Hatte, C., Balesdent, J., & Parent, E. (2015). Deep soil carbon dynamics are driven more by soil type than by climate: a worldwide meta-analysis of radiocarbon profiles. Global Change Biology, 21(11), 4278-4292. doi:10.1111/gcb.13012

Matteucci, M., Gruening, C., Ballarin, I. G., Seufert, G., & Cescatti, A. (2015). Components, drivers and temporal dynamics of ecosystem respiration in a Mediterranean pine forest. Soil Biology & Biochemistry, 88, 224-235. doi:10.1016/j.soilbio.2015.05.017

McCabe, M. F., Rodell, M., Alsdorf, D. E., Miralles, D. G., Uijlenhoet, R., Wagner, W., et al. (2017). The future of Earth observation in hydrology. Hydrology and Earth System Sciences, 21(7), 3879-3914.

McCarthy, H. R., Pataki, D. E., & Jenerette, G. D. (2011). Plant water-use efficiency as a metric of urban ecosystem services. Ecological Applications, 21(8), 3115-3127. doi:10.1890/11-0048.1

Meyer, W. S., & Green, G. C. (1981). COMPARISON OF STOMATAL ACTION OF ORANGE, SOYBEAN AND WHEAT UNDER FIELD CONDITIONS. Australian Journal of Plant Physiology, 8(1), 65-76. doi:10.1071/pp9810065

Midwood, A. J., & Boutton, T. W. (1998). Soil carbonate decomposition by acid has little effect on delta C-13 of organic matter. Soil Biology & Biochemistry, 30(10-11), 1301-1307. doi:10.1016/s0038-0717(98)00030-3

Millennium Ecosystem Assessment, 2005. Ecosystems and Human Well-being: Synthesis. Island Press, Washington, DC.

Minasny B, Malone BP, McBrateny AB., et al. (2017) Soil carbon 4 per mille. Geoderma 292, 59-86

Misson, L., Rocheteau, A., Rambal, S., Ourcival, J. M., Limousin, J. M., & Rodriguez, R. (2010). Functional changes in the control of carbon fluxes after 3 years of increased drought in a Mediterranean evergreen forest? Global Change Biology, 16(9), 2461-2475. doi:10.1111/j.1365-2486.2009.02121.x

Ninari, N., & Berliner, P. R. (2002). The role of dew in the water and heat balance of bare loess soil in the Negev Desert: quantifying the actual dew deposition on the soil surface. Atmospheric Research, 64(1-4), 323-334.

Nowak, D. J., Greenfield, E. J., Hoehn, R. E., & Lapoint, E. (2013). Carbon storage and sequestration by trees in urban and community areas of the United States. Environmental Pollution, 178, 229-236. doi:10.1016/j.envpol.2013.03.019

Nunez-Florez, R., Perez-Gomez, U., & Fernandez-Mendez, F. (2019). Functional diversity criteria for selecting urban trees. Urban Forestry & Urban Greening, 38, 251-266. doi:10.1016/j.ufug.2019.01.005

Nyelele, C., Kroll, C. N., & Nowak, D. J. (2019). Present and future ecosystem services of trees in the Bronx, NY. Urban Forestry & Urban Greening, 42, 10-20. doi:10.1016/j.ufug.2019.04.018

Pacala, S., & Socolow, R. (2004). Stabilization wedges: Solving the climate problem for the next 50 years with current technologies. Science, 305(5686), 968-972. doi:10.1126/science.1100103

Pan, Y. D., Birdsey, R. A., Fang, J. Y., Houghton, R., Kauppi, P. E., Kurz, W. A., et al. (2011). A Large and Persistent Carbon Sink in the World's Forests. Science, 333(6045), 988-993.

Parresol, B. R. (1999). Assessing tree and stand biomass: A review with examples and critical comparisons. Forest Science, 45(4), 573-593.

Pataki, D. E., Alig, R. J., Fung, A. S., Golubiewski, N. E., Kennedy, C. A., McPherson, E. G., . . . Lankao, P. R. (2006). Urban ecosystems and the North American carbon cycle. Global Change Biology, 12(11), 2092-2102. doi:10.1111/j.1365-2486.2006.01242.x

Pataki, D. E., Carreiro, M. M., Cherrier, J., Grulke, N. E., Jennings, V., Pincetl, S., . . . Zipperer, W. C. (2011). Coupling biogeochemical cycles in urban environments: ecosystem services, green solutions, and misconceptions. Frontiers in Ecology and the Environment, 9(1), 27-36. doi:10.1890/090220

Pataki, D. E., Ehleringer, J. R., Flanagan, L. B., Yakir, D., Bowling, D. R., Still, C. J., et al. (2003). The application and interpretation of Keeling plots in terrestrial carbon cycle research. Global Biogeochemical Cycles, 17(1).

Paudel, I., Bar-Tal, A., Rotbart, N., Ephrath, J., & Cohen, S. (2018). Water quality changes seasonal variations in root respiration, xylem CO2, and sap pH in citrus orchards. Agricultural Water Management, 197, 147-157. doi:10.1016/j.agwat.2017.11.007

Paul, E. A., Morris, S. J., Six, J., Paustian, K., & Gregorich, E. G. (2003). Interpretation of soil carbon and nitrogen dynamics in agricultural and afforested soils. Soil Science Society of America Journal, 67(5), 1620-1628. doi:10.2136/sssaj2003.1620

Peddinti, S. R., & Kambhammettu, B. P. (2019). Dynamics of crop coefficients for citrus orchards of central India using water balance and eddy covariance flux partition techniques. Agricultural Water Management, 212, 68-77. doi:10.1016/j.agwat.2018.08.027

Peddinti, S. R., Kambhammettu, B. P., Rodda, S. R., Thumaty, K. C., & Suradhaniwar, S. (2019). Dynamics of Ecosystem Water Use Efficiency in Citrus Orchards of Central India Using Eddy Covariance and Landsat Measurements. Ecosystems. doi: 10.1007/s10021-019-00416-3

Peterjohn, W. T., Melillo, J. M., Steudler, P. A., Newkirk, K. M., Bowles, F. P., & Aber, J. D. (1994). RESPONSES OF TRACE GAS FLUXES AND N AVAILABILITY TO EXPERIMENTALLY ELEVATED SOIL TEMPERATURES. Ecological Applications, 4(3), 617-625.

Philip, J., & De Vries, D. (1957). Moisture movement in porous materials under temperature gradients. Trans Am Geophys Union;38:222–32

Piao, S. L., Fang, J. Y., Ciais, P., Peylin, P., Huang, Y., Sitch, S., et al. (2009). The carbon balance of terrestrial ecosystems in China. Nature, 458(7241), 1009-U1082.

Pilegaard, K., Ibrom, A., Courtney, M. S., Hummelshoj, P., & Jensen, N. O. (2011). Increasing net CO2 uptake by a Danish beech forest during the period from 1996 to 2009. Agricultural and Forest Meteorology, 151(7), 934-946. doi:10.1016/j.agrformet.2011.02.013

Post, W. M., & Kwon, K. C. (2000). Soil carbon sequestration and land-use change: processes and potential. Global Change Biology, 6(3), 317-327. doi:10.1046/j.1365-2486.2000.00308.x

Poulter, B., Frank, D., Ciais, P., Myneni, R. B., Andela, N., Bi, J., . . . van der Werf, G. R. (2014). Contribution of semi-arid ecosystems to interannual variability of the global carbon cycle. Nature, 509(7502), 600-+. doi:10.1038/nature13376

Preisler, Y., Tatarinov, F., Grunzweig, J. M., Bert, D., Ogee, J., Wingate, L., . . . Yakir, D. (2019). Mortality versus survival in drought-affected Aleppo pine forest depends on the extent of rock cover and soil stoniness. Functional Ecology, 33(5), 1-. doi:10.1111/1365-2435.13302

Qubaja, R., Amer, M., Tatrinov, F., Rotenberg, E., Preisler, Y., Sprintsin, M., & Yakir, D. (2019a). Partitioning evapotranspiration and its long-term evolution in a dry pine forest using measurement-based estimates of soil evaporation. Agricultural and Forest Meteorology. doi.org/10.1016/j.agrformet.2019.107831

Qubaja, R., Grünzweig, J., Rotenberg, E., & Yakir, D. (2019). Evidence for large carbon sink and long residence time in semi-arid forests based on 15-year flux and inventory records. Accepted for Global Change Biology

Qubaja, R., Tatarinov, F., Rotenberg, E., & Yakir, D. (2019b). Partitioning of canopy and soil CO2 fluxes in a pine forests at the dry timberline. Biogeosciences Discussions. doi: 10.5194/bg-2019-291

Raich, J. W., & Schlesinger, W. H. (1992). THE GLOBAL CARBON-DIOXIDE FLUX IN SOIL RESPIRATION AND ITS RELATIONSHIP TO VEGETATION AND CLIMATE. Tellus Series B-Chemical and Physical Meteorology, 44(2), 81-99.

Rambal, S. (2001). Hierarchy and Productivity of Mediterranean-Type Ecosystems-14.

Ramirez, D. A., Bellot, J., Domingo, F., & Blasco, A. (2007). Can water responses in Stipa tenacissima L. during the summer season be promoted by non-rainfall water gains in soil? Plant and Soil, 291(1-2), 67-79.

Ramnarine, R., Wagner-Riddle, C., Dunfield, K. E., & Voroney, R. P. (2012). Contributions of carbonates to soil CO2 emissions. Canadian Journal of Soil Science, 92(4), 599-607. doi:10.4141/cjss2011-025

Rana, G., Palatella, L., Scanlon, T. M., Martinelli, N., & Ferrara, R. M. (2018). CO2 and H2O flux partitioning in a Mediterranean cropping system. Agricultural and Forest Meteorology, 260, 118-130. doi:10.1016/j.agrformet.2018.06.007

Raz-Yaseef, N., Rotenberg, E., & Yakir, D. (2010). Effects of spatial variations in soil evaporation caused by tree shading on water flux partitioning in a semi-arid pine forest. Agricultural and Forest Meteorology, 150(3), 454-462. doi:10.1016/j.agrformet.2010.01.010

Raz-Yaseef, N., Yakir, D., Schiller, G., & Cohen, S. (2012). Dynamics of evapotranspiration partitioning in a semi-arid forest as affected by temporal rainfall patterns. Agricultural and Forest Meteorology, 157, 77-85.

Reichstein, M., Falge, E., Baldocchi, D., Papale, D., Aubinet, M., Berbigier, P., . . . Valentini, R. (2005). On the separation of net ecosystem exchange into assimilation and ecosystem respiration: review and improved algorithm. Global Change Biology, 11(9), 1424-1439. doi:10.1111/j.1365-2486.2005.001002.x

Reichstein, M., Falge, E., Baldocchi, D., Papale, D., Aubinet, M., Berbigier, P., . . . Valentini, R. (2005). On the separation of net ecosystem exchange into assimilation and ecosystem respiration: review and improved algorithm. Global Change Biology, 11(9), 1424-1439. doi:10.1111/j.1365-2486.2005.001002.x

Reichstein, M., Rey, A., Freibauer, A., Tenhunen, J., Valentini, R., Banza, J., et al. (2003). Modeling temporal and large-scale spatial variability of soil respiration from soil water availability, temperature and vegetation productivity indices. Global Biogeochemical Cycles, 17(4).

Rey, A., Pegoraro, E., Tedeschi, V., De Parri, I., Jarvis, P. G., & Valentini, R. (2002). Annual variation in soil respiration and its components in a coppice oak forest in Central Italy. Global Change Biology, 8(9), 851-866. doi:10.1046/j.1365-2486.2002.00521.x

Rhode, H. (1992). Modeling biogeochemical cycles. In: Global Biogeochemical Cycles (eds. Charlson, RJ, Butcher, SS, Orians, GH & Wolfe, GV). Academic London, UK.

Rodeghiero M, Cescatti A. (2005). Main determinants of forest soil respiration along an elevation / temperature gradient in the Italian Alps. Glob Chang Biol 11:1024–1041.

Rohatyn, S., Rotenberg, E., Ramati, E., Tatarinov, F., Tas, E., & Yakir, D. (2018). Differential Impacts of Land Use and Precipitation on "Ecosystem Water Yield". Water Resources Research, 54(8), 5457-5470. doi:10.1029/2017wr022267

Roland, M., et al. (2012). Contributions of carbonate weathering to the net ecosystem carbon balance of a mediterranean forest. Thesis submitted to Antwerpen University, Antwerpen, Belgium.

Ross, I., Misson, L., Rambal, S., Arneth, A., Scott, R. L., Carrara, A., et al. (2012). How do variations in the temporal distribution of rainfall events affect ecosystem fluxes in seasonally water-limited Northern Hemisphere shrublands and forests? Biogeosciences, 9(3), 1007-1024.

Rotenberg, E., & Yakir, D. (2010). Contribution of Semi-Arid Forests to the Climate System. Science, 327(5964), 451-454.

Rotenberg, E., & Yakir, D. (2011). Distinct patterns of changes in surface energy budget associated with forestation in the semiarid region. Global Change Biology, 17(4), 1536-1548. doi:10.1111/j.1365-2486.2010.02320.x

Rozenstein, O., Agam, N., Serio, C., Masiello, G., Venafra, S., Achal, S., et al. (2015). Diurnal emissivity dynamics in bare versus biocrusted sand dunes. Science of the Total Environment, 506, 422-429.

Schiller, G. (2000), Ecophysiology of Pinus halepensis Mill. and P. brutia Ten, in Ecology, Biogeography and Management of Pinus halepensis and P. brutia Forest Ecosystems in the Mediterranean Basin, edited by G. Ne'eman and L. Trabaud, pp. 51–65, Backhuys, Leiden, Netherlands.

Schlesinger WH & Amundson R (2019) Managing for soil carbon sequestration: Let's get realistic. Global Change Biology 25, 386-389

Schlesinger, W. H., & Jasechko, S. (2014). Transpiration in the global water cycle. Agricultural and Forest Meteorology, 189, 115-117.

Schmidt, M. W. I., Torn, M. S., Abiven, S., Dittmar, T., Guggenberger, G., Janssens, I. A., . . . Trumbore, S. E. (2011). Persistence of soil organic matter as an ecosystem property. Nature, 478(7367), 49-56. doi:10.1038/nature10386

Schroth, G., D'Angelo, S. A., Teixeira, W. G., Haag, D., & Lieberei, R. (2002). Conversion of secondary forest into agroforestry and monoculture plantations in Amazonia: consequences for biomass, litter and soil carbon stocks after 7 years. Forest Ecology and Management, 163(1-3), 131-150. doi:10.1016/s0378-1127(01)00537-0

Schrumpf, M., Schulze, E. D., Kaiser, K., & Schumacher, J. (2011). How accurately can soil organic carbon stocks and stock changes be quantified by soil inventories? Biogeosciences, 8(5), 1193-1212. doi:10.5194/bg-8-1193-2011

Schulze, E. D., Luyssaert, S., Ciais, P., Freibauer, A., Janssens, I. A., Soussana, J. F., et al. (2009). Importance of methane and nitrous oxide for Europe's terrestrial greenhouse-gas balance. Nature Geoscience, 2(12), 842-850.

Schulze, E.D. & Heimann, M. (1998). Carbon and water exchange of terrestrial ecosystems. In: Galloway, J., Melillo, J.M. (Eds.), Asian change in the context of global change, Cambridge University Press, Cambridge, 145-161.

Schulze, E.-D. (2000). Carbon and Nitrogen Cycling in European Forest Ecosystems: Berlin, Heidelberg : Springer Berlin Heidelberg : Imprint: Springer.

Scott, R. L., & Biederman, J. A. (2017). Partitioning evapotranspiration using long-term carbon dioxide and water vapor fluxes. Geophysical Research Letters, 44(13), 6833-6840.

Scott, R. L., Biederman, J. A., Hamerlynck, E. P., & Barron-Gafford, G. A. (2015). The carbon balance pivot point of southwestern US semiarid ecosystems: Insights from the 21st century drought. Journal of Geophysical Research-Biogeosciences, 120(12), 2612-2624. doi:10.1002/2015jg003181

Seco, R., Karl, T., Turnipseed, A., Greenberg, J., Guenther, A., Llusia, J., . . . Yakir, D. (2017). Springtime ecosystem-scale monoterpene fluxes from Mediterranean pine forests across a precipitation gradient. Agricultural and Forest Meteorology, 237, 150-159. doi:10.1016/j.agrformet.2017.02.007

Segura, M., & Kanninen, M. (2005). Allometric models for tree volume and total aboveground biomass in a tropical humid forest in Costa Rica. Biotropica, 37(1), 2-8. doi:10.1111/j.1744-7429.2005.02027.x

Serrano-Ortiz, P., Roland, M., Sanchez-Moral, S., Janssens, I. A., Domingo, F., Godderis, Y., & Kowalski, A. S. (2010). Hidden, abiotic CO2 flows and gaseous reservoirs in the terrestrial carbon cycle: Review and perspectives. Agricultural and Forest Meteorology, 150(3), 321-329. doi:10.1016/j.agrformet.2010.01.002

Shachnovich, Y., Berliner, P. R., & Bar, P. (2008). Rainfall interception and spatial distribution of throughfall in a pine forest planted in an arid zone. Journal of Hydrology, 349(1-2), 168-177.

Shapland, T. M., Snyder, R. L., Smart, D. R., & Williams, L. E. (2012). Estimation of actual evapotranspiration in winegrape vineyards located on hillside terrain using surface renewal analysis. Irrigation Science, 30(6), 471-484. doi:10.1007/s00271-012-0377-6

Shen, W. J., Jenerette, G. D., Hui, D. F., Phillips, R. P., & Ren, H. (2008). Effects of changing precipitation regimes on dryland soil respiration and C pool dynamics at rainfall event, seasonal and interannual scales. Journal of Geophysical Research-Biogeosciences, 113(G3).

Sheng, H., Yang, Y. S., Yang, Z. J., Chen, G. S., Xie, J. S., Guo, J. F., & Zou, S. Q. (2010). The dynamic response of soil respiration to land-use changes in subtropical China. Global Change Biology, 16(3), 1107-1121. doi:10.1111/j.1365-2486.2009.01988.x

Simonin, K., Kolb, T. E., Montes-Helu, M., & Koch, G. W. (2007). The influence of thinning on components of stand water balance in a ponderosa pine forest stand during and after extreme drought. Agricultural and Forest Meteorology, 143(3-4), 266-276.

Singer, A. (2007). The soils of Israel, Springer Science & Business Media, p. 306.

Singh, G. (2014).Urban Ecology & Ecosystem Inputs - Need of the Urban Era". Urban Ecology.

Siry, J. P., Cubbage, F. W., & Ahmed, M. R. (2005). Sustainable forest management: global trends and opportunities. Forest Policy and Economics, 7(4), 551-561.

Six, J., Conant, R. T., Paul, E. A., & Paustian, K. (2002). Stabilization mechanisms of soil organic matter: Implications for C-saturation of soils. Plant and Soil, 241(2), 155-176. doi:10.1023/a:1016125726789

Smith, K. A., Ball, T., Conen, F., Dobbie, K. E., Massheder, J., & Rey, A. (2003). Exchange of greenhouse gases between soil and atmosphere: interactions of soil physical factors and biological processes. European Journal of Soil Science, 54(4), 779-791.

Song, G. H., Li, L. Q., Pan, G. X., & Zhang, Q. (2005). Topsoil organic carbon storage of China and its loss by cultivation. Biogeochemistry, 74(1), 47-62. doi:10.1007/s10533-004-2222-3

Sorensen, L. (2009). A Spatial Analysis Approach to the Global Delineation of Dryland Areas of Relevance to the CBD Programme of Work on Dry and Sub-Humid Lands (UNEP World Conservation Monitoring Centre).

Sprintsin, M., Cohen, S., Maseyk, K., Rotenberg, E., Grunzweig, J., Karnieli, A., et al. (2011). Long term and seasonal courses of leaf area index in a semi-arid forest plantation. Agricultural and Forest Meteorology, 151(5), 565-574.

Sprintsin, M., Karnieli, A., Berliner, P., Rotenberg, E., Yakir, D., & Cohen, S. (2007). The effect of spatial resolution on the accuracy of leaf area index estimation for a forest planted in the desert transition zone. Remote Sensing of Environment, 109(4), 416-428. doi:10.1016/j.rse.2007.01.020

Steduto, P., & Food and Agriculture Organization of the United Nations. (2012). Crop yield response to water. Rome: FAO, http://www.fao.org/docrep/016/i2800e/i2800e.pdf

Stevens, A., & van Wesemael, B. (2008). Soil organic carbon dynamics at the regional scale as influenced by land use history: a case study in forest soils from southern Belgium. Soil Use and Management, 24(1), 69-79. doi:10.1111/j.1475-2743.2007.00135.x

Stewart, C. E., Paustian, K., Conant, R. T., Plante, A. F., & Six, J. (2009). Soil carbon saturation: Implications for measurable carbon pool dynamics in long-term incubations. Soil Biology & Biochemistry, 41(2), 357-366. doi:10.1016/j.soilbio.2008.11.011

Stoy, P. C., El-Madany, T., Fisher, J. B., Gentine, P., Gerken, T., Good, S. P., Liu, S., Miralles, D. G., Perez-Priego, O., Skaggs, T. H., Wohlfahrt, G., Anderson, R. G., Jung, M., Maes, W. H., Mammarella, I., Mauder, M., Migliavacca, M., Nelson, J. A., Poyatos, R., Reichstein, M., Scott, R. L., and Wolf, S.

(2019). Reviews and syntheses: Turning the challenges of partitioning ecosystem evaporation and transpiration into opportunities, Biogeosciences Discuss., in review.

Stoy, P. C., Katul, G. G., Siqueira, M. B. S., Juang, J. Y., Novick, K. A., Uebelherr, J. M., & Oren, R. (2006). An evaluation of models for partitioning eddy covariance-measured net ecosystem exchange into photosynthesis and respiration. Agricultural and Forest Meteorology, 141(1), 2-18. doi:10.1016/j.agrformet.2006.09.001

Subke, J.-A., Voke, N. R., Leronni, V., Garnett, M. H., & Ineson, P. (2011). Dynamics and pathways of autotrophic and heterotrophic soil CO2 efflux revealed by forest girdling. Journal of Ecology, 99(1), 186-193.

Sulman, B. N., Roman, D. T., Scanlon, T. M., Wang, L. X., & Novick, K. A. (2016). Comparing methods for partitioning a decade of carbon dioxide and water vapor fluxes in a temperate forest. Agricultural and Forest Meteorology, 226, 229-245. doi:10.1016/j.agrformet.2016.06.002

Sun, Z. H., Niinemets, U., Huve, K., Rasulov, B., & Noe, S. M. (2013). Elevated atmospheric CO2 concentration leads to increased whole-plant isoprene emission in hybrid aspen (Populus tremula x Populus tremuloides). New Phytologist, 198(3), 788-800. doi:10.1111/nph.12200

Talsma, C. J., Good, S. P., Jimenez, C., Martens, B., Fisher, J. B., Miralles, D. G., . . . Purdy, A. J. (2018). Partitioning of evapotranspiration in remote sensing-based models. Agricultural and Forest Meteorology, 260, 131-143. doi:10.1016/j.agrformet.2018.05.010

Taneva, L., & Gonzalez-Meler, M. A. (2011). Distinct patterns in the diurnal and seasonal variability in four components of soil respiration in a temperate forest under free-air CO2 enrichment. Biogeosciences, 8(10), 3077-3092.

Tang, J. W., Baldocchi, D. D., & Xu, L. (2005). Tree photosynthesis modulates soil respiration on a diurnal time scale. Global Change Biology, 11(8), 1298-1304.

Tatarinov, F., Rotenberg, E., Maseyk, K., Ogee, J., Klein, T., & Yakir, D. (2016). Resilience to seasonal heat wave episodes in a Mediterranean pine forest. New Phytologist, 210(2), 485-496. doi:10.1111/nph.13791

Taylor, A. J., Lai, C. T., Hopkins, F. M., Wharton, S., Bible, K., Xu, X. M., et al. (2015). Radiocarbon-Based Partitioning of Soil Respiration in an Old-Growth Coniferous Forest. Ecosystems, 18(3), 459-470.

Thomas, C. K., Martin, J. G., Law, B. E., & Davis, K. (2013). Toward biologically meaningful net carbon exchange estimates for tall, dense canopies: Multi-level eddy covariance observations and canopy coupling regimes in a mature Douglas-fir forest in Oregon. Agricultural and Forest Meteorology, 173, 14-27. doi:10.1016/j.agrformet.2013.01.001

Thompson, M. V., & Randerson, J. T. (1999). Impulse response functions of terrestrial carbon cycle models: method and application. Global Change Biology, 5(4), 371-394. doi:10.1046/j.1365-2486.1999.00235.x

Trettin, C. C., Johnson, D. W., & Todd, D. E. (1999). Forest nutrient and carbon pools at Walker Branch Watershed: Changes during a 21-year period. Soil Science Society of America Journal, 63(5), 1436-1448. doi:10.2136/sssaj1999.6351436x

Turpin-Jelfs, T., Michaelides, K., Biederman, J. A., & Anesio, A. M. (2019). Soil nitrogen response to shrub encroachment in a degrading semi-arid grassland. Biogeosciences, 16(2), 369-381. doi:10.5194/bg-16-369-2019

Ucles, O., Villagarcia, L., Canton, Y., Lazaro, R., & Domingo, F. (2015). Non-rainfall water inputs are controlled by aspect in a semiarid ecosystem. Journal of Arid Environments, 113, 43-50.

van Dijk, A., Gash, J. H., van Gorsel, E., Blanken, P. D., Cescatti, A., Emmel, C., et al. (2015). Rainfall interception and the coupled surface water and energy balance. Agricultural and Forest Meteorology, 214, 402-415.

Verhoef, A., Diaz-Espejo, A., Knight, J. R., Villagarcia, L., & Fernandez, J. E. (2006). Adsorption of water vapor by bare soil in an olive grove in southern Spain. Journal of Hydrometeorology, 7(5), 1011-1027.

Villegas, J. C., Dominguez, F., Barron-Gafford, G. A., Adams, H. D., Guardiola-Claramonte, M., Sommer, E. D., et al. (2015). Sensitivity of regional evapotranspiration partitioning to variation in woody plant cover: insights from experimental dryland tree mosaics. Global Ecology and Biogeography, 24(9), 1040-1048.

Volcani, A., Karnieli, A., & Svoray, T. (2005). The use of remote sensing and GIS for spatio-temporal analysis of the physiological state of a semi-arid forest with respect to drought years. Forest Ecology and Management, 215(1-3), 239-250. doi:10.1016/j.foreco.2005.05.063

Wang, L. X., Good, S. P., & Caylor, K. K. (2014). Global synthesis of vegetation control on evapotranspiration partitioning. Geophysical Research Letters, 41(19), 6753-6757. doi:10.1002/2014gl061439

Wang, Q. K., Wang, S. L., Xu, G. B., & Fan, B. (2010). Conversion of secondary broadleaved forest into Chinese fir plantation alters litter production and potential nutrient returns. Plant Ecology, 209(2), 269-278. doi:10.1007/s11258-010-9719-8

Wang, X., Liu, L. L., Piao, S. L., Janssens, I. A., Tang, J. W., Liu, W. X., . . . Xu, S. (2014). Soil respiration under climate warming: differential response of heterotrophic and autotrophic respiration. Global Change Biology, 20(10), 3229-3237. doi:10.1111/gcb.12620

Wang, Y. X., Weng, B. Q., Tian, N., Zhong, Z. M., & Wang, M. K. (2017). Soil Organic Carbon Stocks of Citrus Orchards in Yongchun County, Fujian Province, China. Pedosphere, 27(5), 985-990. doi:10.1016/s1002-0160(17)60459-4

Wei, Z. W., Yoshimura, K., Wang, L. X., Miralles, D. G., Jasechko, S., & Lee, X. H. (2017). Revisiting the contribution of transpiration to global terrestrial evapotranspiration. Geophysical Research Letters, 44(6), 2792-2801.

West, G. B., Brown, J. H., & Enquist, B. J. (1997). A general model for the origin of allometric scaling laws in biology. Science, 276(5309), 122-126. doi:10.1126/science.276.5309.122

West, T. O., & Six, J. (2007). Considering the influence of sequestration duration and carbon saturation on estimates of soil carbon capacity. Climatic Change, 80(1-2), 25-41. doi:10.1007/s10584-006-9173-8

Wheeler, A.J., & Ganji, A.R. (1996). Introduction to Engineering Experimentation. Prentice Hall, Upper Saddle River, New Jersey, United States.

Whiteford, J. R., & Spanu, P. D. (2002). Hydrophobins and the interactions between fungi and plants. Molecular Plant Pathology, 3(5), 391-400.

Wiesmeier, M., Munro, S., Barthold, F., Steffens, M., Schad, P., & Kogel-Knabner, I. (2015). Carbon storage capacity of semi-arid grassland soils and sequestration potentials in northern China. Global Change Biology, 21(10), 3836-3845. doi:10.1111/gcb.12957

Wu, D. H., Piao, S. L., Liu, Y. W., Ciais, P., & Yao, Y. T. (2018). Evaluation of CMIP5 Earth System Models for the Spatial Patterns of Biomass and Soil Carbon Turnover Times and Their Linkage with Climate. Journal of Climate, 31(15), 5947-5960. doi:10.1175/jcli-d-17-0380.1

Xu, M. H., Liu, M., Xue, X., & Zhai, D. T. (2016). Warming effects on plant biomass allocation and correlations with the soil environment in an alpine meadow, China. Journal of Arid Land, 8(5), 773-786. doi:10.1007/s40333-016-0013-z

Xu, M., & Qi, Y. (2001). Soil-surface CO2 efflux and its spatial and temporal variations in a young ponderosa pine plantation in northern California. Global Change Biology, 7(6), 667-677.

Xu, Z. F., Tang, S. S., Xiong, L., Yang, W. Q., Yin, H. J., Tu, L. H., . . . Tan, B. (2015). Temperature sensitivity of soil respiration in China's forest ecosystems: Patterns and controls. Applied Soil Ecology, 93, 105-110. doi:10.1016/j.apsoil.2015.04.008

Yakir, D., & Wang, X. F. (1996). Fluxes of CO2 and water between terrestrial vegetation and the atmosphere estimated from isotope measurements. Nature, 380(6574), 515-517. doi:10.1038/380515a0

Yan, D., Scott, R. L., Moore, D. J. P., Biederman, J. A., & Smith, W. K. (2019). Understanding the relationship between vegetation greenness and productivity across dryland ecosystems through the integration of PhenoCam, satellite, and eddy covariance data. Remote Sensing of Environment, 223, 50-62. doi:10.1016/j.rse.2018.12.029

Yan, Y., Zhou, X. H., Jiang, L. F., & Luo, Y. Q. (2017). Effects of carbon turnover time on terrestrial ecosystem carbon storage. Biogeosciences, 14(23), 5441-5454. doi:10.5194/bg-14-5441-2017

Yang, F. L., Qubaja, R., Tatarinov, F., Rotenberg, E., & Yakir, D. (2018). Assessing canopy performance using carbonyl sulfide measurements. Global Change Biology, 24(8), 3486-3498. doi:10.1111/gcb.14145

Yang, F. L., Qubaja, R., Tatarinov, F., Stern, R., & Yakir, D. (2019). Soil-atmosphere exchange of carbonyl sulfide in a Mediterranean citrus orchard. Atmospheric Chemistry and Physics, 19(6), 3873-3883. doi:10.5194/acp-19-3873-2019

Yosef, G., Walko, R., Avisar, R., Tatarinov, F., Rotenberg, E., & Yakir, D. (2018). Large-scale semi-arid afforestation can enhance precipitation and carbon sequestration potential. Scientific Reports, 8. doi:10.1038/s41598-018-19265-6

Young-Robertson, J. M., Raz-Yaseef, N., Cohen, L. R., Newman, B., Rahn, T., Sloan, V., et al. (2018). Evaporation dominates evapotranspiration on Alaska's Arctic Coastal Plain. Arctic Antarctic and Alpine Research, 50(1).

Yu, S. Q., Chen, Y. Q., Zhao, J., Fu, S. L., Li, Z., Xia, H. P., & Zhou, L. X. (2017). Temperature sensitivity of total soil respiration and its heterotrophic and autotrophic components in six vegetation types of subtropical China. Science of the Total Environment, 607, 160-167. doi:10.1016/j.scitotenv.2017.06.194

Yunusa, I. A. M., Walker, R. R., & Lu, P. (2004). Evapotranspiration components from energy balance, sapflow and microlysimetry techniques for an irrigated vineyard in inland Australia. Agricultural and Forest Meteorology, 127(1-2), 93-107. doi:10.1016/j.agrformet.2004.07.001

Zhang, B. Q., AghaKouchak, A., Yang, Y. T., Wei, J. H., & Wang, G. Q. (2019). A water-energy balance approach for multi-category drought -assessment across globally diverse hydrological basins. Agricultural and Forest Meteorology, 264, 247-265. doi:10.1016/j.agrforrnet.2018.10.010

Zhang, Q., Wang, S., Wang, S. S., Zhao, Y. D., & Wen, X. M. (2016). Influence factors and variation characteristics of water vapor absorption by soil in semi-arid region. Science China-Earth Sciences, 59(11), 2240-2251.

Zhao, P., Kang, S. Z., Li, S., Ding, R. S., Tong, L., & Du, T. S. (2018). Seasonal variations in vineyard ET partitioning and dual crop coefficients correlate with canopy development and surface soil moisture. Agricultural Water Management, 197, 19-33. doi:10.1016/j.agwat.2017.11.004

Zhou, T., Shi, P. J., Hui, D. F., & Luo, Y. Q. (2009). Global pattern of temperature sensitivity of soil heterotrophic respiration (Q(10)) and its implications for carbon-climate feedback. Journal of Geophysical Research-Biogeosciences, 114.

LIST OF PUBLICATIONS

1. Yang, F. L., **Qubaja, R.**, Tatarinov, F., Rotenberg, E., & Yakir, D. (2018). Assessing canopy performance using carbonyl sulfide measurements. Global Change Biology, 24(8), 3486-3498. doi:10.1111/gcb.14145

2. Brugger, P., Banerjee, T., De Roo, F., Kroeniger, K., **Qubaja, R.**, Rohatyn, S., Rotenberg, E., Tatarinov, F., Yakir, D., Yang, F.,& Mauder, M. (2018). Effect of Surface Heterogeneity on the Boundary-Layer Height: A Case Study at a Semi-Arid Forest. Boundary-Layer Meteorology, 169(2), 233-250. doi:10.1007/s10546-018-0371-5

3. Yang, F. L., **Qubaja, R.**, Tatarinov, F., Stern, R., & Yakir, D. (2019). Soil-atmosphere exchange of carbonyl sulfide in Mediterranean citrus orchard. Atmos. Chem. Phys., 19, 3873–3883. doi:10.5194/acp-19-3873-2019

4. **Qubaja, R.**, Grünzweig, J., Rotenberg, E., & Yakir, D. (2019). Evidence for large carbon sink and long residence time in semi-arid forests based on 15-year flux and inventory records. Global Change Biology. doi:10.1111/gcb.14927

5. **Qubaja, R.**, Tatarinov, F., Rotenberg, E., & Yakir, D. (2019). Partitioning of canopy and soil CO_2 fluxes in a pine forest at the dry timberline, Biogeosciences. doi:10.5194/bg-2019-291.

6. **Qubaja, R.**, Tatrinov, F., Yang, F., Amer, M., & Yakir, D. (2019). Assessing CO_2 and H_2O fluxes in a non-commercial urban citrus orchard. Submitted to Agricultural and Forest Meteorology.

7. **Qubaja, R.**, Amer, M., Tatrinov, F., Rotenberg, E., Preisler, Y., Sprintsin, M., & Yakir, D. (2019). Partitioning evapotranspiration and its long-term evolution in a dry pine forest using measurement-based estimates of soil evaporation. Agricultural and Forest Meteorology. doi:10.1016/j.agrformet.2019.107831

8. **Qubaja, R.**, & Yakir, D. (2019). Long-term soil respiration and evaporation under rainfall manipulation in a Mediterranean dry pine forest using chamber-based estimates measurements. In preparation.

9. Three additional papers in preparation stage.